Alfred-Wegener-Institut für Polar- und Meeresforschung
Universität Potsdam, Institut für Geowissenschaften

Land-atmosphere interactions on different scales

**The Exchange of Methane
Between wet Arctic Tundra and the Atmosphere
at the Lena River Delta, Northern Siberia**

**Dissertation
zur Erlangung des akademischen Grades
"doctor rerum naturalium"
(Dr. rer. nat.)
in der Wissenschaftsdisziplin "Geowissenschaften"**

**eingereicht an der
Mathematisch-Naturwissenschaftlichen Fakultät
der Universität Potsdam**

**von
Torsten Sachs**

Potsdam, den 15.01.2009

In all things of nature there is something of the marvelous.

(Aristoteles)

Acknowledgements

Abstract

About 5–8% of the earth's land surface is covered by Arctic tundra, which is the dominant terrestrial ecosystem of the Arctic and plays an important role in the global climate system because of its tight coupling with the atmosphere and the cryosphere. At the same time, these ecosystems are well-adapted to the climatic conditions and characterized by permanently frozen ground (permafrost) rendering them highly vulnerable. Because of recent Arctic warming and a predicted continued warming trend that is more pronounced in the Arctic than on the global average, Arctic ecosystems are changing. These changes are not yet sufficiently understood and quantified, mainly because of a lack of data from remote Arctic regions and the resulting lack of mechanistic understanding.

For example, the amount of methane being released from Arctic ecosystems and the processes involved in it are neither well quantified nor completely understood. Most studies to date have measured methane emission on small spatial scales of typically less than 1 m² by closed chamber methods. The results from these small-scale studies were then upscaled to regional or even global emission estimates associated with large uncertainties.

The aim of this interdisciplinary dissertation at the interface of biosphere, cryosphere, pedosphere, hydrosphere, and atmosphere is the detailed investigation of methane emissions and the relevant processes at two different spatial scales at a Siberian tundra site and to contribute to improved emission estimates and process understanding. First, a model is derived from diffusion theory to accurately describe the concentration change of carbon dioxide in a closed chamber measurement system to improve flux calculations based on this method. This model is valid for methane as well

and is used for methane flux calculation from closed chamber measurements. In addition, the micrometeorological eddy covariance method is used to simultaneously quantify methane fluxes on the ecosystem scale, following a nested approach were small-scale measurements are made within the larger-scale measurements' footprint. This approach allows for a direct comparison of the relevant controls and emissions, and small-scale fluxes upscaled to the ecosystem scale can be checked against real data. Finally, a method is developed to estimate the effect of the spatial heterogeneities characteristic for polygonal tundra directly from eddy covariance data.

The results of this dissertation double the number of published eddy covariance methane flux datasets from Arctic tundra sites and thus constitute an important contribution to the available database as well as to efforts to verify various regional or global models. The measured fluxes on the ecosystem scale are surprisingly low at less than 20 mg m^{-2} d^{-1} (seasonal average from June–September), considering that most published rates based on closed chamber data easily exceed 100 mg m^{-2} d^{-1} which is also true for this study. In addition, previously unrecognized processes and differences in the controls on methane emissions (turbulence and pressure on the ecosystem scale vs. surface temperature on the micro-site scale) are identified and the mechanistic understanding of land-atmosphere exchange processes is improved, in particular with regard to the atmosphere's role in ecosystem-scale emissions on short timescales. The differences affect estimates that were upscaled from micro-site-scale measurements to larger scales and should encourage some restraint in deriving global statements from small-scale measurements. The methods developed in this dissertation could contribute significantly to improved emission estimates on various scales.

Zusammenfassung

Etwa 5–8% der Landfläche der Erde sind von arktischer Tundra bedeckt, die als dominantes terrestrisches Ökosystem der Arktis durch ihre Interaktion mit der Atmosphäre und der Cryosphäre eine wichtige Rolle im globalen Klimasystem spielt. Gleichzeitig sind Tundra-Ökosysteme durch ihre Anpassung an die klimatischen Gegebenheiten und durch das Vorkommen von Dauerfrostboden (Permafrost) extrem sensibel. Durch die in der Arktis stattfindende und auch weiter prognostizierte relativ zum globalen Mittel stärkere Erwärmung, finden Veränderungen statt, die zur Zeit nicht zufriedenstellend verstanden und quantifiziert werden können. Dieses liegt unter anderem in der sehr lückenhaften Datenlage und dem daraus direkt folgenden mangelnden Prozeßverständnis begründet.

Die Mengen des klimawirksamen Treibhausgases Methan und die Prozesse, die an deren Freisetzung aus Permafrost-beeinflußten Tundra-Ökosystemen beteiligt sind, stellen ein derzeit hochaktuelles Beispiel sowohl für die mangelhafte Datenlage als auch für unzureichendes Prozeßverständnis dar. Bisherige Studien zur Methanfreisetzung aus arktischer Tundra wurden fast ausschließlich auf sehr kleinen räumlichen Skalen (bis ca. 1 m²) mittels Gaskammermessungen durchgeführt, von denen die Ergebnisse dann auf die regionale oder globale Skala hochgerechnet wurden. Dieses Vorgehen führte zu erheblichen Unsicherheiten in den globalen Abschätzungen.

Das Ziel der vorliegenden interdisziplinären Arbeit an der Schnittstelle von Biosphäre, Cryosphäre, Pedosphäre, Hydrosphäre und Atmosphäre ist es, Methanemissionen und die daran beteiligten Prozesse an einem sibirischen Tundra-Standort auf zwei verschiedenen Skalen eingehend zu untersuchen und zu einer verbesserten Abschätzung der Emissionen sowie einem genaueren Prozeßverständnis

beizutragen. Dafür wird zunächst theoretisch ein Modell hergeleitet, das die Konzentrationsentwicklung von Kohlendioxid in einem Gaskammer-Meßsystem beschreibt, und mit dessen Hilfe der Fluß des gemessenen Gases (auch für Methan anwendbar) aus dem Boden in die Atmosphäre sicherer bestimmt werden kann als bisher. Zusätzlich zu Messungen mit dem Gaskammersystem wurden zeitgleich mikrometeorologische Messungen mit der sogenannten Eddy-Kovarianz-Methode durchgeführt. Diese Methode erlaubt es, die Methanemission auf einer Fläche von mehreren Hektar bis Quadratkilometern zu bestimmen, wobei die bemessene Fläche die Standorte der Gaskammermessungen einschließt. Dieser zweiskalige Ansatz erlaubt einen direkten Vergleich der relevanten Steuerparameter und eine Möglichkeit, von der kleinen Skala hochgerechnete Emissionen mit den tatsächlich gemessenen auf der nächsthöheren Skala zu vergleichen. Abschließend wird versucht, die beobachteten räumlichen Heterogenitäten direkt aus den Eddy-Kovarianz-Daten abzuschätzen.

Die Ergebnisse der vorliegenden Arbeit verdoppeln die Anzahl der publizierten Eddy-Kovarianz Datensätze zu Methanemissionen aus der Arktis und leisten somit einen wichtigen Beitrag zur Verbesserung der Datenlage sowie zur Verifizierbarkeit verschiedener Computermodelle. Die gemessenen Flüsse sind mit weniger als 20 mg m^{-2} d^{-1} im saisonalen Mittel (Juni–September) überraschend niedrig vor dem Hintergrund, daß publizierte Gaskammer-Methanflußdaten wie auch in der vorliegenden Arbeit durchaus 100 mg m^{-2} d^{-1} übersteigen. Auch werden bisher unbeachtete Unterschiede in den die Methanemission steuernden Prozessen und Parametern (Turbulenz und Druck auf der Ökosystemskala vs. Oberflächentemperatur auf der Mikro-Standortskala) aufgezeigt und das Prozeßverständnis vor allem auf Ökosystemebene und kurzen zeitlichen Skalen erweitert. Die gefundenen Unterschiede haben Auswirkungen auf die Hochrechnungen von Punktmessungen auf größere Skalen und sollten zu etwas Zurückhaltung bei der Ableitung globaler Aussagen aus solchen Punktmessungen anregen. Die in dieser Arbeit entwickelten Methoden könnten wesentlich zu einer verbesserten Abschätzung von Methanemissionen auf verschiedenen Skalen beitragen.

Content

List of Figures

List of Tables

1. LAND-ATMOSPHERE INTERACTIONS ON DIFFERENT SCALES
–
THE EXCHANGE OF METHANE BETWEEN WET ARCTIC TUNDRA AND THE ATMOSPHERE AT THE LENA RIVER DELTA, NORTHERN SIBERIA

1.1 Background

Global mean surface temperatures increased 0.76°C from 1850–1899 to 2001–2005 (IPCC, 2007). During the past 50 years, the rate of warming (0.13°C ± 0.03°C per decade) was almost double the rate over the past 100 years, and the Arctic north of 65°N experienced more than double the warming of the global mean (ACIA, 2005; IPCC, 2007) (Fig. 1.1). All projections of future warming indicate stronger temperature increases in the Arctic relative to the global mean (ACIA, 2005; IPCC, 2007) (Fig. 1.2) and most other changes are expected to be more pronounced in the high latitudes as well.

Arctic tundra ecosystems cover about 7.3–10.5 x 10^{12} m^2 or 5–7% of the earth's land surface (Post et al., 1982; Whalen and Reeburgh, 1992; McGuire et al., 1997; Reeburgh et al., 1998) with the southern boundary being somewhat subjective. The tight coupling between biosphere and atmosphere as well as the permanently frozen ground (permafrost) underneath the shallow seasonally thawed active layer make tundra ecosystems extremely sensitive to disturbance, in particular to changes in climatic conditions. In recent years, permafrost and the vast amounts of frozen organic carbon it contains have attracted significant attention due to concerns about the fate of that
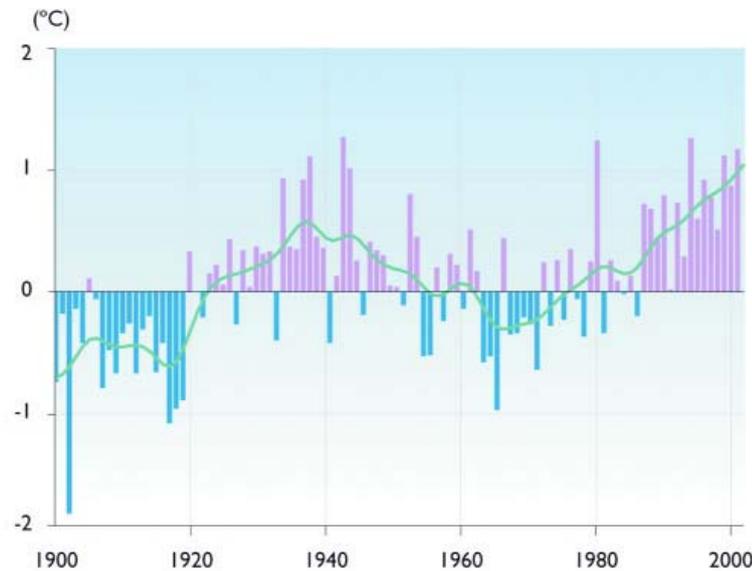
Figure 1.1: Observed Arctic (60°–90°N) near surface temperature during the last century (annual averages) relative to the average for 1961–1990. Note the decadal variability shown by the warm period in the first half of the 20th century. The regional distribution appears to have been different from the current warming (Source: ACIA 2005, updated from Peterson and Vose, 1997).
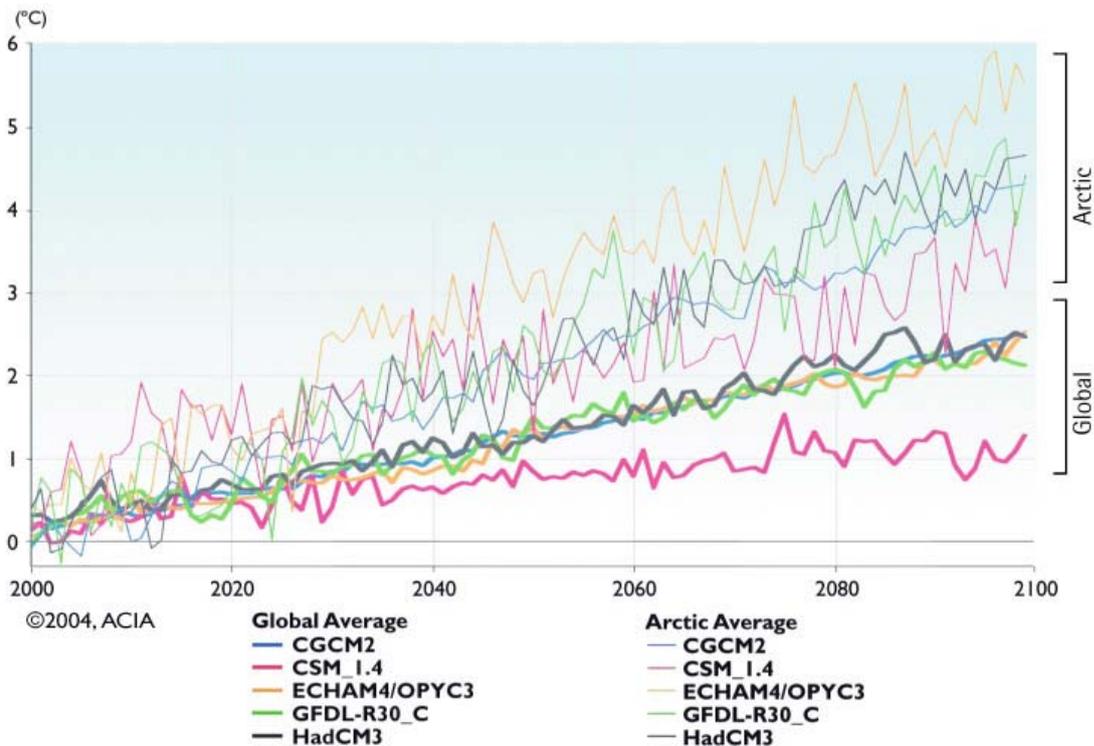
Figure 1.2: Average surface air temperature change (change from 1981–2000 average) projected by the five ACIA-designated Atmosphere–ocean general circulation models (AOGCMs) for the B2 emissions scenario (Source: ACIA, 2005). The models were developed by the Canadian Center for Climate Modelling and Analysis (CGCM2), the National Center for Atmospheric Research, USA (CSM_1.4), the Max Planck Institute for Meteorology, Germany (ECHAM4/OPYC3), the Geophysical Fluid Dynamics Laboratory, USA (GFDL-R30_C), and the Hadley Center for Climate Prediction and Research, UK.

carbon in a warming Arctic and its potential feedback on the climate system. This concern about the possible release of carbon dioxide and methane from thawing, organic-rich permafrost sediments has triggered increased research efforts and a number of alarming reports and estimates about the contribution of high latitude ecosystems to the global atmospheric greenhouse gas burden.

However, despite these increased efforts, data from high latitudes are still extremely sparse and global estimates are associated with large uncertainties. This is particularly true with regard to methane (CH_4), where most studies to date are confined to point measurements and small-scale process studies. These studies delivered important site-specific results and a detailed mechanistic understanding of biological and physical processes and controls governing methane emission, which have partly been converted into process-based models (Cao et al., 1996; Walter and Heimann, 2000; Zhuang et al., 2004). However, often the identified drivers of methane flux are not consistent between different investigation sites and sometimes even contradicting relationships are reported, for example with respect to water levels (Bellisario et al. 1999; Friborg et al., 2000; Zona and Oechel, 2008), thaw depth (Friborg et al., 2000; van Huissteden et al., 2005; Sachs et al., 2008; Wille et al., 2008), or temperature controls (Nakano et al., 2000; Christensen et al., 2001; Hargreaves et al., 2001; Wagner et al., 2003; Wickland et al., 2006). The representation of the known processes on larger scales is highly uncertain due to spatial complexity and heterogeneity, and a comprehensive picture of the Arctic methane budget or of the various interconnected controls and coupled processes operating on different scales and across scales has not yet been proposed. In fact, the significant uncertainties in our current understanding of the Arctic system and in particular of the interactions between biosphere, atmosphere, and cryosphere demonstrate the need for fundamental research to improve our understanding of the complex Earth system dynamics independent from climate feedback concerns.

Detailed understanding of ecosystem functioning on multiple temporal and spatial scales along with comprehensive baseline data is essential for any useful projection into future ecosystem behavior. With regard to future methane emissions, this fundamental understanding includes the ability to project permafrost dynamics, soil moisture, and surface hydrology as the main factors determining the ratio between oxic

and anoxic soil column, the latter of which being a main requirement for methane production by strictly anaerobic methanogenic microbes.

In this dissertation, land-atmosphere interactions and processes controlling the exchange of methane between a wet Arctic tundra ecosystem in Northern Siberia are investigated and some key aspects of the current uncertainties are addressed.

1.2   Objectives of this dissertation

The aim of this study is to broaden our current understanding of land-atmosphere interactions with regard to methane and to identify processes and controls relevant to methane exchange on different spatial scales in the Arctic. Special emphasis is placed on the spatial heterogeneity that is presently limiting our ability to reliably extrapolate results from plot-scale emission measurements to ecosystem-level estimates. However, this study also contributes important baseline data from a region, which is grossly underrepresented in current attempts to quantify and model the terrestrial carbon cycle and it includes the first (Appendix), second (Chapter 4) and currently only published ecosystem-scale methane flux data from the Russian Arctic. This study also contributes two new methods, (1) for flux calculations using closed chamber methods, and (2) for estimating the effect of spatial heterogeneity on eddy covariance data.

More specifically, this dissertation

1. discusses the currently most wide-spread method for flux calculation from enclosure-based concentration data (linear regression) and assesses whether it is appropriate using an extensive data set from four different sites and working groups (Chapter 2).

2. proposes a new exponential regression model for enclosure-based flux calculation (Chapter 2)

3. presents an extensive closed chamber methane flux data set nested in the footprint of eddy covariance measurements and identifies the dominant controls on small-scale methane dynamics (Chapter 3)

4. presents the first eddy covariance methane flux data covering entire growing seasons and identifies the dominant controls on ecosystem-scale methane dynamics (Chapter 4 and Appendix)

5. compares and integrates results from the different scales and scales results from point measurements to the ecosystem scale (Chapter 3)

6. develops a new method based on frequency analysis to estimate the effect of spatial disturbances on eddy covariance data and identify possible emission hot spots and their contribution to ecosystem-scale fluxes (Chapter 5).

Section 1.3 provides an overview of the main components of the methane cycle and of the methods used in this study. Section 1.4 gives an overview of the individual publications and section 1.5 summarizes the author's contribution to each of these publications.

1.3   Present understanding and methods

Methane is a radiatively active trace gas with an atmospheric concentration of $1,774 \pm 1.8$ ppb (2005), a perturbation lifetime of 12 ± 1.8 years, and a global warming potential relative to carbon dioxide of 25 on a 100-year time horizon (IPCC, 2007). Most of the total methane flux into the atmosphere (582 Tg CH_4 year^{-1}) results from anthropogenic sources such as agriculture, natural gas distribution, and landfills. About 40% originate from natural sources with wetlands being the main contributors. The dominant sink of atmospheric methane is oxidation in the troposphere, while stratospheric methane destruction and soils constitute minor sinks (IPCC, 2007). Most of the current uncertainty is associated with the source/sink strength, while the basic processes of methane production and oxidation are well understood.

Methane is produced by methanogenic archaea as the terminal step in the anaerobic decomposition of organic matter. The dominant metabolic pathways in cold environments are the reduction of carbon dioxide to methane using H_2 as a reductant and the fermentation of acetate to methane and carbon dioxide. Methanotrophic bacteria in aerobic soil layers can oxidize a large fraction of the produced methane before it reaches the atmosphere, depending on the dominant transport mechanism at the specific site.

The three mechanisms by which methane can be emitted into the atmosphere are (1) diffusion through soil due to concentration gradients, (2) bubble ebullition from water bodies due to the low solubility of methane in water, and (3) transport through

aerenchyms of vascular plants (Bubier and Moore, 1994; Joabsson and Christensen, 2001). The latter process is the fastest and most important pathway for methane emissions in sedge-dominated ecosystems as it bypasses the oxidation zone in upper soil horizons. Diffusion is slow and most methane transported by diffusion is oxidized before reaching the atmosphere. Convective transport due to pressure differences plays a minor role, and while ebullition can contribute significantly to the net methane emission (Walter et al., 2006), it is a very stochastic process and thus difficult to measure and predict.

Globally, methane emission can be estimated from (1) extrapolation of direct flux measurements, (2) process-based modeling, and (3) inverse modeling from spatially distributed ground, airborne, or satellite observations. Each of these methods requires either good spatial and temporal coverage of ground-truth data or a very solid mechanistic understanding of all relevant processes and their interconnections from the very small-scale processes to large-scale controls.

This dissertation contributes to better coverage of ground data as well as to process understanding on two spatial scales. Methane fluxes were measured directly using two methods relevant to the respective scale, which are described briefly in the following sections.

1.3.1 The closed chamber method

The closed chamber method relies on the concentration change over time of the gas of interest in a closed volume, from which the flux is calculated. Usually, a fixed frame is installed at the investigation site that serves as the base for the chamber. When the chamber is closed and sealed to the base, gas (e.g. methane, carbon dioxide) diffuses into the closed volume. Samples are taken either by syringes or by continuously sampling gas analyzers to monitor the concentration change over time. Most of the work on methane emissions has been conducted using closed chambers (e.g. Whalen and Reeburgh, 1990; Bubier, 1995; Christensen et al., 1995; Reeburgh et al., 1998; Bellisario et al., 1999; Nakano et al., 2000; Wickland et al., 2006; Mastepanov et al., 2008).

The advantages of the closed chamber method include the relatively low costs and the good spatial resolution. However, the method inherently alters the environment

it is used to investigate, and is prone to a variety of errors, which are discussed in more detail in Chapter 2.

1.3.2 The eddy covariance method

The eddy covariance method (EC) is a micrometeorological technique allowing a direct measure of turbulent exchange fluxes between surfaces and the atmosphere (Baldocchi et al. 1988; Foken and Wichura 1996).

Its major advantages include the minimal disturbance of the environment that is investigated and the ability to provide long and continuous time series. It also provides measurements over a relatively large area depending on measurement height, surface roughness conditions and wind speed. However, several important assumptions have to be met, including:

(1) horizontal homogeneity of the surface

(2) atmospheric stationarity during the averaging period (30–60 min)

(3) molecular diffusion is negligible

If these assumptions are met, the vertical exchange flux between a surface and the atmosphere is the covariance of the vertical wind speed w and the concentration of the entity of interest c: $F = \overline{w'c'}$.

Because of the limited frequency response of the measurement instruments and a range of other sources of error, eddy covariance data require sophisticated post-processing and several corrections to compensate for flux losses or violation of basic assumptions. In addition to frequency response corrections, the Webb-Pearman-Leuning (WPL) correction (Webb et al., 1980) is important to compensate for fluctuations of water vapor and temperature, especially in open-path systems. The set-up used in this study, however, did not require the application of a WPL term because the sample gas was dried prior to entering the analyzers and temperature fluctuations were dampened in the trace gas analyzer.

Compared to closed chamber systems, the eddy covariance method is cost-intensive (>100.000 € vs. as low as <1.000 €) and requires several fast-response instruments. To resolve eddies in the atmosphere, every EC system consists of a sonic anemometer for 3D wind observation, which is mounted on a tower of suitable height.

Open-path or closed-path gas analyzers sample air from within few decimeters of the sonic anemometer and a suite of meteorological sensors continuously measures temperature, radiation components, atmospheric pressure, relative humidity and other variables of interest. Closed-path systems capable of measuring methane fluxes currently require generators or line power making their use in remote Arctic regions challenging.

1.4   Overview of the publications

This dissertation consists of four main chapters, each of which constitutes an individual publication, and a short synthesis chapter. A fifth and sixth publication are included in the appendix. The conceptual layout of this study and its specific objectives were formulated in May 2006. From late May through September 2006 eddy covariance and closed chamber measurements were conducted at the Russian-German Research Station Samoylov Island during the expedition LENA 2006 (Boike et al., 2007). The dataset obtained during that expedition forms the basis of this dissertation.

Chapter 2 discusses the traditionally most widely used method for flux calculation from closed chamber concentration data (i.e. linear regression). It is undisputed that the basic underlying principles of the method – if it is applied correctly – do not allow for a linear change of concentration inside the chamber. However, the arguably easier use of linear regression has traditionally been justified by choosing short time spans during which the concentration change appears approximately linear. This approach is tested against alternative models using more than 1760 closed chamber measurements of CO_2 from different German and Finish working groups investigating three boreal peatlands and the wet polygonal tundra site at the center of this dissertation. The linear regression approach was found to not be appropriate. An exponential model developed from theory is proposed for future flux calculations from closed chambers along with several other recommendations.

While chapter 2 focuses on carbon dioxide, the results of this work were found to also apply to methane and therefore, the proposed exponential model is used for the flux calculations in chapter 3. Here, the heterogeneity of small-scale flux data from Samoylov Island is analyzed and the statistically significant controls on methane fluxes on the micro-site scale are identified and discussed. Simple models based on the

identified controls are developed for the high-emission micro-sites and explain most of the variability in measured fluxes. Chapter 3 also introduces and describes the study site on Samoylov Island in detail and thoroughly discusses the processes involved in the methane cycle. The results are compared to the ecosystem-scale, differences are discussed, and a first attempt at up-scaling small-scale fluxes from closed chambers to ecosystem-scale eddy covariance fluxes based on area-weighted contributions from different surface classes obtained from aerial imagery is included.

The ecosystem-scale measurements by eddy covariance are presented in chapter 4. Similar to chapter 3 but with different approaches, the relevant environmental controls, which differ very clearly from those dominating on the small scale, are identified and the processes governing methane fluxes on the ecosystem scale are discussed. A simple model originally proposed in another publication (included in the appendix) and further developed here is able to reproduce the flux time series adequately and explain most of its variability.

In chapter 5 the effect of the spatial heterogeneity shown in chapter 3 and 4 on the eddy covariance time series data is investigated in detail and a new method is developed for estimating the spatially inhomogeneous contributions to ecosystem-scale methane flux. This chapter presents very recent work and constitutes a proof of concept. The proposed method is still under further development and now needs to be generalized and refined by the wider scientific community. If proven beyond the case study in chapter 5, this method may have the potential to become a widely used tool in ecosystem flux research.

In chapter 6, a brief synthesis summarizes the results of the individual chapters and integrates them into the broader context.

The appendix includes an additional publication similar to that in chapter 4 but for earlier data. However, both the study site and the applied methods are the same as those in chapter 4, resulting in strong similarities between these two publications. The publication in chapter 4 builds on this work and further develops the proposed model. The second publication in the appendix is an earlier version of chapter 3 and was prepared for the conference proceedings of the Ninth International Conference on Permafrost in Fairbanks, Alaska.

1.5   The author's contribution to the individual papers

- **Paper 1 (Chapter 2)**: The original idea was born out of unsatisfactory performance of the traditional linear regression flux calculations when applied to data collected during earlier fieldwork. Lars Kutzbach and I initially developed the Matlab Code together until I left for the 2006 field season. The Samoylov closed chamber data set was produced by Michael Giebels under my supervision and guidance in the field. Lars Kutzbach, Michael Giebels and I were involved in data processing, analysis, and interpretation for the Samoylov site, which the other co-authors did for their respective data sets. Lars Kutzbach had the lead in the overall effort and drafted the manuscript, to which all co-authors contributed in several internal revisions and discussions.

- **Paper 2 (Chapter 3)**: I reviewed the relevant literature, did the analyses and wrote the entire manuscript. Michael Giebels did the closed chamber measurements on Samoylov Island and some of the raw data processing based on chapter 2 under my supervision and guidance. All authors critically reviewed and discussed earlier drafts of the manuscript, and Lars Kutzbach and Julia Boike guided the whole process.

- **Paper 3 (Chapter 4)**: I did the entire fieldwork, prepared the relevant literature review, did all analyses, interpreted the data and wrote the entire manuscript. Christian Wille and Lars Kutzbach originally did the relevant EdiRe coding for raw data processing, which I updated and adapted to the data set under their guidance. Christian Wille also introduced me to the technical details of operating the eddy covariance system in the field. Lars Kutzbach and Julia Boike guided me in the whole process and all authors critically reviewed the earlier drafts of the manuscript and contributed in discussions and editing.

- **Paper 4 (Chapter 5)**: I initiated the collaboration with ETHZ and wrote the proposal for the project (funded by DAAD). My initial idea was jointly modified and further developed in close collaboration with Werner Eugster, who also introduced me to the statistical programming language R and time series / frequency analysis. I did the relevant coding under his guidance and with occasional help

where necessary. I wrote the entire manuscript and Werner Eugster contributed in discussions, reviews, and editing.

- **Paper 5 (Appendix)**: Christian Wille and Lars Kutzbach did the relevant fieldwork, raw data processing, all analyses, and most of the interpretation of the flux data. Eva-Maria Pfeiffer provided guidance and resources. Christian Wille had the lead on the manuscript for which I did part of the literature review and writing. All authors contributed to discussing and interpreting the results.

- **Paper 6 (Appendix)**: I reviewed the relevant literature, did the analyses and wrote the entire manuscript. Michael Giebels did the closed chamber measurements on Samoylov Island and some of the raw data processing based on chapter 2 under my supervision and guidance. All authors critically reviewed and discussed earlier drafts of the manuscript, and Lars Kutzbach and Julia Boike guided the whole process.

2. CO$_2$ FLUX DETERMINATION BY CLOSED-CHAMBER METHODS CAN BE SERIOUSLY BIASED BY INAPPROPRIATE APPLICATION OF LINEAR REGRESSION

Lars Kutzbach   Julia Schneider   Torsten Sachs   Michael Giebels

Hannu Nykänen   Narasinha J. Shurpali   Pertti J. Martikainen

Jukka Alm   Martin Wilmking

Abstract

Closed (non-steady state) chambers are widely used for quantifying carbon dioxide (CO$_2$) fluxes between soils or low-stature canopies and the atmosphere. It is well recognised that covering a soil or vegetation by a closed chamber inherently disturbs the natural CO$_2$ fluxes by altering the concentration gradients between the soil, the vegetation and the overlying air. Thus, the driving factors of CO$_2$ fluxes are not constant during the closed chamber experiment, and no linear increase or decrease of CO$_2$ concentration over time within the chamber headspace can be expected. Nevertheless, linear regression has been applied for calculating CO$_2$ fluxes in many recent, partly influential, studies. This approach has been justified by keeping the

closure time short and assuming the concentration change over time to be in the linear range. Here, we test if the application of linear regression is really appropriate for estimating CO_2 fluxes using closed chambers over short closure times and if the application of nonlinear regression is necessary. We developed a nonlinear exponential regression model from diffusion and photosynthesis theory. This exponential model was tested with four different datasets of CO_2 flux measurements (total number: 1764) conducted at three peatlands sites in Finland and a tundra site in Siberia. Thorough analyses of residuals demonstrated that linear regression was frequently not appropriate for the determination of CO_2 fluxes by closed-chamber methods, even if closure times were kept short. The developed exponential model was well suited for nonlinear regression of the concentration over time $c(t)$ evolution in the chamber headspace and estimation of the initial CO_2 fluxes at closure time for the majority of experiments. However, a rather large percentage of the exponential regression functions showed curvatures not consistent with the theoretical model which is considered to be caused by violations of the underlying model assumptions. Especially the effects of turbulence and pressure disturbances by the chamber deployment are suspected to have caused unexplainable curvatures. CO_2 flux estimates by linear regression can be as low as 40% of the flux estimates of exponential regression for closure times of only two minutes. The degree of underestimation increased with increasing CO_2 flux strength and was dependent on soil and vegetation conditions which can disturb not only the quantitative but also the qualitative evaluation of CO_2 flux dynamics. The underestimation effect by linear regression was observed to be different for CO_2 uptake and release situations which can lead to stronger bias in the daily, seasonal and annual CO_2 balances than in the individual fluxes. To avoid serious bias of CO_2 flux estimates based on closed chamber experiments, we suggest further tests using published datasets and recommend the use of nonlinear regression models for future closed chamber studies.

2.1 Introduction

Accurate measurements of carbon dioxide (CO_2) fluxes between soils, vegetation and the atmosphere are a prerequisite for the quantification and understanding of the carbon source or sink strengths of ecosystems and, ultimately, for the development of a global carbon balance. A number of different approaches are used to determine CO_2 exchange

fluxes between ecosystems and the atmosphere, each with its own advantages and limitations. These approaches include micrometeorological methods such as eddy covariance or gradient techniques which are employed on towers or aircrafts, diffusion modelling for bodies of water, and measurements using open (steady state) or closed (non-steady state) chambers (e.g. Matson and Harriss, 1995; Norman et al., 1997).

The closed chamber method is the most widely used approach to measure the CO_2 efflux from bare soil surfaces (e.g. Jensen et al., 1996; Xu and Qi, 2001; Pumpanen et al., 2003, 2004; Reth et al., 2005; Wang et al., 2006). Also, it is often applied to quantify the net CO_2 exchange between the atmosphere and low-stature canopies typical for tundra (Vourlites et al., 1993; Christensen et al., 1998; Oechel et al., 1993, 1998, 2000; Zamolodchikov and Karelin, 2001), peatlands (Alm et al., 1997, 2007; Tuittila et al., 1999; Bubier et al., 2002; Nykänen et al., 2003; Burrows et al., 2004; Drösler, 2005; Laine et al., 2006), forest understorey vegetation (Goulden and Crill, 1997; Heijmans et al., 2004) and agricultural crop stands (Dugas et al., 1997; Wagner et al., 1997; Maljanen et al., 2001; Steduto et al., 2002). Advantageously, the closed-chamber method is relatively low in cost and power consumption, simple to operate and can therefore be used in remote, logistically difficult areas. On the other hand, it is prone to a variety of potential errors (Livingston and Hutchinson, 1995; Welles et al., 2001; Davidson et al., 2002) which the investigator has to consider and to minimise by careful experiment planning and chamber design. Sources of errors are (1) inaccurate determination of the headspace volume (Livingston and Hutchinson, 1995), (2) leakage directly at the chamber components or via the underlying soil pore space (Hutchinson and Livingston, 2001; Livingston et al., 2006), (3) temperature changes of the soil and the atmosphere beneath the chamber (Wagner and Reicosky, 1992; Drösler, 2005), (4) artificial water vapour accumulation which depletes the CO_2 concentration and might influence the stomata regulation of plants (Welles et al., 2001), (5) disturbance of pressure gradients across the soil-atmosphere interface by soil compression or insufficient pressure relief during chamber setting (Hutchinson and Livingston, 2001; Livingston et al., 2006), (6) suppression of the natural pressure fluctuations (Hutchinson and Mosier, 1981; Conen and Smith, 1998; Hutchinson and Livingston, 2001), (7) alteration or even elimination of advection and turbulence and thus modification of the diffusion resistance of the soil- or plant-atmosphere boundary layer (Hanson et al.,

1993; Le Dantec et al., 1999, Hutchinson et al., 2000; Denmead and Reicosky, 2003; Reicosky, 2003), and (8) the concentration build-up or reduction within the chamber headspace that inherently disturbs the underlying concentration gradients that were in effect prior to chamber deployment (e.g. Matthias et al., 1978; Hutchinson et al., 2000; Livingston et al., 2006). This study focuses on the latter problem, which can lead to serious bias of CO_2 fluxes if not accounted for, even if all other potential errors were kept at minimum.

The closed chamber methodology estimates the CO_2 fluxes by analysing the rates of CO_2 accumulation or depletion in the chamber headspace over time. However, every change of the CO_2 concentration from the normal ambient conditions feeds back on the CO_2 fluxes by altering the concentration gradients between the soil or the plant tissues and the surrounding air. In other words, the measurement method itself alters the measurand. Thus, for assessing the predeployment CO_2 flux, the rate of initial concentration change at the moment of deployment ($t=t_0=0$) should be used when the alteration of the concentration gradients in soils and plant tissues is minimal, rather than the mean rate of the CO_2 concentration change over the chamber closure period (Livingston and Hutchinson, 1995).

The nonlinear nature of the gas concentration evolution over time in closed chambers has been recognised and discussed early and at length in the history of chamber-based gas flux measurements. However, most studies concerning this issue were conducted for the gas exchange of bare soil surfaces. Matthias et al. (1978) showed for numerical simulations of closed chamber experiments with closure times of 20 min that N_2O emissions could be underestimated by as much as 55% by linear regression. Quadratic regression still underestimated the real fluxes by up to 25%. An exponential function developed from simplified diffusion theory was best suited for the flux estimate with underestimation of the fluxes of maximal 11%. In the following years, further theoretical and numerical studies came to the same conclusion that the use of linear regression can lead to serious underestimation of gas fluxes between soils and atmosphere (Hutchinson and Mosier, 1981; Healy et al., 1996; Hutchinson et al., 2000; Pedersen, 2000; Pedersen et al., 2001; Welles et al., 2001; Hutchinson and Livingston, 2001). The serious underestimation bias of the linear regression method as predicted by the theoretical and numerical studies was confirmed by Nakano et al. (2004) by

measurements of CO_2 release and CH_4 consumption from soils under actual field conditions. Recently, Livingston et al. (2005, 2006) introduced the so-called nonsteady-state diffusive flux estimator (NDFE) function which is derived from time dependent diffusion theory and can be fitted by nonlinear regression to gas concentration over time data from closed chamber experiments. They demonstrated for numerical model simulations that only the NDFE model was able to accurately determine the predeployment gas fluxes whereas quadratic and also exponential regression still underestimated them. However, the NDFE model is restricted to gas sources in bare soils whereas vegetation and gas sinks are not considered. Only few researchers have applied nonlinear models to determine CO_2 exchange fluxes on vegetated surfaces (Dugas et al., 1997; Wagner et al., 1997; Steduto et al., 2002). The mentioned scientists used the quadratic model proposed by Wagner et al. (1997) which accounts for nonlinear disturbances by the chamber deployment but is not based on the underlying physiology and diffusion physics. Wagner et al. (1997) demonstrated for the CO_2 exchange of different agricultural crop stands that 60% to 100% of all chamber experiments were significantly nonlinear. Even with a short closure time of 60 s, fluxes derived from quadratic regression were 10% to 40% greater than those calculated with linear regression.

Despite the growing evidence against the use of a linear model for the determination of gas fluxes using closed chambers, most of the recent studies on the CO_2 balance of vegetated surfaces and many studies on the CO_2 efflux from bare soil have applied linear regression for estimating CO_2 fluxes (e.g. Vourlites et al., 1993; Oechel et al., 1993, 1998, 2000; Jensen et al., 1996; Alm et al., 1997, 2007; Goulden and Crill, 1997; Christensen et al., 1998; Tuittila et al., 1999; Maljanen et al., 2001; Xu and Qi, 2001; Bubier et al., 2002; Nykänen et al., 2003; Pumpanen et al., 2003; Burrows et al., 2004; Heijmans et al., 2004; Drösler, 2005; Reth et al., 2005; Laine et al., 2006; Wang et al., 2006). Usually, the authors justify the use of linear regression by keeping the closure time short and assuming the concentration change over time to be still in the linear range.

Here, we investigate if the application of linear regression is really appropriate for estimating CO_2 fluxes from bare or vegetated soils using closed chambers with short closure times or if it is necessary to apply a nonlinear model. The performance of the

linear model can be evaluated by comparing its results with the results of nonlinear models developed from biophysical theory. For bare and approximately homogenous soils, we consider nonlinear regression of the NDFE function of Livingston et al. (2005, 2006) as the most advanced approach. However, the extension of this physically-based model of non-steady state diffusion through homogenous soils to the situation of vegetated and substantially heterogeneous soils does not appear feasible to us. Therefore, we develop a conceptual, explicitly simplified biophysical model to include both soils and vegetation processes. The main purpose of this model is to evaluate which type of nonlinear function can be expected to adequately describe the evolution of CO_2 concentrations within closed chambers deployed on vegetated and bare soils. We adopt the exponential model of Matthias et al. (1978) for trace gas efflux from bare soils, which is based on simplified diffusion theory, and expand it for sites with low-stature vegetation. For this purpose, the effect of changing CO_2 concentrations on photosynthesis has to be added to the model.

The developed nonlinear exponential model is tested against the linear model and the quadratic model proposed by Wagner et al. (1997) with four datasets of CO_2 flux measurements (total number = 1764) conducted by four separate working groups at two vegetated boreal peatlands, one vegetated tundra, and one non-vegetated boreal peat excavation site. Furthermore, the exponential model was tested against the NDFE model of Livingston et al. (2005, 2006) using the dataset from the non-vegetated peat excavation site.

The major questions of the test experiment were:

1. How well do the empirical linear and quadratic functions (f_{lin} and f_{qua}) as well as the theory-based exponential and NDFE functions (f_{exp}, f_{NDFE}) describe the chamber CO_2 concentration evolution data from real measurements?

2. Are the linear and quadratic model functions (f_{lin} and f_{qua}) sufficient approximations of the exponential model for the specific experiment set-ups, particularly for short chamber closure times?

3. Is the NDFE function (f_{NDFE}) better fitted to the chamber CO_2 data from the non-vegetated peat excavation site than the exponential function (f_{exp})?
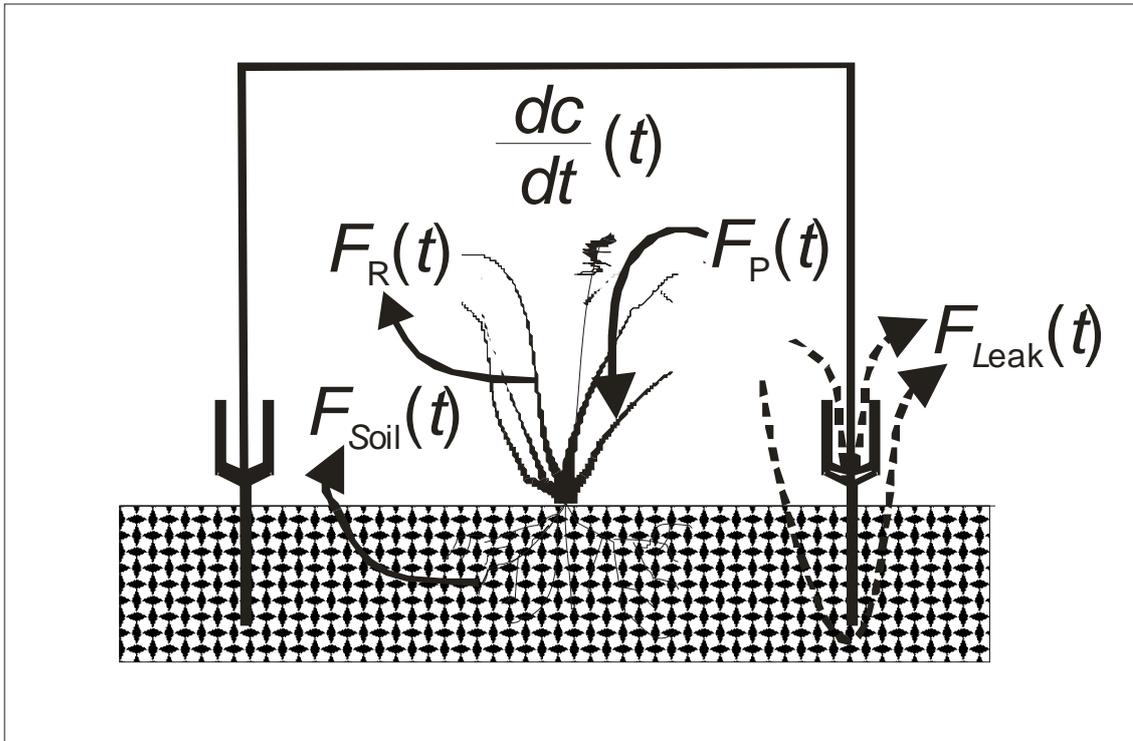
Figure 2.1: Schematic of the CO_2 fluxes in the chamber headspace which make up to the net CO_2 flux F_{net} (details in the text, Eq. (1)). $F_{Soil}(t)$ is the diffusive efflux from the soil, $F_P(t)$ is photosynthesis, $F_R(t)$ is aboveground plant respiration, $F_{Leak}(t)$ is leak flux. $dc/dt(t)$ is the CO_2 concentration change over time t in the chamber headspace.

4. Do the initial slopes $f'(t)$ of the different functions ($f_{lin}, f_{qua}, f_{exp}, f_{NDFE}$), which are directly proportional to the calculated initial CO_2 net fluxes $F_{net}(t_0)$, deviate significantly from each other?

2.2   Development of the nonlinear exponential model

Presuming that the chamber experiment itself alters the measurand, namely the CO_2 flux, a nonlinear evolution of the CO_2 concentration in the chamber headspace must be expected. In the following, a conceptual model based on simplified biophysical theory is developed which shall reflect this nonlinear CO_2 concentration evolution as affected by the main relevant processes which contribute to the net CO_2 flux into or from the chamber headspace. The considered processes are (1) diffusion from the soil, (2) photosynthesis of the plants, (3) respiration of the plants and (4) diffusion from the

headspace to the surrounding atmosphere by leaks at the chamber or through the soil (Fig. 2.1).

The model presented here is based on the assumption that all other potential errors of the closed chamber approach which are not connected to the inherent concentration changes in the closed chamber headspace are negligible thanks to careful experiment planning. This means that during chamber deployment, soil and headspace air temperature, photosynthetically active radiation, air pressure and headspace turbulence are assumed to be constant and approximately equal to ambient conditions. When covering a vegetated soil surface with a closed chamber, the CO_2 concentration change over time in the chamber headspace is the net effect of several individual processes with partly opposing directions (Fig. 2.1). CO_2 is added to or removed from the headspace by different processes at different interface surfaces. The headspace is isolated from the surrounding atmosphere by the chamber walls. Here, relevant CO_2 flux is only possible through leaks (F_{Leak}) which should be avoided but often cannot be ruled out completely. Of course, the headspace is open to the soil surface where CO_2 efflux from the soil (F_{Soil}) to the overlying air takes place. Inside the headspace, plants photosynthesise and respire, meaning CO_2 removal (F_P) from or CO_2 supply (F_R) to the headspace air, respectively. The sum of all CO_2 fluxes into or out of the headspace represents the net CO_2 flux (F_{net}) which can be estimated by the change of the CO_2 concentration over time dc/dt (t) during chamber closure. The sign convention of this study is that fluxes are defined positive when adding CO_2 to the chamber headspace and negative when removing CO_2 from the chamber headspace.

The net CO_2 flux $F_{net}(t)$, which in effect drives the CO_2 concentration change in the chamber headspace over time dc/dt (t), can be written as:

$$F_{net}(t) \;=\; \frac{dc}{dt}(t)\,\frac{p\,V}{R\,T\,A} \;=\; F_{Soil}(t) + F_P(t) + F_R(t) + F_{Leak}(t) \tag{1}$$

where p is air pressure, R is the ideal gas constant, and T is the temperature (in Kelvin). V and A are the volume and the basal area of the chamber, respectively. $F_{Soil}(t)$ is the CO_2 efflux from the soil which originates from the respiration of soil microbes, soil animals and belowground biomass of plants, i.e. roots and rhizomes, $F_P(t)$ is the CO_2

flux associated with the gross photosynthesis of the plants, $F_R(t)$ is the CO_2 flux associated with the dark respiration of the aboveground biomass, and $F_{Leak}(t)$ is the CO_2 flux related to leakage directly at the chamber components or via the soil pore space. These individual process-associated fluxes have to be considered as not constant but more or less variable over time during the chamber deployment. This is due to the direct dependency of some of the individual fluxes on the CO_2 concentration in the headspace which is changing over time.

By reorganising Eq. (1), the concentration change in the chamber headspace over time dc/dt (t), can be written as:

$$\frac{dc}{dt}(t) = \left[F_{Soil}(t) + F_P(t) + F_R(t) + F_{Leak}(t) \right] \frac{R\,T\,A}{p\,V} \tag{2}$$

The CO_2 efflux from the soil to the headspace air $F_{Soil}(t)$ is considered to be mainly driven by molecular diffusion between the CO_2-enriched soil pore space and the headspace air and can be modelled following Matthias et al. (1978), Hutchinson and Mosier (1981) and Pedersen (2000) as:

$$F_{Soil}(t) \quad = \quad D \frac{\left[c_d - c(t) \right]}{d} \frac{p\,V}{R\,T\,A} \tag{3}$$

where D is the soil CO_2 diffusivity, c_d is the CO_2 concentration at some unknown depth d below the surface where the CO_2 concentration is constant and not influenced by the chamber deployment. $c(t)$ is the CO_2 concentration of the headspace air which is assumed equal to the CO_2 concentration at the soil surface, which has to be ensured by adequate mixing of the headspace air.

While the nonlinear models of F_{Soil} over the chamber closure time by the above-mentioned authors are well-accepted and frequently applied, the effect of the CO_2 concentration changes in the chamber headspace on the photosynthesis of enclosed vegetation has not been given much attention. However, this effect can be expected to be substantial considering the underlying enzyme kinetics of photosynthesis whose main substrate is CO_2.

As photosynthesis is limited either by the electron transport rate at the chloroplast, which is dependent on irradiation, or the activity of Rubisco, which is mainly dependent on the intercellular CO_2 concentration (Farquhar et al., 1980), F_P can be either strongly dependent on or nearly independent of changes of the headspace CO_2 concentration $c(t)$ depending on the irradiation level. The complex dependence of photosynthetic activity on irradiation and CO_2 concentration which is reflected in full detail by the model of Farquhar et al. (1980) must and can be strongly simplified for our approach. Under non-irradiation-limited conditions, the photosynthesis of C3 plants and mosses is considered to correlate approximately linearly with the ambient CO_2 concentration at CO_2 concentrations between 300 ppm and 400 ppm. This has been shown by several previous studies (Morison and Gifford, 1983; Grulke et al., 1990; Stitt, 1991; Sage, 1994; Luo et al., 1996; Luo and Mooney, 1996; Williams and Flanagan, 1998; Griffin and Luo, 1999). Consequently, $F_P(t)$ can be modelled for periods with nonirradiation-limited photosynthesis of a canopy consisting of C3 plants and/or mosses, which is typical for tundra and peatlands, as:

$$F_P(t) \quad = \quad k_P \, c(t) \frac{p \, V}{R \, T \, A} \tag{4}$$

where k_p is the constant of proportionality of the approximately linear relationship between CO_2 concentration and photosynthesis-associated flux.

On the other hand, $F_P(t)$ is not a function of $c(t)$ but invariant with changing $c(t)$ if photosynthesis is limited by the irradiation – consequently also during dark conditions – or if the canopy consists mainly of C4 plants. Thus, if the other environmental controls such as irradiation, temperature or air moisture can be assumed constant, $F_P(t)$ can be defined as:

$$F_P(t) \quad = \quad F_P(t_0) \tag{5}$$

where t_0 is t=0.

As the effect of ambient CO_2 concentration changes on dark respiration has been shown to be very low or none (Grulke et al., 1990; Drake et al., 1999; Amthor, 2000;

Tjoelker et al., 2001; Smart, 2004; Bunce, 2005), $CO2$ flux associated with the dark respiration of aboveground biomass $F_R(t)$ is considered invariant with changing $c(t)$ in a considered CO_2 concentration range of 200 ppm to 500 ppm. Thus, if the other environmental controls such as temperature or air moisture can be assumed constant, $F_R(t)$ can be defined as:

$$F_R(t) \quad = \quad F_R(t_0)$$
(6)

As leakage often cannot be ruled out completely, CO_2 flux associated with potential leakages $F_{Leak}(t)$ should be integrated into the model. $F_{Leak}(t)$ is considered to be driven by diffusive transport and can therefore be modelled similarly to $F_{Soil}(t)$:

$$F_{Leak}(t) \quad = \quad \left\{ D_{Chamber} \frac{[c_a - c(t)]}{d_{Chamber}} + D_{Soil} \frac{[c_a - c(t)]}{d_{Soil}} \right\} \frac{p V}{R T A} \quad = \quad K_{Leak} [c_a - c(t)] \frac{p V}{R T A}$$

(7)

where $D_{chamber}$ is the mean diffusivity of leaks directly at the chamber components, $d_{chamber}$ is the distance between headspace and the surrounding air, D_{Soil} is the mean diffusivity of leaks by air-filled soil pore space, and d_{Soil} is the distance between the headspace and the surrounding air via the air-filled soil pore space. K_{Leak} is a constant which combines $D_{chamber}$, $d_{chamber}$, D_{Soil}, and d_{soil} and indicates leakage strength. c_a is the CO_2 concentration in the air outside of the chamber which is considered well-mixed and therefore constant during chamber deployment.

For situations with non-irradiation-limited photosynthesis, the concentration change in the chamber headspace over time dc/dt (t) can be derived by inserting the Eqs. (3), (4), (6) and (7) into Eq. (2):

$$\frac{dc}{dt}(t) \quad = \quad D \frac{[c_d - c(t)]}{d} + k_P\, c(t) + F_R(t_0) \frac{R T A}{p V} + K_{Leak} [c_a - c(t)]$$
(8)

which can be reorganised to

$$\frac{dc}{dt}(t) = \left[\frac{D}{d}c_d + F_R(t_0)\frac{R\,T\,A}{p\,V} + K_{Leak}\,c_a\right] + \left[-\frac{D}{d} + k_P - K_{Leak}\right]c(t) \qquad (9)$$

This differential equation expresses mathematically the previously emphasised fact that the measurement method itself alters the measurand. The measurand dc/dt (t) is altered by the change of the headspace concentration $c(t)$ which is forced by the chamber deployment to determine dc/dt (t). The differential equation Eq. (9) is solved by computing its indefinite integral:

$$c(t) = -\frac{\left[\dfrac{D}{d}c_d + F_R(t_0)\dfrac{R\,T\,A}{p\,V} + K_{Leak}\,c_a\right]}{\left[-\dfrac{D}{d} + k_P - K_{Leak}\right]} + \exp\left[\left(-\frac{D}{d} + k_P - K_{Leak}\right)t\right]B \qquad (10)$$

where B is the integral constant.

For situations with irradiation-limited photosynthesis, the concentration change in the chamber headspace over time dc/dt (t) can be derived by inserting the Eqs. (3), (5), (6) and (7) into Eq. (2):

$$\frac{dc}{dt}(t) = D\frac{[c_d - c(t)]}{d} + [F_P(t_0) + F_R(t_0)]\frac{R\,T\,A}{p\,V} + K_{Leak}[c_a - c(t)] \qquad (11)$$

which can be reorganised to:

$$\frac{dc}{dt}(t) = \left\{\frac{D}{d}c_d + F[_P(t_0) + F_R(t_0)]\frac{R\,T\,A}{p\,V} + K_{Leak}\,c_a\right\} + \left(-\frac{D}{d} - K_{Leak}\right)c(t) \qquad (12)$$

This differential equation is solved by computing its indefinite integral:

$$c(t) = -\frac{\left\{\dfrac{D}{d}c_d + [F_P(t_0) + F_R(t_0)]\dfrac{R\,T\,A}{p\,V} + K_{Leak}\,c_a\right\}}{\left(-\dfrac{D}{d} - K_{Leak}\right)} + \exp\left[\left(-\frac{D}{d} - K_{Leak}\right)t\right]B \qquad (13)$$

where B is the integral constant.

For both situations, with non-irradiation-limited photosynthesis and with irradiation-limited photosynthesis, the evolution of $c(t)$ over time as given by Eq. (10) and Eq. (13), respectively, can be described and fitted by an exponential function $f_{exp}(t)$ of the form:

$$c(t) = f_{exp}(t) + \varepsilon(t) = p_1 + p_2 \exp(p_3\, t) + \varepsilon(t) \tag{14}$$

where $\varepsilon(t)$ is the residual error at a specific measurement time t. The parameters p_1 and p_3 have different meanings for each situation. For the situation with non-irradiation-limited photosynthesis, p_1 is given by

$$p_1 = -\frac{\left[\dfrac{D}{d}\, c_d + F_R(t_0)\dfrac{R\,T\,A}{p\,V} + K_{Leak}\, c_a\right]}{\left(-\dfrac{D}{d} + k_P - K_{Leak}\right)} \tag{15}$$

and p_3 is given by

$$p_3 = \left(-\frac{D}{d} + k_P - K_{Leak}\right) \tag{16}$$

For the situation with irradiation-limited photosynthesis, p_1 is given by

$$p_1 = -\frac{\left\{\dfrac{D}{d}\, c_d + [F_P(t_0) + F_R(t_0)]\dfrac{R\,T\,A}{p\,V} + K_{Leak}\, c_a\right\}}{\left(-\dfrac{D}{d} - K_{Leak}\right)} \tag{17}$$

and p_3 is given by

$$p_3 = \left(-\frac{D}{d} - K_{\text{Leak}} \right) \tag{18}$$

For both situations, p_2 is equal to the integral constant B of the solution of the respective differential equation:

$$p_2 = B \tag{19}$$

As shown clearly by Eqs. (15) to (19), the parameters of the exponential model p_1, p_2, and p_3 cannot directly be interpreted physiologically or physically since they represent a mathematical combination of several physiological and physical parameters of the investigated soil-vegetation system and the applied closed chamber technique. However, the given derivation demonstrates that an exponential or near-exponential form of the regression model should be applicable for describing the evolution of $c(t)$ over time in the chamber headspace. The initial slope of the exponential regression curve $f'_{\text{exp}}(t_0)=(p_2\,p_3)$ can be used to estimate the CO_2 flux rate at the beginning of the chamber deployment $F_{\text{net}}(t_0)$, which is considered to be the best estimator of the net CO_2 exchange flux under undisturbed conditions:

$$F_{\text{net}}(t_0) = \frac{dc}{dt}(t_0) \frac{p\,V}{R\,T\,A} = f'_{\text{exp}}(t_0) \frac{p\,V}{R\,T\,A} = p_2\,p_3\,\frac{p\,V}{R\,T\,A} \tag{20}$$

Regarding the results of Matthias et al. (1978) and Livingston et al. (2006), nonlinear regression of the exponential function to the $c(t)$ data is still likely to underestimate the predeployment fluxes. However, we consider the application of exponential regression as the most accurate approach which is practicable at all when measuring CO_2 fluxes from complex vegetation-soil systems.

2.3   Least squares regression of model functions

The evolution of the CO_2 concentration in the chamber headspace $c(t)$ over time was analysed by fitting the following model functions to the experimental data: (1) the exponential model function $f_{\text{exp}}(t)$ developed in Chapter 2, (2) a quadratic model function $f_{\text{qua}}(t)$ as proposed previously by Wagner et al. (1997), (3) the linear model

function $f_{lin}(t)$, which was used in many other studies and (4) the NDFE function proposed by Livingston et al. (2006) only for the non-vegetated peat excavation site Linnansuo. The quadratic model function has the form:

$$c(t) \;=\; f_{exp}(t) + \varepsilon(t) \;=\; a + b\,t + c\,t^2 + \varepsilon(t) \tag{21}$$

where a, b, and c are the fit parameters of the second-order polynomial. The linear model function has the form:

$$c(t) \;=\; f_{exp}(t) + \varepsilon(t) \;=\; a + b\,t + \varepsilon(t) \tag{22}$$

The NDFE function has the form:

$$c(t) \;=\; f_{NDFE}(t) + \varepsilon(t) \;=\; c_0 + f_0\,\tau\left(\frac{A}{V}\right)\left[\frac{2}{\sqrt{\pi}}\sqrt{t/\tau} + \exp\left(t/\tau\right)erfc\left(\sqrt{t/\tau}\right) - 1\right] + \varepsilon(t)$$
$$\tag{23}$$

where c_0 and f_0 represent initial chamber headspace CO_2 concentrations and initial CO_2 flux at $t_0 = 0$, the time constant τ is an indicator of how fast the concentration gradient of the gas in the soil responds to changes in chamber CO_2 concentration (Livingston et al., 2005, 2006).

The parameters of the best-fitted functions were estimated by least-squares regression, i.e. by minimizing the sum of the squared residuals between the observed data and their fitted values. Both, the nonlinear and the linear regressions were conducted with an iterative Gauss-Newton algorithm with Levenberg-Marquardt modifications for global convergence (function *nlinfit* of the Statistics Toolbox of MATLAB® Version 7.1.0.246 (R14)).

The parameters of the exponential and quadratic regression functions (Eqs. 20, 21) can only be interpreted by the theoretical model if the curves are convex, i.e. if the absolute value of the slope of the $c(t)$ curve is decreasing with time. However, the parameter estimations of the exponential and quadratic regressions were not restricted

to such curvatures only, thus allowing for the detection of clearly nonlinear $c(t)$ curves with curvatures not explainable by the theoretical model. Curves with such "unexplainable" curvatures were separated after the fitting procedure. The parameters of the NDFE model were restricted to positive values as was done also by Livingston et al. (2006).

2.4   Statistical evaluation and comparison of different models

The first step to test the theory-based models f_{exp} and f_{NDFE} with respect to their ability to describe the $c(t)$ evolution within the chambers was to check if the curvatures of the quadratic f_{qua} and exponential f_{exp} regression functions were consistent with the theoretical considerations (see Sect. 3). Curves with the absolute values of the slopes increasing with time are neither explainable by the exponential model developed in this study nor by the NDFE model of Livingston et al. (2006). They were considered to be caused by violations of the basic assumptions of the developed theoretical models, which means that one of the factors soil temperature, headspace air temperature, photosynthetically active radiation, the pressure gradient across the soil-atmosphere interface or the headspace turbulence were apparently neither constant nor approximately equal to ambient conditions. Then, the different regression functions f_{lin}, f_{qua}, f_{exp}, f_{NDFE} were evaluated by thorough analyses of residuals. These analyses included the *Durbin-Watson* test for autocorrelation and the *D'Agostino-Pearson* test for normality of the residuals (Durbin andWatson, 1950; D'Agostino, 1971). Furthermore, the goodness of fit of the different regression functions was compared using the adjusted nonlinear coefficient of determination R^2_{adj} (Rawlings et al., 1998), the *Akaike* information criterion AIC_c (with small sample second order bias correction; Burnham and Anderson, 2004) and an F-test of the residual variances of two compared regression functions (Fisher, 1924).

Autocorrelation of the residuals would indicate that the fitted model does not reflect all important processes governing the $c(t)$ evolution over time. Indeed, autocorrelation of the residuals is a very sensitive indicator of a too simple model. With significantly autocorrelated residuals, the least-squares estimators would no longer be the best estimators of the function parameters (violation of the third *Gauss-Markov* assumption). Also the variance (error) estimators of the parameters would be seriously

biased (Durbin and Watson, 1950; Rawlings et al., 1998). That means that autocorrelation must be removed (by data reduction) before correct estimations of the errors of the regression parameters and consequently also of the errors of the flux estimates are possible. For the $c(t)$ evolution data from the closed chamber experiments, checking for autocorrelation becomes particularly important since these data represent time series which are often susceptible to residual autocorrelation. The assumption of normality of the residuals has to be valid for tests of significance and construction of confidence intervals for the regression function (Rawlings et al., 1998). For the $c(t)$ data, the *D'Agostino-Pearson* test is a stricter test for normality than the often used Kolmogorov-Smirnov test, which has to be considered outdated (D'Agostino, 1986). A well-fitted model should neither show autocorrelation nor non-normality of the residuals. Thus, in our case, if autocorrelation and/or non-normality of the residuals are found to be more serious for f_{lin} or f_{qua} compared to f_{exp}, this would indicate that the respective function would be less appropriate for modelling the measurement data than f_{exp}.

The question whether the initial slopes $f'(t_0)$ of two different regression functions deviate significantly from each other was then evaluated by plotting them against each other as x-y scatter diagrams. The differences between the absolute values of $f'(t_0)$ of two regression functions were separated by their sign and tested for their significance by one-tailed *Student's* t-tests following Potthoff (1965, cited in Sachs, 1992). The error estimates of the initial slopes were determined after removing autocorrelation by block-averaging the data. The necessary data number for block averages were automatically adjusted to the degree of observed autocorrelation by a routine included in the applied MATLAB® regression program. The error estimates of the initial slope of the exponential function were derived by fitting a Taylor power series expansion of 17th order to the data whose curve form and initial slope is practically identical with the original exponential function. Advantageously, the power series expansion is more resistant against overparameterisation than the exponential function and directly estimates the initial slope of the $c(t)$ curve as one of its fit parameters which results in lower error estimates for the initial slopes.

2.5   Field measurements

2.5.1 Investigation sites

The closed chamber experiments were conducted at three peatland sites in Finland (Salmisuo, Vaisjeäggi, Linnansuo) and one tundra site in Siberia (Samoylov) by four separate working groups. Salmisuo is a pristine oligotrophic lowsedge-pine fen and is located in eastern Finland (62°46'N, 30°58'E) in the boreal zone. A total of twelve plots were established in different microsite types: four in flarks, four in lawns, and four in hummocks. The hummocks are elevated above the surrounding area and represent the driest conditions. They are covered by *Sphagnum fuscum*, *Pinus sylvestris* and/or *Andromeda polifolia* as well as *Rubus chamaemorus*. The lawns are intermediate microsites with respect to water level. Their vegetation consists mostly of *Eriophorum vaginatum*. The flarks represent the wettest microsites and are covered primarily by *Sphagnum balticum* and *Scheuchzeria palustris*. More information on Salmisuo mire can be found in Alm et al. (1997) and Saarnio et al. (1997).

Vaisjeäggi is a pristine palsa mire in northern Finland (69°49'N, 27°30'E). The climate is subarctic. To consider the different functional surfaces within the mire, four study transects were established. Transects T_1 and T_2 were located on the wet surfaces dominated by *Sphagnum lindbergii* or *Sphagnum lindbergii* and *Sphagnum riparium*. The most common vascular plants were *Eriophorum angustifolium* and *Eriophorum russeolum*, *Vaccinium microcarpum* and *Carex limosa*. Transect T_3 was set at a wet palsa margin and was covered by *Sphagnum riparium*, *E. angustifolium* and *E. Russeolum*. Transect T_4 was on the top of the palsa and was occupied by *Vaccinium vitis-idaea*, *Betula nana*, *Empetrum nigrum*, *Rubus chamaemorus*, *Ledum palustre*, *Dicranum polysetum*, *Andromeda polifolia* and lichens like *Cladina rangiferina* and *Cladonia* species. More detailed information is given by Nykänen et al. (2003).

Linnansuo is a cutover peatland complex in eastern Finland (62°30'N, 30°30'E) in the boreal zone. The measurements were done in a drained, actively harvested peat production area. No vegetation was present and the bare peat was laid open. No microsites were differentiated. More detailed information will be given by Shurpali et al. (2008).

Samoylov is an island in the southern central Lena River Delta in Northern Siberia (72°22'N, 126°30'E). The climate is true-arctic and continental. Samoylov Island is characterised by wet polygonal tundra. In the depressed polygon centers, drainage is strongly impeded due to the underlying permafrost, and water-saturated soils or small ponds are common. In contrast, the elevated polygon rims are characterised by a moderately moist water regime. The vegetation in the swampy polygon centers and at the edges of ponds is dominated by hydrophytic sedges (*Carex aquatilis*, *Carex chordorrhiza*, *Carex rariflora*) and mosses (e.g. *Limprichtia revolvens*, *Meesia longiseta*, *Aulacomnium turgidum*). At the polygon rims, various mesophytic dwarf shrubs (e.g. *Dryas octopetala*, *Salix glauca*), forbs (e.g. *Astragalus frigidus*) and mosses (e.g. *Hylocomium splendens*, *Timmia austriaca*) gain a higher dominance. More detailed information is given in Pfeiffer et al. (1999), Kutzbach et al. (2004) and Kutzbach (2006). A total of 15 plots were established in five different microsite types: three at a polygon rim and three at each of four polygon centers which differed by their moisture and vegetation conditions. More details on the Samoylov site will be given by a manuscript in preparation by T. Sachs et al. (2007).

2.5.2 Experimental methods

The closed chamber experiments were conducted from July to September 2005 at Salmisuo, from June to August 1998 at Vaisjeäggi, from June to November 2004 at Linnansuo and from July to September 2006 on Samoylov Island to determine the net ecosystem exchange of CO_2. An overview of the set-up characteristics for the four investigation sites is given in Table 2.1. For illustration of the differences between the datasets, examples of the $c(t)$ evolution over time for all investigation sites are given in Figure 2.2. Permanent and robust boardwalks supported by poles driven in the soils vertically as well as permanently installed collars were established at Salmisuo, Vaisjeäggi and Samoylov. At Linnasuo, neither boardwalks nor permanent collars could be installed due to ongoing peat excavation activities. All chamber experiments were performed manually. Transparent chambers were used at the vegetated sites Salmisuo, Vaisjeäggi and Samoylov while opaque chamber were used at the bare peat site Linnansuo. Experiments were conducted during day and night time at Salmisuo and Samoylov whereas they were conducted only during daytime at Vaisjeäggi and
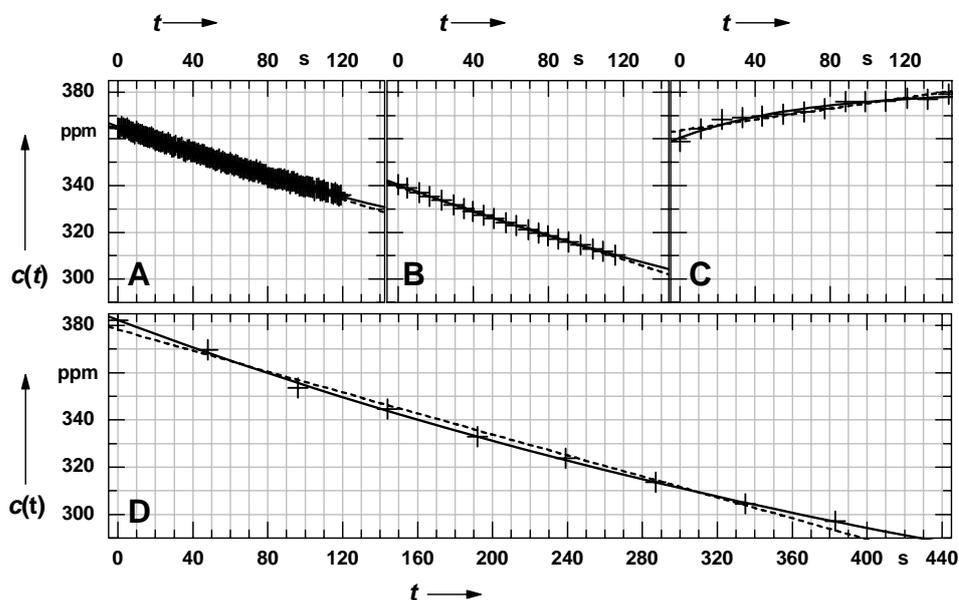
Figure 2.2: Examples of the CO_2 concentration $c(t)$ evolution over time t for the different investigation sites. **(A)** Salmisuo, 11 August 2005, **(B)** Vaisjeäggi, 17 August 1998, **(C)** Linnansuo, 12 November 2004, **(D)** Samoylov, 26 July 2006. The dashed lines indicate linear regression functions f_{lin}, the solid lines indicate exponential regression functions f_{exp}. The absolute values of the initial slopes of the exponential functions $f'_{exp}(t_0)$ are around 0.3 ppm s^{-1} for all examples. An overview of the different set-up characteristics is given in Table 2.1.

Linnansuo. The chamber headspace air was automatically cooled and mixed by a fan at Salmisuo and Vaisjeäggi. For Samoylov chambers, headspace air was mixed by air cycling through dispersive tubes by a membrane pump but not cooled. For Linnansuo chambers, neither an air mixing device nor a cooling system was provided. Initial pressure shocks during the chamber setting were minimised by additional openings on top of the chambers.

Closure times were rather short at Salmisuo (120 s), Vaisjeäggi (120–160 s) and Linnasuo (150 s), and much longer at Samoylov (480–600 s). Also, the concentration measurement intervals differed considerably in length: 1 s at Salmisuo, 5 s at Vaisjeäggi, 10 s at Linnasuo and 45 s at Samoylov. To avoid initial large noise in the $c(t)$ data which would disturb the regressions seriously, we discarded data points at the start of the chamber deployment and delayed the start point of the experiment $t_0 = 0$. The discarding interval was 10 s at Salmisuo, 30 s at Linnansuo and 45 s at Samoylov. No data discarding was done for the Vaisjeäggi data. The chamber experiments were

Table 2.1: Overview of set-up characteristics for the different investigation sites Salmisuo, Vaisjeäggi, Linnasuo and Samoylov.

	Salmisuo	Vaisjeäggi	Linnansuo	Samoylov
chamber type	manual, transparent	manual, transparent	manual, opaque	manual, transparent
time schedule	24-hour runs	only daytime	only daytime	partly day, partly night
chamber basal area	0.36 m^2	0.36 m^2	0.075 m^2	0.25 m^2
chamber height	32 cm	25 cm	30 cm…32 cm	5 cm…15 cm
robust boardwalks	yes	yes	no	yes
permanent collars	yes	yes	no	yes
insertion depth of collar/chamber in soil	15 cm…20 cm	15 cm…30 cm	5 cm	10 cm…15 cm
cooling system	yes	yes	no	no
air mixing	fan	fan	no	air cycling by pump
pressure relief provision	only during chamber setting	vent tube open over closure period	relief valve in function over closure period	only during chamber setting
CO$_2$ analyser	LI-840, LI-COR	LI-6200, LI-COR	LI-6200, LI-COR	Gas monitor 1412, Innova Airtech Instruments
closure time	120 s	120 s…160 s	150 s	480 s…600 s
interval length	1 s	5 s	10 s	45 s
data discard interval at experiment start	10 s	no	30 s	45 s
instrument noise RMSE	±0.5 ppm	±0.1 ppm	±0.3 ppm	±0.8 ppm
threshold of residual standard deviation used for coarse error filtering	1.6 ppm	1.2 ppm	2.2 ppm	1.7 ppm

filtered to exclude data which appeared strongly disturbed. For Linnasuo data, a visual inspection of $c(t)$ curves was done, and curves that looked strongly disturbed were discarded right away (6.1% of the experiments). All datasets were filtered after regression analysis using the standard deviation of the residuals of the exponential regression function as indicator of experiment noise. Thresholds of residual standard deviation, which indicated unacceptable noise levels, were 1.6 ppm for Salmisuo, 1.2 ppm for Vaisjeäggi, 2.2 ppm for Linnansuo and 1.7 ppm for Samoylov. It should be noted that data screening and flux calculations of the already published data from Vaisjeäggi and Linnasuo was performed using different approaches than in this study (Nykänen et al, 2003; Shurpali et al., 2008).

Table 2.2: Goodness-of-fit statistics of linear (lin) and exponential (exp) regression curves for example datasets as shown in Figure 3. Goodness of fit can be compared by the adjusted coefficient of determination R^2_{adj}, the Akaike information criterion AIC_c (with small sample second order bias correction) and an F-test checking if the residual variance of the exponential regressions is smaller than that of the linear regression (P is significance level).

ID	site, date, time	R^2_{adj}		AIC_c		F-test
		lin	exp	lin	exp	Var(exp)<Var(lin)
A	Salmisuo, 13/09/2005, 13:10	0.994	0.998	−56	−180	$P < 0.0001$
B	Salmisuo, 18/8/2005, 10:40	0.994	0.996	−137	−177	$P < 0.05$
C	Salmisuo, 9/9/2005, 2:50	0.979	0.992	−54	−175	$P < 0.0001$
D	Salmisuo, 9/9/2005, 3:30	0.971	0.980	−136	−179	$P < 0.05$
E	Vaisjeäggi, 27/8/1998, 14:40	0.992	0.999	−83	−123	$P < 0.0001$
F	Vaisjeäggi, 22/6/1998, 15:00	0.998	0.9998	−85	−143	$P < 0.0001$

2.6 Results

2.6.1 Residual analyses

Examples of the observed $c(t)$ data and fits of the linear and exponential model are given in Figure 2.3. The respective goodness-of-fit statistics are given in Table 2.2. Many of the measured $c(t)$ curves were clearly nonlinear even if chamber closure times were only 120 s (e.g. Fig. 2.3a–f). However, a rather large fraction of the nonlinear curves showed curvatures which were not consistent with the theoretical model developed in Chapter 2 (e.g. Fig. 2.3b, d, f). A summary of the residual analyses for all chamber experiments from the four investigation sites is given in Table 2.3. The residual analyses were conducted for all regression functions without parameter restrictions. Thus, regression curves with curvatures not consistent with the theoretical model were also included. In general, the residual analyses showed that the exponential model was frequently significantly better suited than the linear model to describe the measured $c(t)$ evolution in the chamber headspace. However, a substantial fraction (20% to 40%) of the fitted curves showed curvatures which did not conform to the theoretical model. The quadratic and the exponential model performed very similarly with respect to their residual statistics. The extent to which the nonlinear models were better suited than the linear model was different for the four datasets depending on the specifics of the respective experiment set-ups, i.e. measurement intervals, measurement

Table 2.3: Summary of residual analyses for the linear (lin), quadratic (qua) and exponential (exp) regression models applied to the datasets Salmisuo, Vaisjeäggi, Linnansuo and Samoylov. Autocorrelation of the residuals was examined with the *Durbin-Watson* test. If $d > d_U$, there is statistical evidence that the residuals are not positively autocorrelated ($P < 0.05$). If $d > d_L$, neither positive autocorrelation nor non-autocorrelation could be proved ($P < 0.05$). The *D'Agostino-Pearson* test was applied for checking normality of the residuals. If $P_N > 0.05$, no deviation from normal distribution could be detected. Goodness of fit of the linear (lin) and nonlinear (nlin) regression curves was compared by the adjusted coefficient of determination R^2_{adj}, the Akaike information criterion AIC_c (with small sample second order bias correction) and an F-test checking if the residual variance of the nonlinear regressions is smaller than that of the linear regression ($P < 0.1$). The percentages of the experiments of a respective dataset which match the test conditions are given in the columns (n_e: total number of experiments in the respective dataset). Residual analyses were conducted for regression functions without parameter restrictions. For the exponential regression, percentages for regressions restricted to parameter combinations explainable by the theoretical model are given in parentheses.

		autocorrelation		normality	goodness-of-fit comparisons		
test		*Durbin-Watson*		*D'Agost.-Pearson*	adjusted R^2	Akaike IC	F-test
test condition		$d > d_U$	$d > d_L$	$P_N > 0.05$	$R^2_{adj}(nlin)$ $> R^2_{adj}(lin)$	$AIC_c(nlin)$ $< AIC_c(lin)$	$Var(nlin)$ $< Var(lin)$
				percentage of n_e (%)			
Salmisuo 1 s intervals ($n_e= 542$)	lin	44	46	84	–	–	–
	qua	67	73	86	84	77	37
	exp	68	72	87	83 (63)	77 (58)	37 (30)
Vaisjeäggi 5 s intervals ($n_e = 389$)	lin	10	12	87	–	–	–
	qua	30	47	93	90	86	60
	exp	30	48	92	89 (55)	86 (58)	60 (42)
Linnansuo 10 s intervals ($n_e = 368$)	lin	27	44	90	–	–	–
	qua	48	88	93	79	66	33
	exp	49	88	92	78 (49)	64 (41)	36 (23)
Samoylov 45 s intervals ($n_e = 465$)	lin	67	92	98	-	-	-
	qua	75	100	97	70	35	15
	exp	75	100	98	68 (43)	37 (26)	19 (15)

noise, and presumably also by the ecosystem characteristics of the different sites.

Autocorrelation was less often detected by the Durbin-Watson test for the exponential and quadratic models than for the linear model. For the Salmisuo dataset, significant positive autocorrelation ($d>d_U$) could be excluded for 68% of the exponential regressions, 67% of the quadratic regressions and for only 44% of the linear regressions. For the Vaisjeäggi and Linnansuo datasets, autocorrelation was generally a bigger problem: For the Vaisjeäggi dataset, significant positive autocorrelation ($d>d_U$) could be excluded for 30% of the exponential regressions, 30% of the quadratic regressions and for only 10% of the linear regressions. For the Linnasuo dataset, significant positive autocorrelation ($d>d_U$) could be excluded for 49% of the exponential regressions, 48% of the quadratic regressions and for only 27% of the linear
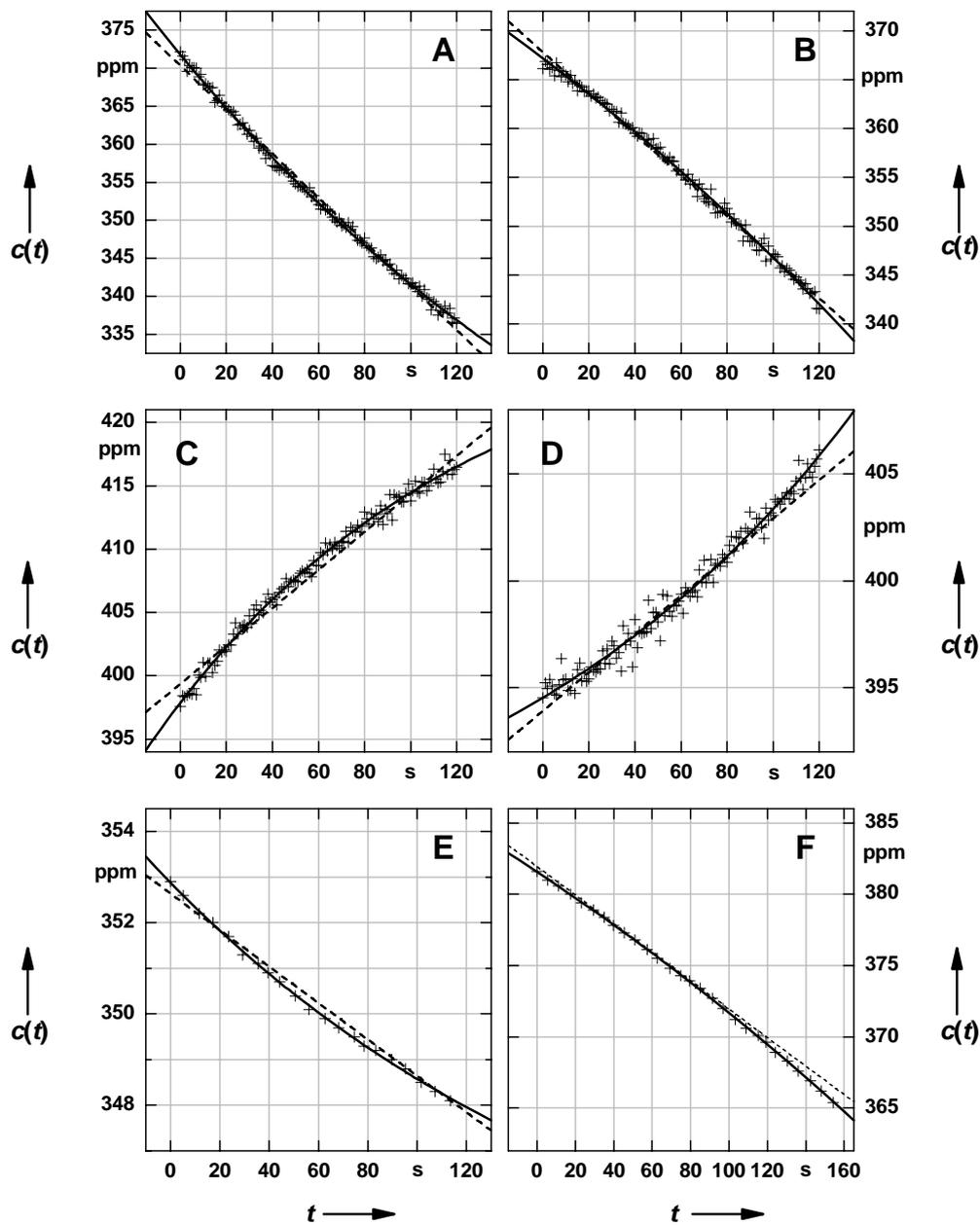
Figure 2.3: Examples of the CO_2 concentration $c(t)$ evolution within the chamber and fitted linear and exponential functions. **(A)** Salmisuo, 13 September 2005 13:10 LT, **(B)** Salmisuo, 18 August 2005 10:40 LT, **(C)** Salmisuo, 9 September 2005 3:30 LT, **(D)** Salmisuo, 9 September 2:50 LT, **(E)** Vaisjeäggi, 27 August 1998 14:40 LT, **(F)** Vaisjeäggi, 22 June 1998 15:00 LT. The dashed lines indicate linear regression functions f_{lin}, the solid lines indicate exponential regression functions f_{exp}. (A), (C) and (E) show exponential regression functions with curvature consistent with the developed theoretical model. (B), (D) and (F) show exponential regression functions with curvature not consistent with the theoretical model. Statistics for the regression functions are given in Table 2.2.

regressions. For the Samoylov dataset, autocorrelation was less of a problem due to a lower number of data points and a higher noise level: Significant positive autocorrelation (d>d_U) could be excluded for 75% of the exponential and quadratic regressions and for 67% of the linear regressions.

Evaluated with the D'Agostino-Pearson test, normality of the residuals was found to be a minor problem compared to autocorrelation. For the Salmisuo dataset, 84% of the linear regressions, 86% of the quadratic regressions, and 87% of the exponential regressions showed normally distributed residuals. The percentages of regressions with normally distributed residuals are even greater for the other datasets with longer measurement intervals (Vaisjeäggi, Linnansuo, Samoylov). For Salmisuo, removal of autocorrelation by block-averaging also eliminated most of the non-normality problems in the residuals (data not shown).

The different goodness-of-fit indicators for regression model comparison R^2_{adj}, AIC_c and the F-test of the residual variances showed rather differing results between the different indicators and datasets (Table 2.3). However, it could be demonstrated that for the majority of experiments of all datasets the exponential and quadratic models were significantly better fitted than the linear model. For the Salmisuo dataset, R^2_{adj} was greater for 84% of the quadratic regressions and 83% of the exponential regressions than for the respective linear regressions indicating a better fit. However, only 63% of the exponential regressions showed a greater R^2_{adj} than the linear regressions while also showing a curvature conforming with the theoretical model. The AIC_c appeared to penalize somewhat stronger the higher number of parameters in the nonlinear models than the R^2_{adj}: The AIC_c was smaller for only 77% of the quadratic and exponential regressions than for the respective linear regressions indicating a better fit. The F-test of the residual variances indicated that the quadratic and exponential regressions had a significantly (P<0.1) lower residual variance than the respective linear regressions for 37% of the Salmisuo experiments. Thirty percent of the exponential regressions had a significantly lower residual variance than the linear regressions while also showing a curvature conforming with the theoretical model.

Compared to Salmisuo, the Vaisjeäggi dataset showed a greater percentage of experiments which were better fitted by the nonlinear regressions than the linear regression. The F-test of the residual variances proved that the quadratic and

exponential regressions had a significantly ($P<0.1$) lower residual variance than the respective linear regressions for 60% of the Vaisjeäggi experiments. 42% of the exponential regressions had a significantly lower residual variance than the linear regressions while also showing a curvature conforming with the theoretical model.

The percentage of the Linnansuo experiments which were better fitted by the nonlinear than by the linear model was comparable to that of the Salmisuo dataset. However, rather many of these regressions showed curvatures not consistent with the theoretical model.

The Samoylov data set showed a lower percentage of experiments which were better fitted by the nonlinear than by the linear model compared to the other datasets. The F-test of the residual variances indicated that the quadratic and exponential regressions had a significantly ($P<0.1$) lower residual variance than the respective linear regressions for only 15% and 19% of the Samoylov experiments, respectively. Only 15% of the exponential regressions had a significantly lower residual variance than the linear regressions while also showing a curvature conforming with the theoretical model.

The F-test of the residual variances revealed that the residual variance of the linear regression was never significantly ($P<0.1$) lower than the residual variances of the nonlinear regressions in all four datasets (data not shown). Furthermore, the residual variance of the exponential regression was only significantly smaller than the residual variance of the quadratic regression in less than 1% of the experiments of all datasets (data not shown).

An F-test of the residual variances of the exponential and the NDFE function (Livingston et al., 2006) fitted to the Linnansuo data showed that less than 1% of 335 $c(t)$ curves were significantly ($P<0.1$) better fitted by the NDFE function compared to the exponential regression function whereas 13% of the $c(t)$ curves were significantly ($P<0.1$) better fitted by the exponential model (data not shown).

2.6.2 The effect of different regression models on the flux estimates

A comparison of the initial slopes of the linear and exponential regression functions $f'_{lin}(t_0)$ and $f'_{exp}(t_0)$ by x-y scatter diagrams is shown in Figure 2.4 for all investigation sites. The initial slopes of the regression functions are directly proportional to the CO_2
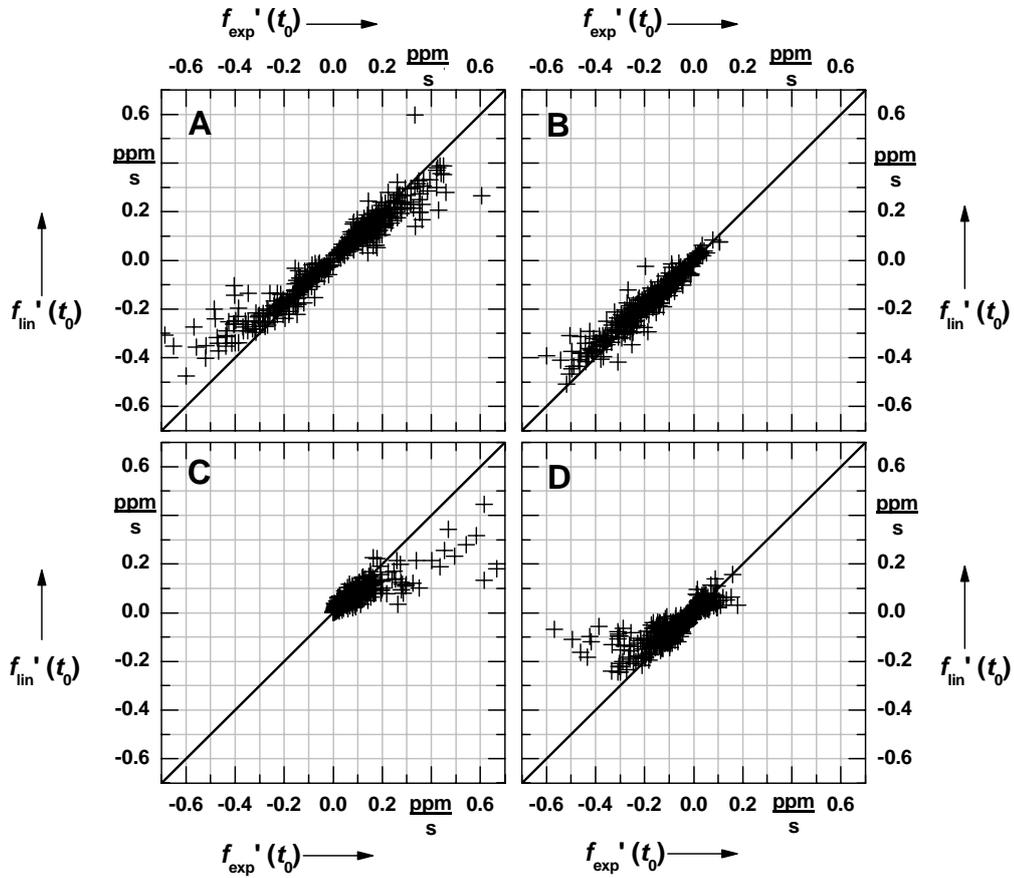
Figure 2.4: Comparison of initial slopes of the linear and exponential regression curves for the different investigation sites. A Salmisuo, B Vaisjeäggi, C Linnansuo, D Samoylov. On the x-axes, the initial slopes of the exponential regression $f_{exp}'(t_0)$ are plotted. On the y-axes, the initial slopes of the linear regression curves $f_{lin}'(t_0)$ are plotted. The $y = x$ relationship is given as solid line. As the initial slopes of the regression curves are directly proportional to the CO_2 flux estimates, a deviation between $f_{lin}'(t_0)$ and $f_{exp}'(t_0)$ indicates a bias of the CO_2 flux estimate by the application of the linear model presuming that the undisturbed CO_2 fluxes are better reflected by the exponential model.

flux at the beginning of chamber closure $F_{net}(t_0)$ which is considered to be the best estimate of the undisturbed flux before chamber closure (Eq. 20). Considering the exponential model as more correct, deviating values of $f'_{lin}(t_0)$ and $f'_{exp}(t_0)$ would represent a bias of the CO_2 flux estimate by the linear regression approach. As illustrated in Figure 2.4, $f'_{lin}(t_0)$ and $f'_{exp}(t_0)$ partly deviated considerably from each other, in particular for great values of the initial slopes. Mostly, the absolute values of $f'_{lin}(t_0)$ were smaller than the absolute values of $f'_{exp}(t_0)$, which means an underestimation bias of the linear regression approach both for CO_2 uptake and CO_2

release situations, which is expected by the theoretical exponential model. However, the inverse relationship was also frequently observed, which means an overestimation bias by the linear regression compared to the

exponential regression, which indicated apparent violations of the basic assumptions of the theoretical model. The effect of the underestimation of the absolute values of the initial slopes increased with increasing absolute values of the initial slopes and thus with increasing absolute values of CO_2 fluxes. The underestimation bias by linear regression could be observed for all four datasets although to different degrees. The strongest underestimation effects were found for the Linnansuo and Samoylov datasets (Fig. 2.4c, d). For high absolute values of the initial slopes in these datasets, $f'_{lin}(t_0)$ could be as low as 50% or even 20% of the values of $f'_{exp}(t_0)$. On the other hand, the weakest effects were found for the Vaisjeäggi dataset (Fig. 2.4b). Also for highest absolute values of the initial slopes in this dataset, $f'_{lin}(t_0)$ was not below 60% of the value of $f'_{exp}(t_0)$. The Salmisuo dataset was intermediate in this regard (Fig. 2.4a). For high absolute values

of the initial slope in these datasets, $f'_{lin}(t_0)$ was often between 40% and 80% of the value of $f'_{exp}(t_0)$. Salmisuo is the only dataset with nearly equally distributed numbers of experiments for CO_2 uptake and CO_2 release situations. For this dataset, it could be observed that the underestimation effect of the linear regression was on average stronger for CO_2 uptake situations than for CO_2 release situations.

An overview of the significances of the deviations between $f'_{lin}(t_0)$ and $f'_{exp}(t_0)$ is given in Table 2.4. The percentages of experiments with significant (*Student's* t-test, $P<0.1$) deviations between $f'_{lin}(t_0)$ and $f'_{exp}(t_0)$ are listed separately for situations with underestimation (H1) and overestimation (H2) by the linear regression. The absolute values of $f'_{exp}(t_0)$ were significantly greater than the absolute values of $f'_{lin}(t_0)$ (H1 is true at $P<0.1$) for 57% of the Salmisuo experiments, 55% of the Vaisjeäggi experiments, 42% of the Linnasuo experiments and only 29% of the Samoylov experiments. These portions of experiments showed that a nonlinearity of an exponential form as predicted by the theoretical model often produced a significant underestimation effect of the initial slopes by linear regression. On the other hand, the absolute values of $f'_{exp}(t_0)$ were significantly smaller than the absolute values of $f'_{lin}(t_0)$ (H2 is true at $P<0.1$) for 19% of the Salmisuo experiments, 30% of the Vaisjeäggi

Table 2.4: Significance of deviations between the slope estimates at $t = 0$ as yielded by the exponential $f_{exp}'(t_0)$ and linear $f_{lin}'(t_0)$ regression models. The hypothesis H1 states that the absolute value of the initial slope of the exponential regression is greater than the absolute value of the initial slope of the linear regression. The hypothesis H2 states that the absolute value of the initial slope of the exponential regression is smaller than the absolute value of the initial slope of the linear regression. The null hypothesis H0 states that the absolute value of the initial slope of the exponential regression is equal to the absolute value of the initial slope of the linear regression. While H1 is conforming with the developed theoretical model, H2 is not which implies the occurrence of disturbing processes not considered by the model. The hypotheses were tested by one-tailed *Student*'s t-tests ($P < 0.1$) following Potthoff (1965, cited in Sachs, 1992). The percentages of the experiments of a respective dataset for which the respective hypotheses could be confirmed are given in the columns (n_e: total number of experiments in the respective dataset).

	Student's t-test of hypotheses ($P < 0.1$)		
	H1: $|f_{exp}'(t_0)|-|f_{lin}'(t_0)| > 0$	H2: $|f_{exp}'(t_0)|-|f_{lin}'(t_0)| < 0$	H0: $|f_{exp}'(t_0)|-|f_{lin}'(t_0)| = 0$
	percentage of n_e (%)		
Salmisuo ($n_e = 542$)	57.4	18.5	24.2
Vaisjeäggi ($n_e = 389$)	55.3	30.3	14.4
Linnansuo ($n_e = 368$)	42.4	25.8	31.8
Samoylov ($n_e = 465$)	29.0	19.3	51.6

experiments, 26% of the Linnasuo experiments and 19% of the Samoylov experiments. These portions of experiments were not consistent with the theoretical model because of their curvature but showed that unexplained nonlinearity can occur and can cause a significant overestimation effect of the initial slopes by linear regression. The absolute values of $f'_{exp}(t_0)$ and $f'_{lin}(t_0)$ did not deviate significantly from each other (H0 could not be rejected at $P<0.1$) for 24% of the Salmisuo experiments, 14% of the Vaisjeäggi experiments, 32% of the Linnansuo experiments and 52% of the Samoylov experiments. Thus, although the nonlinearity effects on the flux estimates of the Linnansuo and Samoylov datasets were pronounced, they were significant for a rather small percentage of experiments compared to the Salmisuo and Vaisjeäggi datasets. On the other hand, the Vaisjeäggi dataset had a high percentage of significant effects on the flux estimates but these effects were comparatively moderate. Here, the importance of the closure time, measurement interval length, and instrument precision (Table 2.1) on the nonlinearity problem became obvious.

A comparison of the initial slopes of the quadratic and the exponential regression functions $f'_{qua}(t_0)$ and $f'_{exp}(t_0)$ by *x-y* scatter diagrams is shown in Figure 2.5 for all investigation sites. An overview of the significances of the deviations between $f'_{qua}(t_0)$ and $f'_{exp}(t_0)$ is given in Table 2.5. The initial slopes $f'_{qua}(t_0)$ and $f'_{exp}(t_0)$ differ
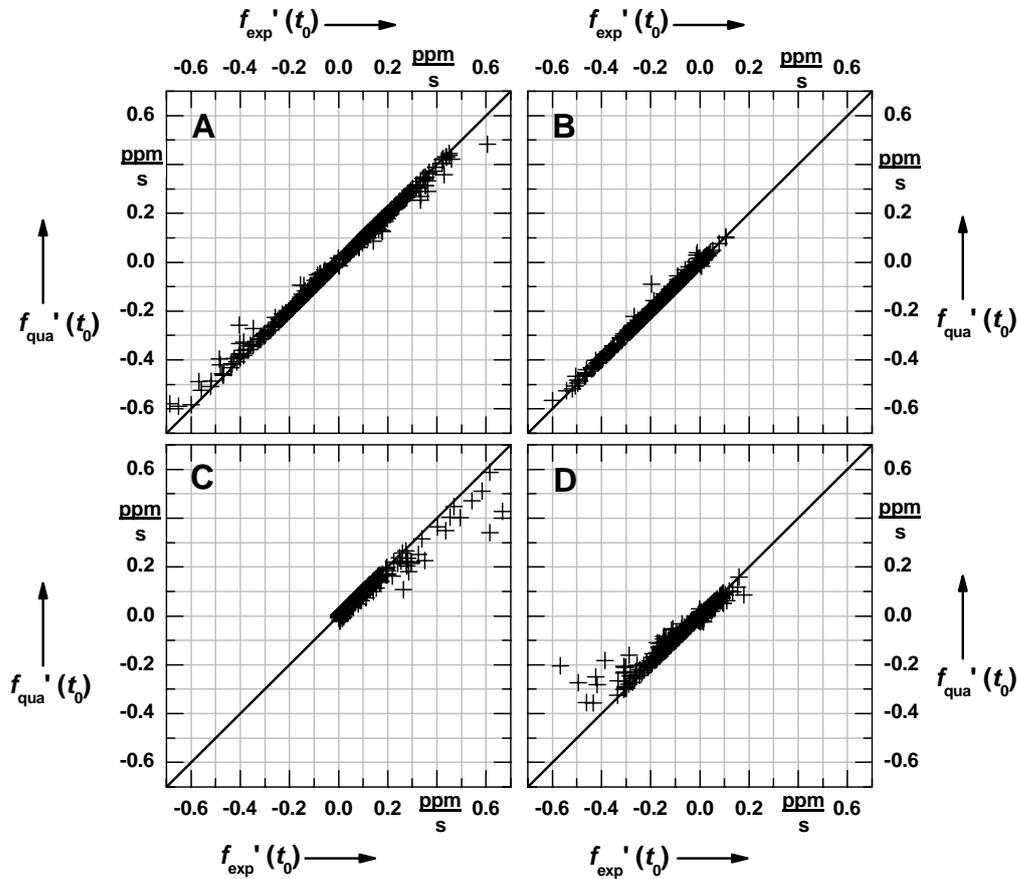
Figure 2.5: Comparison of initial slopes of the exponential and quadratic regression curves for the different investigation sites. **(A)** Salmisuo, **(B)** Vaisjeäggi, **(C)** Linnansuo, **(D)** Samoylov. On the x-axes, the initial slopes of the exponential regression $f_{exp}'(t_0)$ are plotted. On the y-axes, the initial slopes of the quadratic regression curves $f_{qua}'(t_0)$ are plotted. The $y = x$ relationship is given as solid line. As the initial slopes of the regression curves are directly proportional to the CO_2 flux estimates, a deviation between $f_{qua}'(t_0)$ and $f_{exp}'(t_0)$ indicates a bias of the CO_2 flux estimate by the application of the quadratic model presuming that the undisturbed CO_2 fluxes are better reflected by the exponential model.

significantly ($P<0.1$) for only 5%–9% of the experiments of the four datasets. However, the quadratic regression functions tended to show lower absolute values of the initial slopes than the exponential regression functions, in particular for situations with strong CO_2 uptake or release. The underestimation of the absolute value of the initial slope of the quadratic regression compared to the exponential regression was strongest for the Linnansuo and Samoylov datasets and lowest for the Vaisjeäggi dataset. The Salmisuo dataset was intermediate in this regard.

A comparison of the initial slopes of the exponential $f'_{exp}(t_0)$ and the NDFE function proposed by Livingston et al. (2005, 2006) $f'_{NDFE}(t_0)$ by x-y scatter and
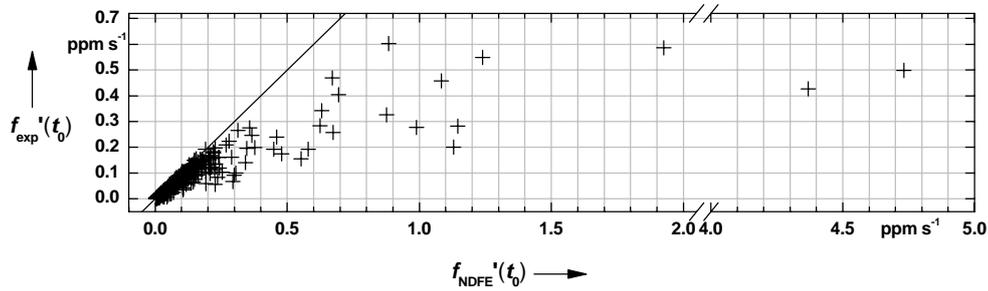
Figure 2.6: Comparison of initial slopes of the NDFE (Livingston et al., 2006) and the exponential regression curves for the non-vegetated peat excavation site Linnansuo. On the x-axes, the initial slopes of the NDFE regression function $f_{NDFE}'(t_0)$ are plotted. On the y-axes, the initial slopes of the exponential regression curves $f_{exp}'(t_0)$ are plotted. The $y = x$ relationship is given as solid line. The NDFE curves have drastically higher initial slopes than the exponential curves particularly for high fluxes. Notice the break in the x-axis.

diagrams is shown in Figure 2.6 for the non-vegetated peat excavation site Linnasuo. The $f'_{NDFE}(t_0)$ was generally higher as $f'_{exp}(t_0)$. The steeper the fluxes and thus the initial slopes the stronger was the deviation between $f'_{exp}(t_0)$ and $f'_{NDFE}(t_0)$. The $f'_{NDFE}(t_0)$ was often 1.5 to 3 times higher than $f'_{exp}(t_0)$ and in extreme cases up to 10 fold higher.

2.7 Discussion

This study presents the first derivation of a theory-based model function of gas concentration changes over time $c(t)$ in closed chambers above vegetated land surfaces. Residual analyses demonstrated that the developed exponential model could be significantly better fitted to the data than the linear model even if closure times were kept short, for example two minutes as for the Salmisuo experiments. On the other hand, application of linear regression was often not appropriate and led to underestimation of the absolute values of the initial slope of the $c(t)$ curves and thus of the CO_2 flux estimates. The exponential model was not significantly better fitted than the quadratic model with respect to the residual analyses. However, the absolute values of initial slopes of the $c(t)$ curves were often systematically lower for the quadratic compared to the exponential regression function. The exponential model could be better fitted to the $c(t)$ curves observed on the non-vegetated peat excavation site Linnansuo than the physically most profound NDFE model function proposed by Livingston et al. (2005, 2006). This can be explained by the probable serious violations of the underlying

model assumptions of the NDFE model, in particular by the likely leakage through the peat pore space since no permanent collars were installed at Linnansuo. The great difference between the initial slopes of the NDFE and the exponential model demonstrates the sensibility of CO_2 flux estimation to the choice of the applied model. If applying physically based nonlinear models, violations of model assumptions have to be minimised with great care.

Modelling of the CO_2 concentration changes over time in chamber headspaces is more complicated for vegetated surfaces than for bare soil surfaces since additional processes such as photosynthesis and plant respiration have to be considered. The complex processes in plants and soils had to be substantially simplified for the development of a model that is simple enough for nonlinear regression of actual, often noisy data. Furthermore, some strong assumptions have to be made as basis for such a model development: Soil and headspace air temperature, photosynthetically active radiation, air pressure and headspace turbulence were assumed to be constant and approximately equal to ambient conditions. Apparently, however, these assumptions were not valid for all experiments. Whereas the majority of fitted $c(t)$ curves were consistent with the proposed theoretical model, a substantial fraction of the experiments were not. These unexplainable curvatures are considered to have been caused by violations of the basic assumptions of the theoretical model. The obvious violation of model assumptions indicates that the experiment design was sub-optimal and that the reason for it must be identified and accounted for. Otherwise, the calculated fluxes would be biased to an unknown extent. As at least the closed chambers at Salmisuo and Vaisjeäggi were temperature-controlled by an effective cooling system, we consider the change in headspace turbulence by the closed chamber, which is not yet covered by the theoretical model, as a likely problematic process which could introduce nonlinearity difficult to model. An additional reason for the unexplainable curvature could have been small positive pressure perturbations during chamber placement (Hutchinson and Livingston, 2001). Although the possible disturbing effects of altering turbulence or pressure conditions by closed chambers were discussed previously by several studies (Hanson et al., 1993; Le Dantec et al., 1999; Hutchinson et al., 2000; Livingston and Hutchinson, 2001; Denmead and Reicosky, 2003; Reicosky, 2003; Livingston et al., 2006), additional investigations are certainly needed concerning these issues.
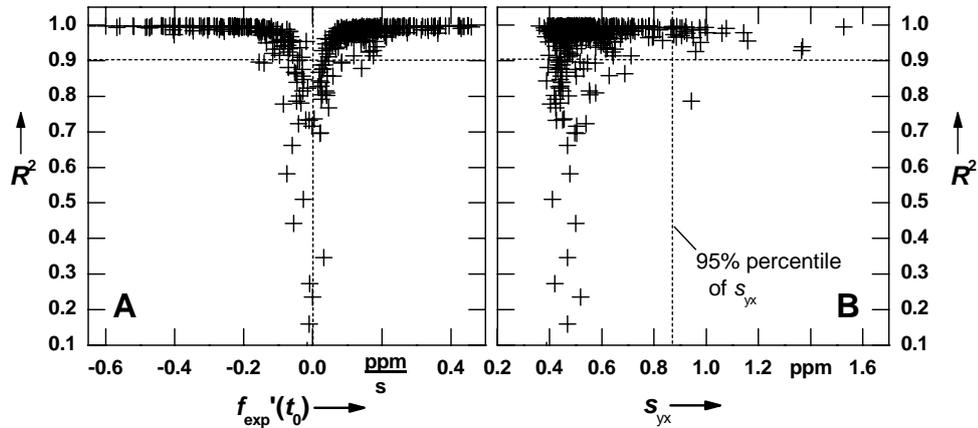
Figure 2.7: The relationships of the nonlinear coefficient of determination R^2 with the initial slope $f_{exp}'(t_0)$ of the regression function and the standard deviation of the residuals s_{yx} exemplified by the dataset Salmisuo 2005. **(A)** The R^2 value is plotted against the initial slope $f_{exp}'(t_0)$. The use of R^2 as a filter criterion (e.g. $R^2 = 0.9$) would discriminate strongly the regressions with low slope values $f_{exp}'(t_0)$. **(B)** The R^2 value is plotted against the standard deviation of residuals s_{yx} which is a better filter criterion for measurement performance. The application of R^2 (e.g. $R^2 = 0.9$) or s_{yx} (e.g. the 95 % percentile of s_{yx}: 0.87 ppm) as filter criteria would identify completely different experiments as disturbed.

To evaluate the validity of candidate models, we recommend the use of residual analysis including tests for autocorrelation and normality. In particular, autocorrelation has to be excluded for unbiased estimates of the uncertainty of regression parameters. Goodness of fit can be evaluated by the adjusted nonlinear coefficient of determination R^2_{adj}, the Akaike Information Criterion AIC and by an F-test of the residual variances.

We note that the linear coefficient of determination r^2 was frequently misused during the history of closed chamber measurements. The linear r^2 and the nonlinear R^2 are neither appropriate measures of regression model correctness (often used for checking linearity) nor appropriate filter criteria for measurement performance (Granberg et al., 2001; Huber, 2004; Hibbert, 2005). The expressions $(1-r^2)$ and $(1-R^2)$ are measures of the unexplained variance normalized to the total variance. The significance of r^2 and R^2 is strongly dependent on the number of data points n which is often disregarded. In extreme cases, the r^2 values were calculated for only three data points and were considered as evidence of linearity when greater than typically 0.95. However, applying the F-test to check if a R^2 value of 0.95 for three data points is significantly different from zero reveals an error probability P of 0.14, which is higher than the typically used significance levels of 0.05 or 0.1. Furthermore, even an R^2 value significant at the 0.05 level does not prove linearity and cannot exclude serious bias of

the flux estimates. A linear regression can show a rather high r^2 value of above 0.99 although significant nonlinearity can be demonstrated by more appropriate statistical methods like the F-test for the residual variances (Huber, 2004; Hibbert, 2005). Only for comparison of two regression functions with the same numbers of data points n and parameters k, r^2 or R^2 can give an indication which function is better suited. Moreover, r^2 as well as R^2 are not usable as filter criteria for measurement performance because they arbitrarily discriminate the lower fluxes: r^2 and R^2 values increase with constant unexplained variance and increasing total variance which is inherently higher for greater fluxes (Fig. 2.7a). In this context, a better filter criterion would be the standard deviation of the residuals s_{yx} (Fig. 2.7b).

The measurement interval length, the number of measurement points and the precision of the CO_2 concentration measurements determine whether the nonlinearity can be detected with sufficient statistical significance. It has to be stressed that strong nonlinearity can be present even when it cannot be detected because of long measurement intervals, few data points or low measurement precision.

Considering the results of this study, a list of practical recommendations for closed chamber measurements follows:

- A nonlinear model should be favoured over a linear model to reflect the various biophysical processes in effect and thus to better estimate the predeployment flux.

- We recommend to fit an exponential function as given in Eq. (14) to the observed $c(t)$ curves for experiments on vegetated soils. For experiments on non-vegetated soils, the NDFE model function proposed by Livingston et al. (2005, 2006) should be applied. When applying the NDFE model, however, violations of the underlying assumptions of the NDFE model, i.e. no-leakage, must be strictly avoided.

- When adopting a nonlinear approach, investigators should employ chambers with smaller headspace volumes and longer deployment times as warranted to emphasize the non-linearity of the $c(t)$ response. For vegetated soils, however, the advantages of this approach must be carefully balanced with the risk of unpredictable plant responses due to strongly lowered CO_2

concentrations or artificially high water vapour contents in the chamber headspace.

– Light, temperature and humidity conditions as well as wind speed and turbulence during chamber closure should be as similar as possible to the ambient conditions. Changes of light, temperature and humidity would change plant physiology and thus complicate the form of the $c(t)$ curve whereas artificial changes of pressure, wind and turbulence may additionally impact transport processes and thus even compromise the assumption that the initial slope of the $c(t)$ is the best estimator of the predeployment CO_2 flux (Hutchinson et al., 2000; Hutchinson and Livingston, 2001).

– Generally, leaks should be avoided (Hutchinson and Livingston, 2001; Livingston et al., 2006). If this is not possible, fitting of an exponential function would allow for better approximation of the initial slopes of the $c(t)$ curves and thus for more realistic estimation of predeployment fluxes compared to linear regression.

– High noise levels at the start of the chamber deployment due to eventual pressure or turbulence disturbances or insufficient purging of residual gases in the analyser lines have to be avoided since this noise would be very critical regarding the results of nonlinear regression. If initial noise is obviously present, the data from the respective time period has to be discarded, and the starting time of the experiment $t_0=0$ should be delayed accordingly. It has to be stressed that this initial data discarding would lead to inherent underestimation of fluxes because the slope of the $c(t)$ evolution curve is expected to be greatest and changing most strongly at the start of the chamber closure time (Hutchinson et al., 2000; Livingston et al., 2006, this study). Still, this underestimation would be less when applying a nonlinear model compared to the use of linear regression. Anyhow, experimental set-ups should be improved to make an initial data discarding unnecessary. The interval of initial data discarding must be as short as possible.

– When using the presented exponential or quadratic regression functions (number of parameters $k=3$), not less than seven data points ($n \geq 7$) should be collected over the closure time to achieve an acceptable value for the

degrees of freedom ($n-k{\geq}4$). More data points are recommended, particularly if the measurement precision is not optimal.

– The better the measurement precision and the more data points are available for the regression, the better the nonlinearity can be detected and its significance demonstrated.

– Autocorrelation and non-normality of residuals should be checked for and can be reduced by block-averaging to avoid biased estimations of parameters and their errors.

One scientific question for which the possible bias of closed chamber CO_2 flux measurements is important is the comparison of micrometeorological eddy covariance data and chamber data where often a considerable mismatch can be observed. Mostly, this mismatch is attributed to methodological problems of the eddy covariance approach (e.g. Law et al., 1999; Van Gorsel et al., 2007). While the methodological problems of the eddy covariance method are undoubtedly real, it has to be stated that also the flux estimates by closed chambers can be prone to significant biases and should be interpreted using much caution (see also Reicosky, 2003; Livingston et al., 2005, 2006).

The underestimation effect by linear and quadratic regression compared to exponential regression increases with increasing absolute values of the CO_2 fluxes. Thus, the underestimation of the CO_2 fluxes by the linear regression method not only disturbs the quantitative but also the qualitative evaluations since differences between sites with strong and weak CO_2 exchange would be smoothed. Furthermore, the effect should be dependent on ecosystem characteristics such as soil texture, peat density, soil moisture status or vegetation composition (Hutchinson et al., 2000; Nakano et al., 2004). Here, the uneven underestimation bias between sites can lead to the conclusion that CO_2 fluxes differ greatly between sites although, in fact, only the response to the chamber disturbance on of soil gas diffusion and plant physiology differs.

As the underestimation of the absolute values of the initial slope of the $c(t)$ curves by linear regression was observed to be of different magnitude for CO_2 uptake and CO_2 release situations, there is a high potential for serious bias of carbon balances which can, in extreme cases, lead to changing of the sign, which determines an ecosystem as CO_2 source or sink. This high potential for serious bias of the CO_2 balances is exemplified by Figure 2.8 for a diurnal cycle of CO_2 exchange fluxes at the
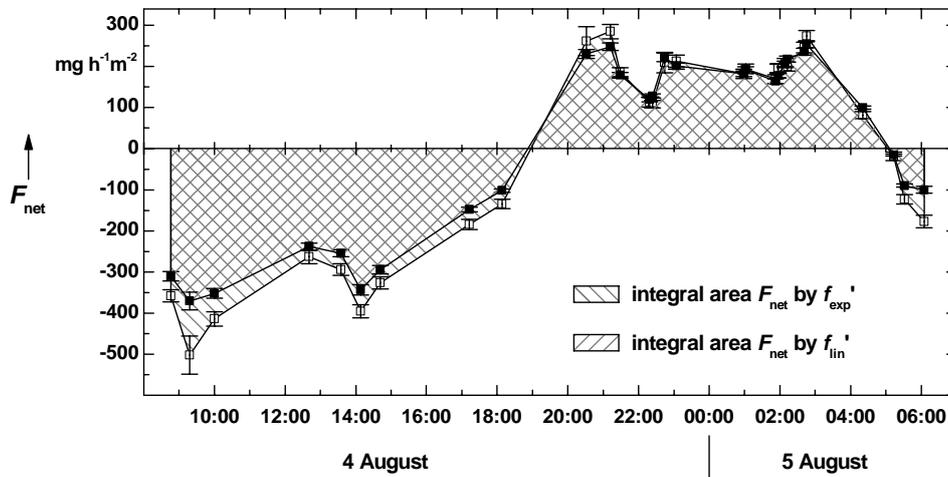
Figure 2.8: Example of the effect of the different regression approaches on the estimated CO_2 balance over one diurnal cycle (04/08/2005 8:45 to 05/08/205 6:05 LT) at the flark sites of Salmisuo. The black squares indicate CO_2 flux estimates F_{net} by the linear model approach, the white squares indicate CO_2 flux estimates F_{net} by the exponential model approach. The error bars indicate the standard errors of the flux estimates. Simple integrations of the two CO_2 flux estimate time series according to the trapezoidal rule yield carbon balances over the 21.33 h of -0.86 g CO_2 and -1.30 g CO_2 for the linear and exponential model approaches, respectively. Thus, the estimate of CO_2 uptake using the exponential model is 150 % of the estimate using the linear model!

flark sites of Salmisuo. The bias on the daily balance can be very large because it is equal to the sum of integrated daytime uptake and integrated night time release. The sum is much smaller than the two summands due to their similar magnitude but opposing signs. If the bias of one summand is stronger than for the other summand, the relative bias of the balance can be much more pronounced than the relative bias of the respective summands. This high sensitivity of the CO_2 balance to asymmetric biases of CO_2 uptake and CO_2 release is of major importance as closed chamber CO_2 flux measurements based on linear regression are used for local, regional and global carbon budgets and for the evaluation of the carbon source or sink characteristics of ecosystems or even vegetation zones (e.g. Oechel et al., 1993, 1998, 2000).

In this context, we fully agree with Hutchinson et al. (2000) and Livingston et al. (2005, 2006) who emphasised that the bias of flux estimates by using linear regression for closed chamber experiments is systematic, not random. Therefore, "although such errors are relatively small in comparison to the temporal and spatial variability characteristic of trace gas exchange, they bias the summary statistics for each

experiment as well as larger-scale trace gas flux estimates based on them" (Hutchinson et al., 2000).

2.8 Conclusions

Thorough analyses of residuals demonstrate that linear regression is frequently not appropriate for the determination of CO_2 fluxes by closed-chamber methods, even if closure times are kept short.

The coefficient of determination R^2 should not be used as proof of linearity. For comparing the performance of models, goodness-of-fit measures such as the adjusted R^2, the *Akaike* Information Criterion or an F-test of the residual variances are recommended. Additionally, the residuals should be checked for autocorrelation and normality to allow for unbiased estimations of the parameters and their errors.

The assumptions inherent in the proposed exponential model fit the majority of the observations examined in this investigation, thus suggesting the potential value of biophysical models in future chamber-based emissions studies.

However, the curvature of the nonlinear $c(t)$ curves is for a substantial percentage of the experiments not explainable with the proposed theoretical model. This is considered to be caused by violations of the basic assumptions of the theoretical model. In particular, the effects of turbulence alteration and pressure disturbances across the soil-atmosphere interface by setting a closed chamber on the ecosystem should be investigated in more detail in the future.

In many cases, a quadratic model as proposed by Wagner et al. (1997) can be equally well fitted to the data as the exponential model. However, the estimates of the absolute values of the initial slopes of the $c(t)$ curves tended to be systematically lower for quadratic than the exponential regression. This can have a considerable effect on the CO_2 flux estimates for situations with strong CO_2 uptake or release.

The NDFE model proposed by Livingston et al. (2005, 2006) could not be better fitted to the $c(t)$ observations at the bare peat site Linnansuo than the exponential function. This was probably due to violations of the NDFE model assumptions, in particular the required non-existence of leakage.

Inappropriate application of linear regression can lead to serious underestimation of CO_2 fluxes. Initial slopes of linear regression can be as low as 40 % of the initial slope of exponential regression for closure times of only 2 min.

The degree of underestimation increased with increasing CO_2 flux strength and is dependent on soil and vegetation conditions which can disturb not only quantitative but also qualitative evaluation of CO_2 flux dynamics.

The underestimation effect by linear regression was observed to be different for CO_2 uptake and CO_2 release situations which can lead to stronger bias in the daily, seasonal and annual CO_2 balances than in the individual fluxes.

The fitting of observed closed-chamber data to biophysical models in combination with thorough statistical tests of the different models' validities offers at least two major advantages over the simple use of linear regression: (1) the ability to control the quality of observations, detect major problems of the methodology and thus to improve experimental protocols, and (2) improved accuracy and lower uncertainty in resultant flux estimates.

To avoid serious bias of CO_2 balance estimates on the local, regional or even global scale, we suggest further tests for biases of published flux estimates and recommend the use of nonlinear regression models for future closed-chamber studies.

We developed a MATLAB® routine which can perform linear and nonlinear regression including residual analyses for data of a wide range of chamber experiment setups. This routine is available online at http://biogeo.botanik.uni-greifswald.de/index.php?id=264.

Acknowledgements

3. ENVIRONMENTAL CONTROLS ON CH$_4$ EMISSION FROM POLYGONAL TUNDRA ON THE MICRO-SITE SCALE IN THE LENA RIVER DELTA, SIBERIA

Torsten Sachs   Michael Giebels   Julia Boike   Lars Kutzbach

Abstract

The carbon budgets of the atmosphere and terrestrial ecosystems are closely coupled by vertical exchange fluxes of carbon dioxide and methane. However, uncertainties remain especially with respect to high latitude ecosystem and the processes driving their temporally and spatially highly variable exchange of methane with the atmosphere. To address this uncertainty and analyze the complex network of coupled processes and interconnected controls of tundra methane emissions, we conducted intensive field studies on two spatial scales in Northern Siberian tundra. Methane fluxes on the micro-site scale (0.1–100 m^2) were measured in the Lena River Delta from July through September 2006 by closed chambers and were compared to simultaneous ecosystem-scale (1 ha–1 km^2) methane flux measurements by the eddy covariance method at the same study site. Our study adds results from an area that is seriously underrepresented in current efforts to quantify carbon emissions from high latitude ecosystems. Closed chamber measurements of methane fluxes were conducted daily on 15 plots in four differently developed polygon centers and on a polygon rim. Controls on methane emission were identified by a stepwise multiple regression procedure. In contrast to the

relatively low ecosystem-scale fluxes which were mainly controlled by near-surface turbulence and to a lesser extend by atmospheric pressure and soil temperature, fluxes on the micro-site scale were almost an order of magnitude higher at the wet polygon centers and near zero at the drier polygon rim and a high-center polygon. Micro-site-scale methane fluxes varied strongly even within the same micro-sites. The only statistically significant control on chamber-based fluxes was surface temperature in the wet polygon centers, while no significant control was found for the low emissions from the dry sites. The comparison with the eddy covariance measurements hints at the importance of open water surfaces and potential problems of chamber-methods in wet polygonal tundra environments.

3.1 Introduction

In recent decades, methane (CH_4) has increasingly become a focus of studies investigating the carbon cycle and carbon budget as well as the feedback mechanisms increasing greenhouse gas emissions may have on the climate system. Despite these increased efforts, atmospheric concentration data and earth surface emissions still cannot be reconciled and large uncertainties remain with regard to both mechanistic understanding of methane emissions and the distribution and strength of sources and sinks. Even new sources (Walter et al., 2006; Keppler et al., 2006) and mechanisms (Mastepanov et al., 2008; Sachs et al., 2008) are still being identified and discussed. While a general scarcity of data from the Arctic, especially from the extensive Russian tundra areas, is a major factor in this lack of understanding, it is exacerbated by the heterogeneity of the methane sink/source distribution as well as the large variability of methane emissions and the processes controlling these emissions, which vary over different spatial and temporal scales. This heterogeneity contributes to uncertainties in the global methane budget, especially by complicating any attempts at up-scaling emissions from point measurements to larger areas or even global estimates, as small-scale variability can substantially affect the statistics of large-scale variables (von Storch, 2004).

Therefore, measurements of methane fluxes and their controls are required on multiple spatial and temporal scales in order to comprehensively understand methane dynamics (Bubier and Moore, 1994). At key sites, each measurement should ideally be

nested within the footprint of the next larger-scale measurements to develop up-scaling methods in small, verifiable steps.

Closed-chamber techniques are widely used for small-scale measurements and allow for good spatial coverage (Whalen and Reeburgh, 1990; Christensen et al., 1995; Reeburgh et al., 1998; Wickland et al., 2006). However, they represent an intrusive method and can affect the measured variable even if care is taken to avoid the many potential biases this method is prone to. In a nested approach, results can be checked against other methods such as the eddy covariance (EC) technique, thus helping to reduce uncertainties (Fan et al., 1992; Kulmala et al., 2007; Riutta et al., 2007; Fox et al., 2008).

We applied such a nested approach in our investigation of methane emissions from northern Siberian wet polygonal tundra in the Lena River Delta. An eddy covariance system capable of continuous high-resolution methane flux measurements was installed at the site in 2002 and has delivered valuable flux data on the ecosystem scale (Sachs et al., 2008; Wille et al., 2008). Existing closed chamber sites for studies of the effect of microrelief and vegetation on methane emission (Wagner et al., 2003; Kutzbach et al., 2004) were located 700 m south of the tower site in an area that was generally drier and more elevated. Thus, in 2005, fifteen closed chambers were installed at five different micro-sites within the eddy covariance footprint and operated simultaneously to the EC system.

The objectives of this paper are to (1) investigate the spatial variability of methane fluxes from wet polygonal tundra within the eddy covariance footprint, (2) identify the dominant processes and controls governing small-scale methane dynamics, and (3) compare the results to eddy covariance measurements in order to identify differences or similarities in the dominant processes and controls.

3.2 Study area

The study site was located on Samoylov Island near the Russian-German Research Station Samoylov Island, 120 km south of the Arctic Ocean in the southern central Lena River Delta (72°22'N, 126°30'E) (Fig. 3.1). Samoylov Island is located in the active delta landscape, which covers about 65% of the total 32,000 km² delta. During the past
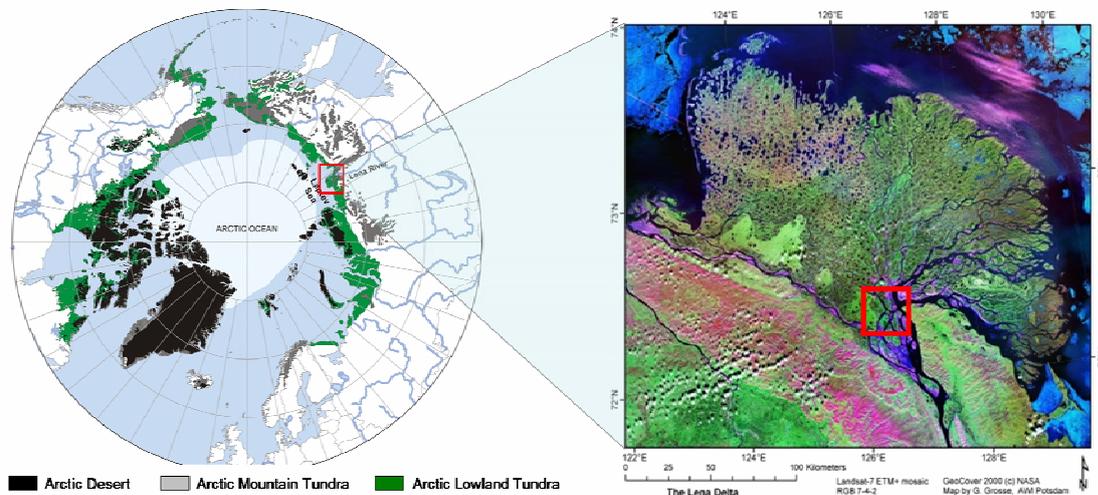
Figure 3.1: (left) Location of the investigation area and vegetation zones in the Arctic (modified after work by UNEP/GRID-Arendal (1996)). **(right)** Location of the study site Samoylov Island in the Lena River Delta (marked by the square (satellite image: Landsat 7 Enhanced Thematic Mapper (on Nimbus 6)+ GeoCover 2000, NASA (Landsat imagery courtesy of NASA Goddard Space Flight Center and U.S. Geological Survey) (Map by G. Grosse, AWI Potsdam))).

ten years, Samoylov Island has been the focus of a wide range of studies on surface-atmosphere gas and energy exchange, soil science, hydrobiology, microbiology, cryogenesis, and geomorphology (Schwamborn et al., 2002; Boike et al., 2003, 2008; Kutzbach et al., 2004, 2007; Liebner and Wagner, 2007; Abramova et al., 2007; Sachs et al., 2008; Wille et al., 2008).

Samoylov Island covers an area of about 7.5 km². The western part of the island (3.4 km²) is a modern floodplain with elevations from 1 to 5 meters above sea level (a.s.l.), which is flooded annually during river break-up. The study site is located in the center of the eastern part of the island (4.1 km²) with elevations from 10 to 16 meters a.s.l. which is composed of sediments of a Late-Holocene river terrace (Fig. 3.2). The surface of the terrace is characterized by wet polygonal tundra with a flat meso-relief and a pronounced regular micro-relief caused by the development of low-center ice wedge polygons. The typical elevation difference between depressed polygon centers and elevated polygon rims is up to 0.5 m (Kutzbach, 2006). The poorly drained and hence mostly inundated centers are characterized by *Typic Historthels*, while *Glacic* or *Typic Aquiturbels* dominate at the dryer but still moist polygon rims (Soil Survey Staff, 1998; Kutzbach et al., 2004). As the summer progresses, these soils typically thaw to a
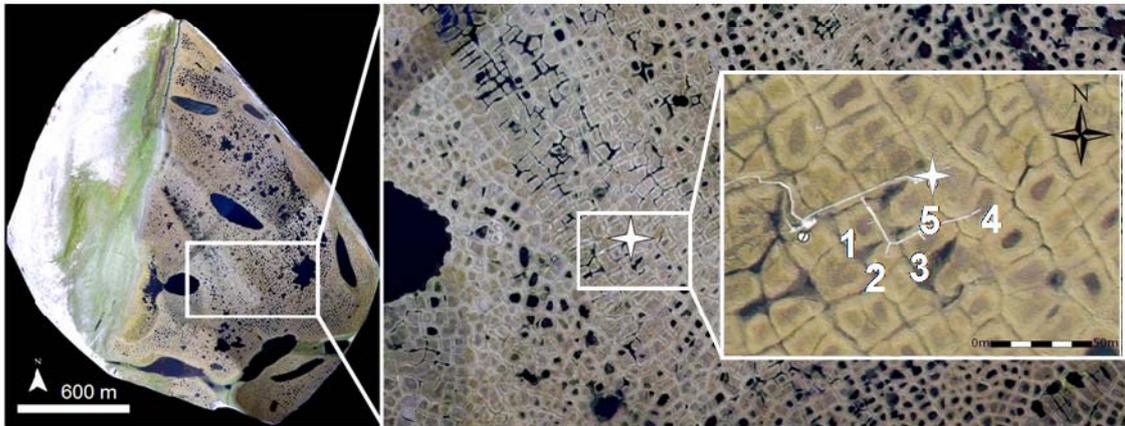
Figure 3.2: Aerial images of the study site. **(left)** Mosaic of aerial images of Samoylov Island taken in August 2007 (Boike et al., 2009). **(right)** The central part of Samoylov Island in August 2007. The asterisk marks the position of the micrometeorological tower. The inset shows the closed chamber study area in direct proximity to the tower. The numbers refer to the micro-sites 1-5.

depth of 30 cm to 50 cm. Hydrophytic sedges as well as mosses dominate the vegetation in the wet polygon centers (Kutzbach et al., 2004). Polygon rims are dominated by mesophytic dwarf shrubs, forbs, and mosses. Surface classification of aerial photographs shows that elevated and dryer areas cover approximately 60% of the tundra surrounding the study site, while depressed and wet polygon centers and troughs cover only about 10%. Open and overgrown water makes up 30% of the area (S. Muster, personal communication).

The climate in the region is arctic continental climate characterized by very low temperatures and low precipitation. Mean annual air temperature at the meteorological station on Samoylov Island was –14.7°C and mean liquid precipitation was 137 mm, ranging from 72 mm to 208 mm in a period from 1999 to 2005 (Boike et al., 2008). Meteorological conditions can change rapidly throughout the growing season depending on the prevailing synoptic weather conditions, which cause either advection of cold and moist air from the Arctic Ocean or warm and dry air from continental Siberia, respectively. The region experiences polar day from 7 May to 8 August and polar night from 15 November to 28 January. Snowmelt and river break-up typically start in the first half of June, and the growing season lasts from mid-June through mid-September. The continuous permafrost in the delta reaches depths of 500 to 600 meters

(Grigoriev, 1960) and is characterized by very low temperatures with the top-of-permafrost temperature on Samoylov being approximately −10°C (Boike et al., 2003).

3.3   Investigation sites

Five different micro-sites (four polygons and a rim) characteristic of the prevalent surface and vegetation features in the eddy covariance fetch were established within 40 m of the EC tower and equipped with boardwalks, wells for water level measurements, and three chamber collars each (Fig. 3.2).

Polygon 1 was a low-center polygon with standing water in the center. The northern side of the polygon rim showed signs of beginning degradation, which might serve as a hydraulic connection to surrounding polygon troughs. Polygon 2 was a high-center polygon with no standing water in the center due to drainage into surrounding thermokarst cracks and troughs. Polygon 3 was a low-center polygon with a massive rim on the western side and a completely degraded rim on the eastern side, where a large thermokarst crack of more than 2 m depth was located. There was standing water in the polygon center throughout most of the growing season. Polygon 4 was a low-center polygon with no apparent rim degradation and no apparent hydraulic connection to surrounding cracks or troughs. It usually maintained the highest water level of all investigated polygon centers. The polygon rim micro-site was underlain by a massive ice wedge and draining into polygon 3 to the east and the crack.

Detailed vegetation cover is given in Table 2.1 (data provided by Merten Minke, 2006). A schematic overview and exemplary photographs of the dominant micro-site types are given in Figure 3.3. The organic layer is about 5 cm thick on polygon rims and about 30 cm in polygon centers. The root density is high within the top 15 cm of the soil and then decreases towards deeper horizons. At our site, the active layer is deeper in low-center polygons (up to 40 cm) than on polygon rims and high-center polygons (about 20 cm). At the climate station 700 m south of the closed chamber sites, this relationship is reversed with a deeper active layer at the top of the polygon rims than in the centers. Generally, a measurable water table is only present in low-center polygons, but high-center polygons and rims remain very moist at least right above the permafrost table as indicated in the figure. Temperature gradients are generally steeper in rims and high-center polygons, which also reach higher surface temperatures than

Table 3.1: Species and percent coverage for each 50x50cm closed chamber plot (data provided by Merten Minke, 2006).

plot	Polygon 1: wet low-center; early degradation — species	%	Polygon 2: well-drained high-center; final stage of degradation — species	%	Polygon 3: wet low center; advanced degradation — species	%	Polygon 4: inundated low-center; no visible degradation — species	%	Polygon 5: polygon rim; no standing water — species	%
1	*Scorpidium scorpidioides*	99	*Hylocomium splendens*	90	*Drepanoladus cf. vernicosus*	50	*Scorpidium scorpidioides*	100	*Hylocomium splendens*	50
	Carex chordorrhiza	10	*Tomentypnum nitens*	10	*Drepanoladus revolvens*	40	*Carex chordorrhiza*	7	*Rhytidium rugosum*	40
	Comarum palustre	1	*Carex concolor*	2	*Carex chordorrhiza*	30	*Carex concolor*	3	*Polytrichum cf. alpinum*	5
	Aulacomnium turgidum	0.5	*Peltigera sp.*	1	*Aulacomnium turgidum*	10	*Comarum palustre*	3	*Carex concolor*	3
	Meesia triquetra	0.5	*Salix glauca or S.reptans*	1	*Carex concolor*	3	*Calliergon giganteum*	0.1	*Aulacomnium turgidum*	1
	Calliergon giganteum	0.1	*Aulacomnium turgidum*	0.5	*Comarum palustre*	2			*Dryas punctata*	1
	Carex concolor	0.1	*Lagotis*	0.1	*Meesia triquetra*	1			*Pyrola rotundifolia*	0.1
			Poa arctica	0.1	*Calliergon giganteum*	0.1			*Astragalus frigidus*	0.5
			Polygonum viviparum	0.1					*Cetraria laevigata*	0.5
									Peltigera sp.	0.5
									Parrya nudicaulis	0.1
									Saussurea sp.	0.1
2	*Scorpidium scorpidioides*	100	*Hylocomium splendens*	80	*Drepanoladus revolvens*	85	*Scorpidium scorpidioides*	100	*Rhytidium rugosum*	60
	Carex chordorrhiza	8	*Tomentypnum nitens*	20	*Aulacomnium turgidum*	10	*Carex chordorrhiza*	7	*Hylocomium splendens*	30
	Carex concolor	1	*Carex concolor*	1	*Carex chordorrhiza*	10	*Carex concolor*	3	*Carex concolor*	3
	Comarum palustre	1	*Aulacomnium turgidum*	1	*Carex concolor*	5	*Comarum palustre*	3	*Polytrichum cf. alpinum*	2
	Meesia triquetra	0.1	*Dryas punctata*	0.1	*Comarum palustre*	5	*Calliergon giganteum*	0.1	*Astragalus frigidus*	1
	Calliergon giganteum	0.1	*Salix glauca or -reptans*	0.1	*Meesia triquetra*	3			*Peltigera sp.*	1
			Poa arctica	0.1	*Calliergon giganteum*	0.1			*Pyrola rotundifolia*	0.5
			Polygonum viviparum	0.1					*Cetraria laevigata*	0.1
									Dactylina arctica	0.1
									Poa arctica	0.1
									Saussurea sp.	0.1
3	*Scorpidium scorpidioides*	99	*Hylocomium splendens*	85	*Drepanoladus revolvens*	95	*Scorpidium scorpidioides*	100	*Hylocomium splendens*	99
	Carex chordorrhiza	3	*Aulacomnium turgidum*	5	*Carex concolor*	10	*Carex chordorrhiza*	10	*Carex concolor*	5
	Comarum palustre	2	*Peltigera sp.*	5	*Aulacomnium turgidum*	5	*Carex concolor*	3	*Pyrola rotundifolia*	2
	Meesia triquetra	0.5	*Tomentypnum nitens*	5	*Carex chordorrhiza*	5	*Comarum palustre*	2	*Rhytidium rugosum*	2
	Calliergon giganteum	0.1	*Dryas punctata*	1	*Comarum palustre*	1			*Astragalus frigidus*	1
	Carex concolor	0.1	*Carex concolor*	0.5	*Calliergon giganteum*	0.1			*Peltigera sp.*	1
	Drepanoladus cf. vernicosus	0.1	*Equisetum arvense*	0.1	*Meesia triquetra*	0.1			*Aulacomnium turgidum*	0.5
			Hierochloe pauciflora	0.1					*Cetraria laevigata*	0.5
			Polygonum viviparum	0.1					*Dactylina arctica*	0.5
			Salix glauca or S.reptans	0.1					*Draba pilosa*	0.1
									Polytrichum cf. alpinum	0.1
									Saussurea sp.	0.1
									Stereocaulon sp.	0.1
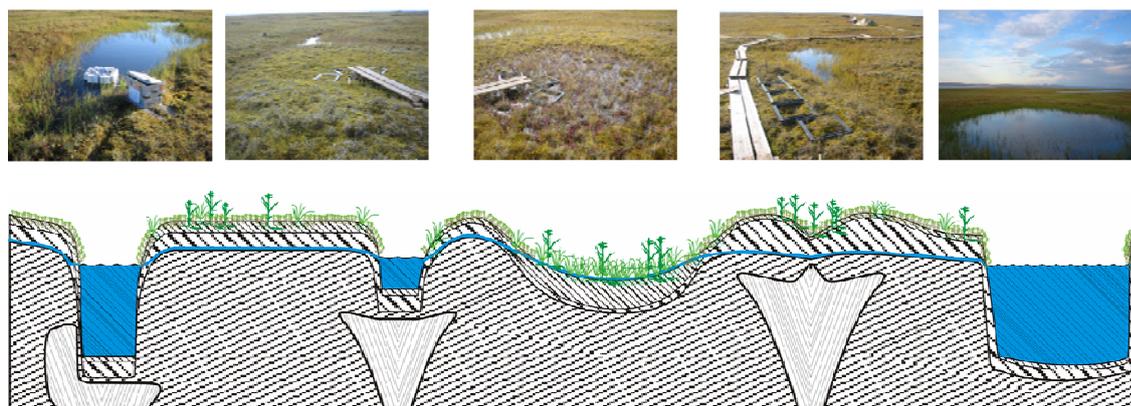
Figure 3.3: Schematic overview of the dominant micro-sites. From left to right: thermokarst crack (not explicitly covered in this study), high-center polygon (Polygon 2) surrounded by cracks or troughs, wet low-center polygon (Polygon 1, 3, and 4), polygon rim (Polygon 5), and pond/lake (not explicitly covered). The dense diagonal hatching from bottom left to top right marks the permafrost. The wider diagonal hatching in the opposite direction shows mineral soil layers within the seasonally thawed active layer and the denser diagonal hatching on the top denotes the organic layer. The water level is represented by the blue line.

water-inundated low-center polygons. The CH_4 concentration in the noninundated soil is close to ambient in the aerobic soil horizons and increases strongly just above the permafrost table, where anaerobic conditions dominate (S. Liebner, personal communication).

3.4 Methods

3.4.1 Closed chamber set-up and measurements

Three 50 cm x 50 cm PVC chamber collars with a water-filled channel as a seal were installed in each of the four polygon centers and along the rim and inserted 10–15 cm into the active layer. Chambers were made of opaque PVC and clear PVC, respectively, for light and dark measurements. Chamber volume was 12.5 l at the high-center and rim micro-sites and 37.5 l at the other sites where higher vegetation did not allow for the use of small chambers.

Manual chamber measurements at all 15 plots were made daily from 13 July through 19 September 2006 with both clear and opaque chambers, resulting in 6 measurements per day and micro-site. Sample air was drawn from a port on top of the chamber every 45 s for eight to ten minutes for simultaneous analysis of CO_2, CH_4, and water vapor using a photo-acoustic infrared gas spectrometer Innova 1412 with optical

filters UA0982 for CO$_2$, UA0969 for CH$_4$, and SB0527 for water vapor (INNOVA AirTech Instruments, Denmark). A membrane pump was connected to two other ports and circulated chamber headspace air through perforated dispersive tubes for mixing.

Because of water interference with the CH$_4$ optical filter, sample air was dried prior to entering the analyzer using 0.3 nm molecular sieve (beads, with moisture indicator; Merck KGaA, Darmstadt, Germany). Temperature and pressure inside the chamber were logged continuously by a MinidanTemp 0.1° temperature logger (Esys GmbH, Berlin, Germany) and the Innova 1412, respectively.

Additional variables measured at the eddy covariance system and an automated long-term monitoring station 700 m south of the EC tower include air temperature, relative humidity, incoming and outgoing solar and infrared radiation, photosynthetically active radiation (PAR), barometric pressure, precipitation, and soil temperature at various depths.

Manual measurements at each micro-site during chamber deployment included thaw depth using a steel probe, soil temperatures in 5 cm depth intervals, and water level.

3.4.2 Non-linear flux calculation

The most widely used method for calculating fluxes from the change of concentration in the chamber headspace over time is by linear regression under the assumption that by keeping chamber closure time short, the concentration change is approximately linear. However, Kutzbach et al. (2007) showed that linear regression is frequently not appropriate based on four sets of closed chamber CO$_2$ data, including those gathered during the measurement campaign reported on here. We found the conclusions for the CO$_2$ data to also hold for CH$_4$ (e.g. in Fig. 3.4) and therefore used the non-linear exponential regression model proposed by Kutzbach et al. (2007) to describe CH$_4$ evolution over time in the chamber headspace:

$$c(t) = f_{\exp}(t) + \varepsilon(t) = \beta_1 + \beta_2 \exp(\beta_3\, t) + \varepsilon(t) \qquad (1)$$

where $\varepsilon(t)$ is the residual error at measurement time t.
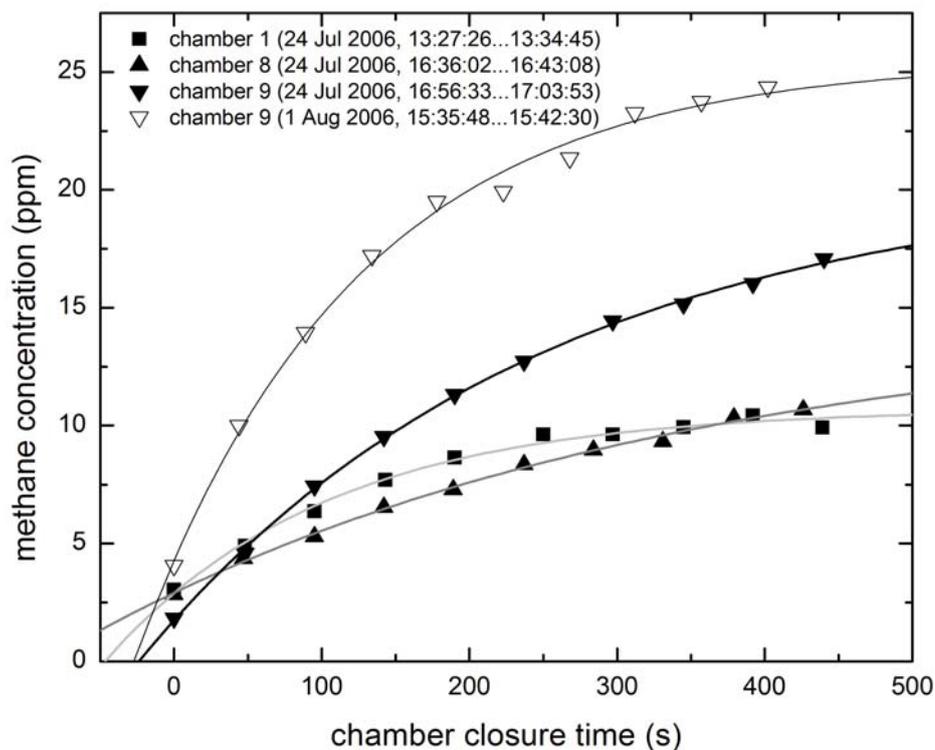
Figure 3.4: Examples for non-linear evolution of CH_4 concentration in the closed chamber headspace for different micro-sites and dates. The exponential fits of the form $cCH_4 = \beta_1 + \beta_2 \exp(\beta_3 t)$ are also given for each concentration curve.

At the beginning of the measurement, gas fluxes are assumed to be least disturbed by chamber deployment, and thus, the initial slope of the regression curve $f_{exp}'(t_0) = (\beta_2 \beta_3)$ is used for flux calculation:

$$F_{CH4}(t_0) \;=\; \frac{dc}{dt}(t_0)\frac{p\,V}{R\,T\,A} \;=\; f'_{exp}(t_0)\frac{p\,V}{R\,T\,A} \;=\; \beta_2\,\beta_3\,\frac{p\,V}{R\,T\,A} \qquad (2)$$

where p is air pressure, R is the ideal gas constant, T is the temperature (in Kelvin) and V and A are the volume and basal area of the chamber.

Calculated fluxes were thoroughly screened and all fluxes with a residual standard deviation greater than 0.3 ppm were excluded from further analysis.

3.4.3 Model development

Measurements were summarized by averaging the six individual measurements at each micro-site and day. In order to identify statistically significant explanatory variables for the measured methane fluxes, we used multiple linear regressions, starting with a descriptive regression model including all available variables:

$$F_{CH4} = c_0 + c_1 \cdot x_1 + c_2 \cdot x_2 + ... + c_n \cdot x_n \qquad (3)$$

We then eliminated all non-significant variables in a stepwise procedure:

First, data were tested for multi-collinearity following Schuchard-Ficher (1982). If multi-collinearity was present, variables were dropped until all remaining variables were approximately orthogonal. Next, the residuals of the reduced model were tested for autocorrelation using the Durbin-Watson test (or d-test).

If no autocorrelation was found, the multiple regression coefficient of determination R^2 was tested for significance using the F-test:

$$F(df_1 = q, df_2 = n - q - 1) = \frac{R^2 \cdot (n - q - 1)}{q \cdot (1 - R^2)} \qquad (4)$$

where df indicates degrees of freedom, n is the number of data points and q is the number of predictor variables.

If R^2 was significant, the correlation coefficients c ($i = 1, 2, ..., n$) were tested for significance using the t-test. The reduced model that passes these tests provides predictors of the methane flux with a statistically significant explanatory power, i.e. it identifies not necessarily the best fit to the data but the significant and most likely process drivers.

After the parameter selection process, the resulting regression model was fitted to the means of the six replicate measurements per day and micro-site using the inverse square of the mean standard error of these six measurements as a weight, such that points with large errors were given less weight in the fitting process. Cumulative CH$_4$ fluxes over the measurement period were calculated by integrating the modeled hourly
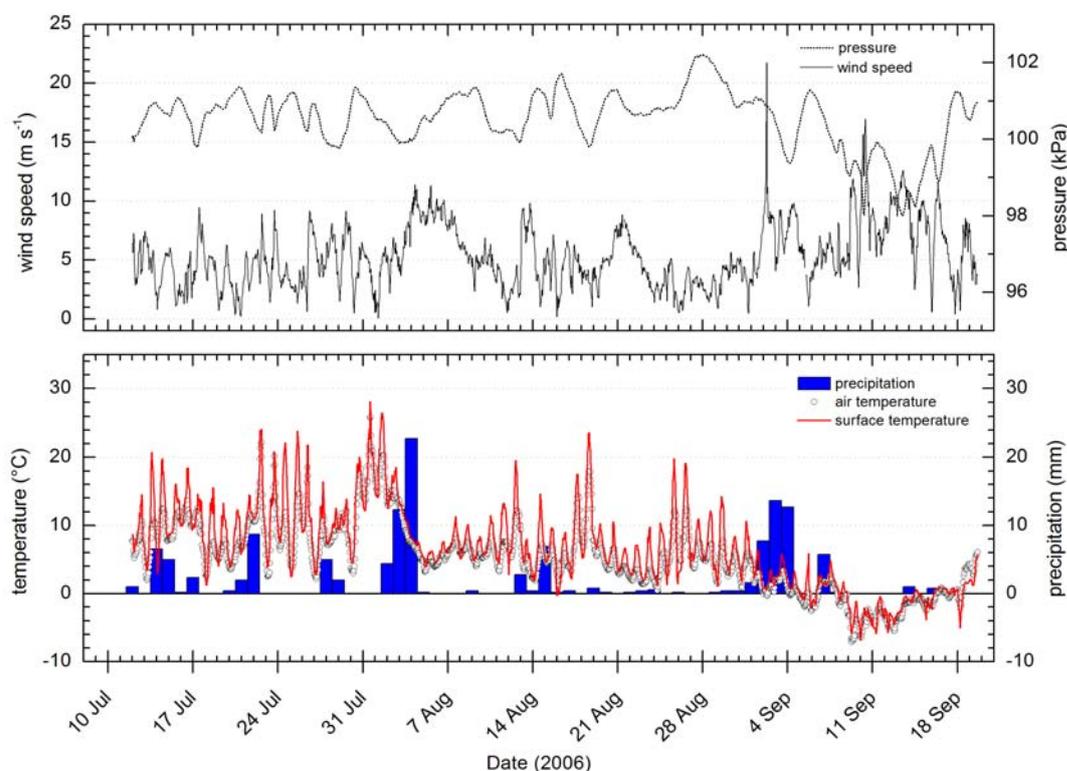
Figure 3.5: Meteorological conditions during the measurements campaign. **(top)** hourly wind speed and atmospheric pressure measured at the eddy covariance tower. **(bottom)** daily precipitation measured at the long-term climate station 700 m south of the closed chamber site, hourly air temperature in 2 m height measured at the eddy covariance tower, and surface temperature calculated from outgoing long-wave radiation using the Stefan-Boltzmann equation.

flux time series. The uncertainty of the cumulative fluxes was assessed by error propagation using the RMSE of the regression models as uncertainty indicator for the hourly modeled flux values.

3.5 Results

3.5.1 Meteorology

At the beginning of the measurement period, air temperatures had just dropped from a daytime summer record of up to 28.9°C on 11 July (mean 18.3°C, minimum 8.9°C) to well below 10°C (Fig. 3.5). Fluctuations between daytime and nighttime temperatures were strong throughout July with mean temperatures rising from 8.4°C in the first week of measurements to 12.2°C in the third week. The maximum daily mean temperature

during the measurements period was reached on 31 July at 18.5°C. A storm system with heavy precipitation of up to 23 mm per day and prolonged periods of mean hourly wind speeds around 10 m s^{-1} caused daily mean temperatures to drop sharply to as low as 4.2°C in the first week of August. Mean daily temperatures never exceeded 11.9°C for the remaining season and remained between 2.3°C and 11.9°C during August. Another storm system in the first week of September yielded 34 mm of precipitation within three days and wind speeds exceeding 20 m s^{-1}. Temperatures continued to decrease and reached a daily minimum at –5.2°C on 9 September. Mean daily temperature was well below zero for the entire week from 8 September to 15 September and caused the mean September temperature (1 September – 19 September) to be below freezing despite increasing temperatures during the last week of the measurement period. The second week of September was characterized by extremely low atmospheric pressure (down to 98 kPa) and frequent snow storms with wind speeds above 10 m s^{-1}. Snow started to accumulate on 12 September and reached depths of 8–10 cm in polygon centers and 2–6 cm on elevated areas, but all snow had disappeared on 18 September after advection of warmer air from the south. By mid-September, all water bodies except for the large thermokarst lakes were covered with ice up to 8 cm thick and soils were frozen up to approximately 10 cm depth. Long-term temperature data are available from Tiksi, which is located 110 km south-east of Samoylov Island but characterized by very similar temperatures. Temperature conditions in 2006 were within ±1°C of the long-term average in July (7°C), August (7°C), and September (1°C). The average daily wind speed was 5.3 m s^{-1} during the study period, which is 0.6 m s^{-1} higher than in 2003 and 2004 (Kutzbach, 2006). Winds from east southeast were clearly predominant, but west-northwesterly and southern winds also occurred frequently (data not shown).

3.5.2 Methane fluxes and controls

Fluxes were averaged across six measurements per micro-site and day (two measurements on each of three plots per micro-site) and are reported with the standard deviation as a measure of within-site spatial variability and the averaged standard error of the measurements (Fig. 3.6). In general, methane emission was similar among the wet and inundated low-center polygons and differed from fluxes at the high-center and rim micro-sites by an order of magnitude. At the low-center polygons, the
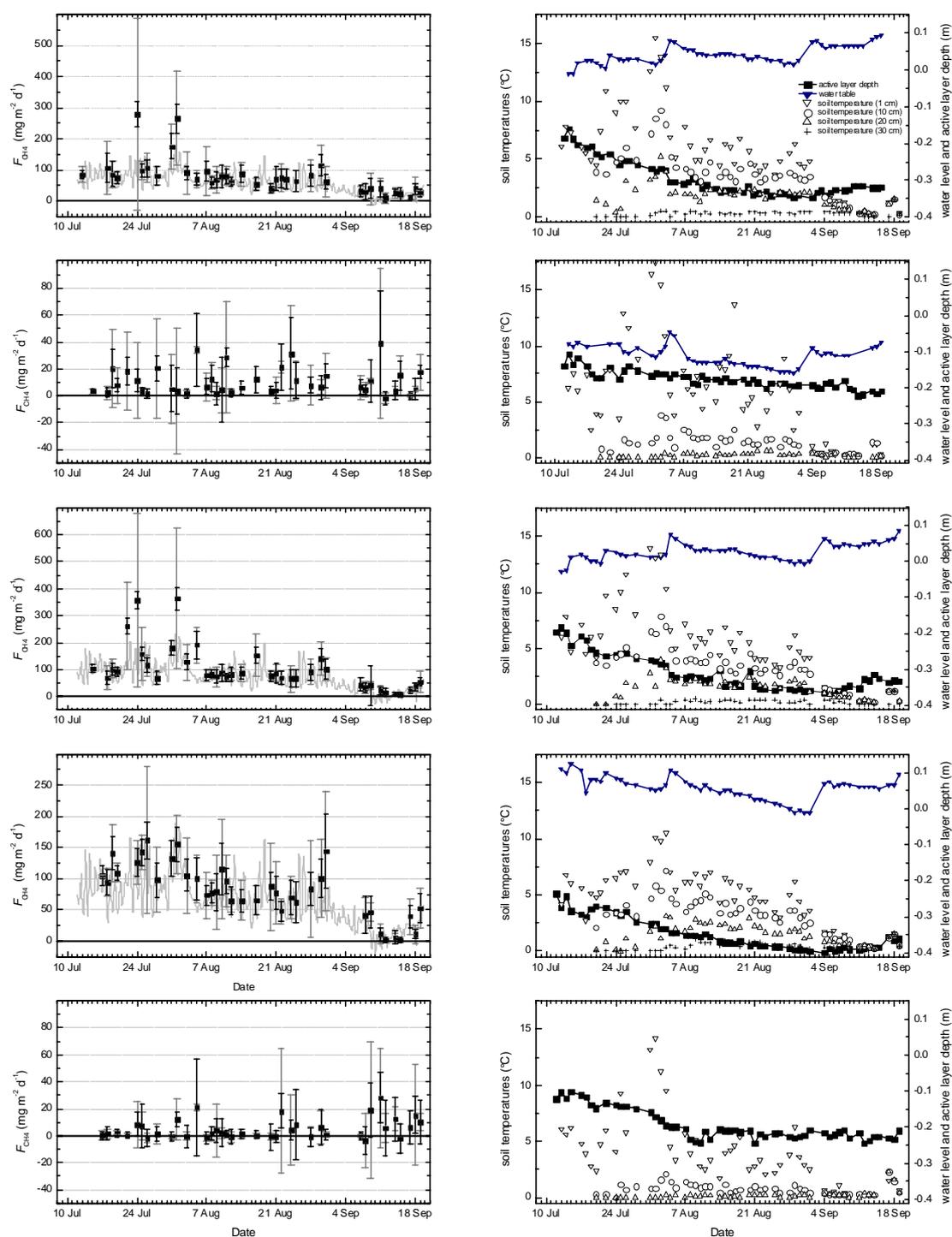
Figure 3.6: (left) from top to bottom: closed chamber methane fluxes from micro-sites 1–5. Black error bars denote the mean of the standard error of each of the six replicate measurements per micro-site. Grey error bars denote the standard deviation of the replicate measurements within a micro-site, providing information about the spatial variability. The grey line shows the modeled fluxes for micro-site 1, 3, and 4. **(right)** water table, active layer depth, and soil temperatures in 1, 10, 20, and where possible 30 cm depth for each of the micro-sites.

monthly averaged emissions decreased by about 30% from July to August and by about 70% from August to September.

At the wet and low-centered Polygon 1 (Fig. 3.6a), the average methane flux during the measurement period was 77.88 mg m^{-2} d^{-1} decreasing from a July average of 121.16 mg m^{-2} d^{-1} to 83.81 mg m^{-2} d^{-1} in August and 27.69 mg m^{-2} d^{-1} in September. The maximum methane flux occurred on 24 July at 278.40 ± 307.18 mg m^{-2} d^{-1} (standard error: 39.34 mg m^{-2} d^{-1}), when surface temperatures exceeded 22°C and a day after air temperatures exceeded 20°C. The minimum flux was recorded on 12 September at 9.33 ± 15.77 mg m^{-2} d^{-1} (standard error: 14.08 mg m^{-2} d^{-1}) during the frost period. The water level in this polygon never dropped below the surface during the entire measurement period and ranged from 0 to 9.5 cm above the surface. Peak water levels were reached after precipitation events at the beginning of August and the beginning of September as well as after snow melt and thawing at the end of the campaign. The active layer depth gradually increased from 18 cm at the beginning of the measurement period to a maximum of 35 cm, which was reached on 4 September. During the frost period a refreezing from the bottom decreased the active layer depth to 32 cm by 19 September.

At the relatively "dry" and high-centered Polygon 2 (Fig. 3.6b), the average methane flux during the measurement period was significantly lower at 10.49 mg m^{-2} d^{-1} with no clear seasonal trend from a July average of 9.43 mg m^{-2} d^{-1} to 11.28 mg m^{-2} d^{-1} in August and 10.05 mg m^{-2} d^{-1} in September. The maximum methane flux occurred on 11 September at 39.07 ± 55.28 mg m^{-2} d^{-1} (standard error: 38.75 mg m^{-2} d^{-1}), and the minimum flux was recorded on 12 September at -1.87 ± 4.13 mg m^{-2} d^{-1} (standard error: 5.12 mg m^{-2} d^{-1}). The water level in this polygon remained slightly above the permafrost table and never reached the surface during the entire measurement period. It ranged from 16 cm to 4.5 cm below the surface and peak water levels were reached after the precipitation event at the beginning of August and after thawing towards the end of the campaign. The active layer depth increased less than in the low-center polygons from 14 cm to 21 cm. No clear refreezing from the bottom was observed.

The wet and low-centered Polygon 3 (Fig. 3.6c) showed the largest methane emissions. The average methane flux during the measurement period was 99.98 mg m^{-2} d^{-1} decreasing from a July average of 150.93 mg m^{-2} d^{-1} to 110.58 mg m^{-2} d^{-1} in August

and 28.91 mg m^{-2} d^{-1} in September. The maximum methane flux occurred on 1 August at 363.82 ± 259.81 mg m^{-2} d^{-1} (standard error: 42.39 mg m^{-2} d^{-1}) when daytime temperature exceeded 20°C and a day after daytime temperatures had reached 26°C. The minimum flux was recorded on 15 September at 8.81 ± 7.29 mg m^{-2} d^{-1} (standard error: 7.29 mg m^{-2} d^{-1}) during the frost period. Except on the first two days of measurements, the water level in this polygon never dropped below the surface and ranged from 0 to 8.5 cm above the surface. Peak water levels were reached after precipitation events at the beginning of August and the beginning of September as well as after snow melt and thawing at the end of the campaign. The active layer depth gradually increased from 19 cm at the beginning of the measurement period to a maximum of 37 cm, which was reached on 4 September. During the frost period a refreezing from the bottom decreased the active layer depth to 33 cm by 19 September.

At the inundated and low-centered Polygon 4 (Fig. 6d), the average methane flux during the measurements period was 80.75 mg m^{-2} d^{-1} decreasing from a July average of 123.21 mg m^{-2} d^{-1} to 87.76 mg m^{-2} d^{-1} in August and 23.49 mg m^{-2} d^{-1} in September. The spatial variability in this polygon was much lower than in Polygon 1 and 3, as were the peak fluxes. The maximum methane flux occurred on 26 July at 161.58 ± 118.10 mg m^{-2} d^{-1} (standard error: 29.91 mg m^{-2} d^{-1}) when surface temperatures exceeded 21°C. The minimum flux was recorded on 15 September at 1.78 ± 3.34 mg m^{-2} d^{-1} (standard error: 5.03 mg m^{-2} d^{-1}) during the frost period. This polygon had the highest water level after precipitation events (up to 12.5 cm) and throughout July but also showed a more pronounced drying in August, causing the water level to drop slightly below the surface at the end of August. In September, the water level resembled that of Polygon 1. The active layer depth gradually increased from 24 cm at the beginning of the measurement period to a maximum of 40 cm, which was reached on 4 September. During the frost period a refreezing from the bottom decreased the active layer depth to 36 cm by 19 September.

At the elevated and well-drained polygon rim (Fig. 6e), the average methane flux during the measurements period was the lowest of all sites at 4.94 mg m^{-2} d^{-1}, increasing from a July average of 2.14 mg m^{-2} d^{-1} to 4.07 mg m^{-2} d^{-1} in August and 9.15 mg m^{-2} d^{-1} in September. The maximum methane flux occurred on 11 September at 28.22 ± 36.86 mg m^{-2} d^{-1} (standard error: 18.60 mg m^{-2} d^{-1}) and the minimum flux was

Table 3.2: Results of the error-weighted linear regressions given by y = a + bx.

Polygon	Parameter	Value	Error	t-value	p>|t|	[a]LCI	[b]UCI	R	[c]R²$_{adj}$	[d]RMSE (mg m^{-2} d^{-1})
1	a (mg m^{-2} d^{-1})	23.165	4.305	5.381	<0.0001	14.435	31.895	0.82	0.66	1.162
	b (°C^{-1})	5.137	0.513	10.015	<0.0001	4.097	6.178			
3	a (mg m^{-2} d^{-1})	21.422	3.355	6.386	<0.0001	14.625	28.219	0.85	0.72	1.803
	b (°C^{-1})	7.549	0.425	17.777	<0.0001	6.688	8.409			
4	a (mg m^{-2} d^{-1})	22.255	2.280	9.762	<0.0001	17.627	26.883	0.91	0.83	1.330
	b (°C^{-1})	5.957	0.335	17.769	<0.0001	5.277	6.638			

[a]LCI is the lower confidence interval, [b]UCI is the upper confidence level, [c]R²$_{adj}$ is the adjusted R² taking into consideration the number of explanatory variables and [d]RMSE is the root mean squared error.

recorded on 8 September at –3.57 ± 20.31 mg m^{-2} d^{-1} (standard error: 10.14 mg m^{-2} d^{-1}) when temperatures dropped below freezing. Typically, the standard error of the measurements was around ± 25 mg m^{-2} d^{-1} for Polygon 1, 3, and 4, and about ± 10 mg m^{-2} d^{-1} for the drier micro-sites. The spatial standard deviation was around ± 43 mg m^{-2}d^{-1} in Polygon 1, 3, and 4, and about ± 10…15 mg m^{-2} d^{-1} at the drier sites. Polygon 4 showed less spatial variability than Polygon 1 and 3. Except on the polygon rim, spatial standard deviation decreased strongly towards the end of the season, most pronouncedly in the low-center polygons.

It was not possible to construct multidimensional regression models with independent and significant parameters. The predictor variable with the highest explanatory power within the final one-dimensional model for the low-center polygons was surface temperature (Table 3.2; Fig. 3.7). Except for the underestimation of the extreme flux peaks on 24 July and 1 August at Polygon 1 and Polygon 3, the modeled methane flux agreed well with measured fluxes (mean RMSE = 1.43 mg m^{-2} d^{-1}). The best fit (RMSE = 1.33 mg m^{-2} d^{-1}) was obtained at Polygon 4, which did not show any major outliers in the flux data.

At Polygon 2 (high-center) and at the polygon rim, very low methane concentrations in the closed chamber system frequently caused the analyzer to reach its detection limit, resulting in noisy data and a high exclusion rate during flux calculation. No statistically significant correlation with any of the observed environmental parameters was found.

Cumulative fluxes during the measurement period were similar at Polygon 1 and 4 with 3.95 ± 0.0020 g m^{-2} and 4.26 ± 0.0023 g m^{-2}, respectively. Polygon 3 emitted
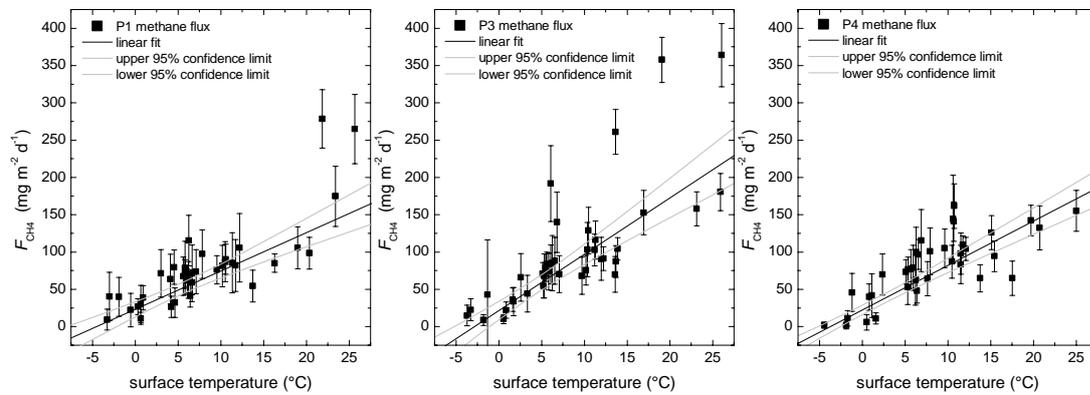
Figure 3.7: Standard-error weighted linear regression models with surface temperature as the best predictor for methane fluxes from polygons 1, 3, and 4.

about 25% more methane than Polygon 1 amounting to a cumulative flux of 4.93 ± 0.0031 g m^{-2}. At the drier micro-sites, cumulative fluxes were 0.72 ± 0.078 g m^{-2} at the high-center site and 0.34 ± 0.047 g m^{-2} at the rim site.

3.6 Discussion

3.6.1 Environmental controls on micro-site methane emission

The single parameter with the highest explanatory power for the observed CH$_4$ fluxes and statistical significance at the three low-center polygon sites was surface temperature while no significant predictor was found for the high-center and rim site flux data, which were often low enough to reach the detection limit of the analyzer. Many studies found relationships between soil temperature in different depths and methane flux (Whalen and Reeburgh, 1988; Bubier, 1995; Christensen et al., 1995; Bellisario et al., 1999; Nakano et al., 2000), but only few (Hargreaves et al., 2001) identified surface temperature as a predictor of methane flux or even measured it. This finding might be due to our strict exclusion criteria and the significantly dampened variability of soil temperatures at our site. A shallow active layer and cold permafrost reduce short-term variability already close below the surface, and thus the highly variable surface temperature is better suited to predict highly variable methane fluxes than soil temperature with little variability. Nevertheless, soil temperatures are closely correlated

with surface temperature, and thus surface temperature can be seen as a master variable representing the entire soil thermal regime.

Temperature directly influences microbial activity (Arrhenius, 1909; Conrad, 1989) and several studies found relationships between soil or peat temperature and methane flux (Whalen and Reeburgh, 1988; Bubier, 1995; Christensen et al., 1995; Bellisario et al., 1999; Nakano et al., 2000), while others did not find a relationship (Wickland et al., 2006; Wagner et al., 2003). In principal, a temperature change affects both methanogens and methanotrophs and thus, its net effect on methane flux could be expected to cancel out. However, microbial populations on Samoylov Island were found to be well adapted to their environment and in particular, methanotrophic bacteria are characterized by lower temperature optima (Liebner and Wagner, 2007). With methanotrophs more sensitive to increased temperatures, the balance can be expected to shift towards more methane production at higher temperatures.

Kutzbach et al. (2007) found surface temperature and not soil temperature as the best predictor variable for ecosystem respiration at the same study site, which was explained by the importance of above-ground plant respiration. Vegetation might also explain the controlling influence of surface temperature in this study if surface temperature is seen as an indicator for plant productivity. Vegetation plays an important role in the methane cycle, supplying substrate for methanogens, in some cases (e.g. sedges) oxygen for methanotrophs, and a conduit for methane release to the atmosphere (Morrissey et al., 1993; Whiting and Chanton, 1993; Bubier, 1995; Schimel, 1995; Bellisario et al., 1999; King et al., 1998, 2002; Joabsson and Christensen, 2001). At our site, plant-mediated methane transport was found to account for 27…66% of overall methane fluxes (Kutzbach et al., 2004). We did not find significantly different emission rates between measurements with clear chambers and those with opaque chambers, suggesting that there was no stomatal effect in plant-mediated methane flux.

Another effect of increased temperatures is decreasing solubility of methane in the water inundating the low-center polygon, thus resulting in increased diffusion of methane from the water column into the atmosphere. For example, at the typical thaw depth of 30 cm in a water-saturated polygon center, with an assumed porosity of 0.7 and a maximum CH$_4$ saturation of the water column, a temperature change of 1.5°C (over the entire depth) leads to an additional loss of about 272 mg CH$_4$ m^{-2} d^{-1}.

While methane emission was found to increase with higher water levels in many studies (e.g. Friborg et al., 2000; Suyker et al., 1996; Wagner et al., 2003), there was no correlation between water level and methane emission at our site. This may be due to the fact that in low-center polygons, where most of the methane was emitted, the water level remained at or above the soil surface at all times and thus fluctuations in water level did not change the ratio of oxic/anoxic soil column. In fact, the dampened methane emission dynamics at Polygon 4, which had the highest water level during the measurement period, suggests that water levels above the surface may actually hinder methane emission by submerging vegetation and presenting a barrier to both soil-diffusive flux and plant-mediated flux. Bellisario et al. (1999) also found an inverse relationship between water table and methane flux but did not discuss the finding further. Zona and Oechel (2008) found that in certain conditions, a drop in water table caused increased methane flux in a large-scale manipulation experiment in Arctic tundra in Barrow, Alaska.

Increased emissions from the polygon rim and high-center micro-sites coincided more with heavy precipitation and the transient rises in water levels. This may be due to a change in the distribution of the anoxic/oxic fraction of the soil column which favours methane production over methane consumption for as long as the water level is elevated. Lower temperatures usually accompanying precipitation events may also inhibit methane oxidation in the upper soil layers, further shifting the balance towards methane production. This is supported by Whalen and Reeburgh (1996) who found the lowest methane oxidation rates in boreal soils during experiments combining high moisture contents and low temperatures. Another effect of precipitation could be an increased advective flux of methane, as water percolates down into the pore space and displaces methane-enriched pore air.

3.6.2 Comparison of closed chamber vs. eddy covariance methane fluxes and their controls on different scales

Simultaneous eddy covariance measurements of methane flux at the same site are described in Sachs et al. (2008) and – in combination with the results reported here – constitute the first study of methane emission from a Siberian arctic tundra site on different but nested scales.
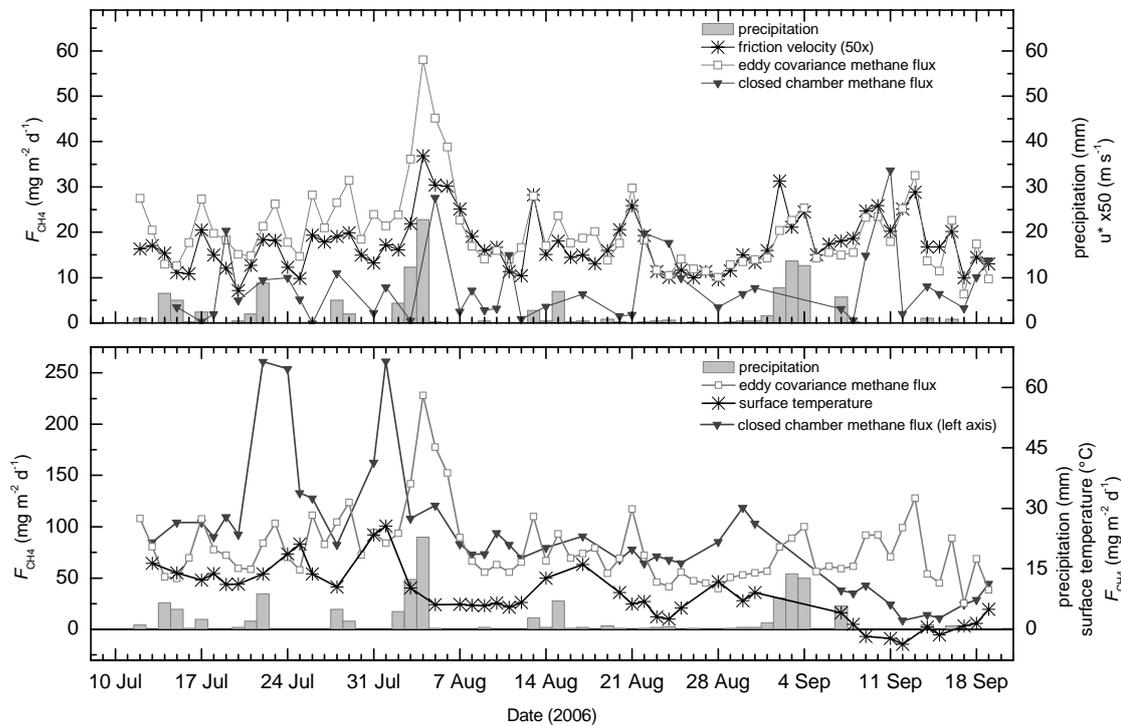
Figure 3.8: Comparison of closed chamber vs. eddy covariance methane fluxes and the dominant controls. **(top)** closed chamber methane fluxes from micro-sites 2 and 5 are extremely low and peaks tend to coincide with peaks in the eddy covariance flux time series, which is best predicted by near-surface turbulence u_*. **(bottom)** closed chamber methane fluxes from micro-sites 1, 3, and 4 are at least an order of magnitude larger (left axis) than those from micro-sites 2 and 5 and also several times larger than those obtained by eddy covariance. Their seasonal dynamics do not match that of the eddy covariance time series and the best predictor of these chamber-based fluxes is surface temperature.

The comparison of micro-site fluxes from closed chamber data and ecosystem-scale fluxes of the eddy covariance system (Sachs et al., 2008) reveals differences both in terms of the dominant controls on methane flux as well as the seasonal variation of the fluxes (Fig. 3.8). On the ecosystem scale, no clear seasonal course was visible, although maximum fluxes did occur during the first week of August. On the micro-site scale, however, low-center polygons showed a decrease of methane emission from July to August by about 30% and a pronounced decrease from August to September by 70%, which is more in line with most studies (e.g. Whalen and Reeburgh, 1988; Christensen et al., 1998; Wagner et al., 2003). The drier micro-sites, on the other hand, did not show any seasonal course and thus appear more comparable to the seasonal dynamics on the ecosystem scale.

In addition to the differing seasonal dynamics, peak methane emissions on the different scales did not occur on the same dates. Ecosystems-scale emission peaks were usually associated with high wind speed, low atmospheric pressure, and precipitation events, and the best predictor of ecosystem-scale methane emission was near-surface turbulence. The very few identifiable peaks at the drier micro-sites also coincide with these weather conditions, while emission peaks at low-center polygons typically occurred during warm and dry days. At the end of the season, methane fluxes on the different scales diverge completely, with ecosystem-scale and drier micro-site fluxes increasing during the last week while low-center polygon emissions reached their minima during the frost period.

To reconcile the results from these two different scales, we developed a conceptual model that includes the prevalent micro-site types in the eddy covariance footprint, not all of which were included in this closed chamber investigation, as well as the following two scenarios for environmental conditions:

(1)   high temperatures and incident radiation, high pressure system, no precipitation, moderate wind speed ("good weather")

(2)   low temperatures, cloudy sky, low pressure system, precipitation and high wind speed ("storm system").

Very wet polygon center (micro-sites 1, 3, and 4)

Under scenario (1) increased temperatures result in increased microbial activity, increased diffusive methane loss from the water column, and increased plant productivity, which in turn provides methanogens with more substrate, further improving methane production. Longer warm periods increase evaporation and cause the water table to fall which exposes previously submerged vegetation and results in more plants being able to transport methane to the atmosphere.

Under scenario (2) decreased temperatures have a negative effect on methane production and emission. Additionally, precipitation and rising water tables submerge vegetation that would otherwise transport methane from the CH_4-producing horizons to the atmosphere. Stronger winds could presumably cause some methane ebullition; however, methane bubbles are likely to get trapped in the dense vegetation characterizing low-center polygons. A possible transport mechanism resulting in

increased emissions under high wind conditions would be convective transport induced by the Venturi-effect, where methane is sucked out of the rhizosphere through dead stems. However, this mechanism is more likely to be relevant during senescence and in winter. The overall effect of the "bad weather" scenario thus depends on the state of the vegetation: during summer, scenario (2) may well result in decreased methane emission from this type of micro-site while during fall and winter it may increase emissions.

Polygon rims and high-center polygons (micro-sites 2 and 5)

Polygon rims and high-center polygons appear to behave similarly despite strongly differing soil conditions (i.e. cryoturbated mineral soils on the rims vs. organic layers and peat in the high-center). Higher temperatures do not affect the methanogenic communities as much as in low-center polygons since these are mostly closer to the permafrost table where temperatures are dampened. Higher temperatures might increase the diffusive flux of methane but at the same time, drying of pore space and an increasing fraction of air-filled pores decreases the anaerobic soil volume needed for methane production. In addition, the anaerobic zone of methane production is usually deeper than the root horizon, and thus the net effect of increased temperature at drier sites is either negligible or at most a slight decrease in emissions.

Under scenario (2), however, colder temperatures inhibit methanotrophic activity in the upper soil layers, where the temperature optimum was found to be 21°C (Liebner and Wagner, 2007), while not affecting the deeper layers of methane production. The most pronounced effect is expected to be that of precipitation and temporarily rising water levels which shift the distribution of aerobic/anaerobic soil volume towards anaerobic conditions, favoring methane production. At the same time, water percolating down into the pore space will displace methane left in those pores and increase the advective flux. The net effect is a transient increase in methane production and emission from these micro-sites.

Open water surfaces

Open water surfaces are an important feature of the polygonal tundra and include relatively small but deep thermokarst cracks as well as ponds and larger lakes. Only exploratory closed chamber measurements were conducted on open water surfaces in

Table 3.3: Surface classes and average August methane emissions in the eddy covariance footprint. The area-weighted chamber fluxes add up to the flux measured by eddy covariance.

Surface class	Area coverage (%)	CH4 emission (August average)	Total flux (mg m^{-2} d^{-1})	Source of emission rate
Very wet soils (inundated low-center polygons)	10	94.05	9.41	This study
Drier or moderately moist soils (high-center polygons and rims)	62	7.68	4.76	This study
Open water (+ ebullition estim.) (ponds, lakes, cracks)	14	2.37 (+ 4…30)	0.33 (+0.56…4.20)	Spott (2003)
Overgrown water (small ponds, cracks, shores)	14	44.9	6,29	Spott (2003)
Eddy covariance footprint	100	20.58	20.79 (21.35…24.99)	Sachs et al. (2008)

this study. At these micro-sites, higher temperatures can increase the diffusive flux of methane but will most likely not affect methane production in the sediments underneath deeper water columns, unless the water bodies are clear and shallow enough for the sun to reach and warm the bottom sediments.

Open water surfaces are mostly affected by increased wind speeds under scenario (2). Diffusive and turbulent gas transfer between water and atmosphere is known to be proportional to the third power of the wind speed (Wanninkhof and McGillis, 1999). In addition, storm systems are associated with decreasing atmospheric pressure, which was observed to increase methane flux by ebullition (Spott, 2003). These micro-sites must be included in future small-scale measurements within the eddy covariance footprint in order to accurately scale chamber flux measurements to larger areas. Spott (2003) measured methane fluxes from water bodies of the polygonal tundra on Samyolov Island by closed chambers and found open water surfaces to emit between 1.9…9.9 mg m^{-2} d^{-1} during calm conditions while vegetated areas emitted up to 88.65 mg m^{-2} d^{-1}.

Surface classification and flux weighting

Surface classification of high resolution aerial images reveals a distribution of these micro-sites which is likely to be wrongly estimated by simple visual assessment in the field: the very wet high methane emission sites only constitute 24% of the area while relatively drier and moderately moist sites occupy 62% of the area (Schneider et al.,
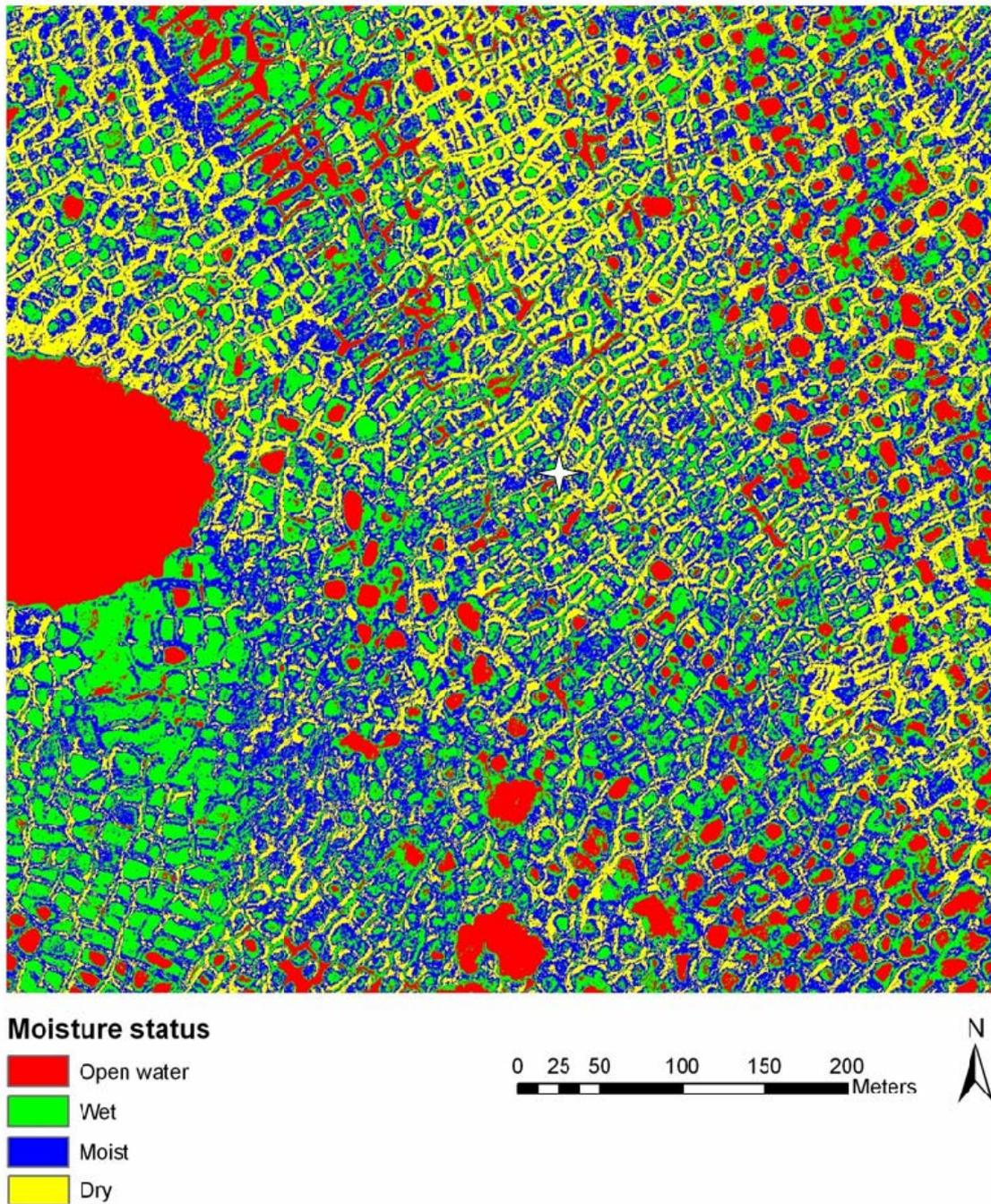
Figure 3.9: Surface classification of a high-resolution aerial image (S. Muster, unpublished data). The white asterisk in the center of the image marks the position of the eddy covariance tower.

2009; S. Muster, personal communication). If water with emergent vegetation is classified separately from inundated low-center polygons where water levels are just at or slightly above the surface, the fraction of low-center polygons is reduced to about

10%, while overgrown water covers about 14% of the area (Schneider et al., 2009). Open water without vegetation is present in about 14% of the area (Schneider et al, 2009; S. Muster, personal communication). Table 3.3 provides typical methane emissions for each surface class and the fraction of the surface it covers during August, reflecting an average of scenario (1) and scenario (2) conditions. Ebullition fluxes according to Spott (2003) were 4.17 mg m^{-2} d^{-1} on average (measured at three water bodies) but may have been underestimated due to the applied closed chamber approach which reduces water turbulence. Adding ebullition flux to the emissions from open water surfaces can change the total flux but would have to be at least three times higher than the diffusive flux to change the total flux estimate by 5% or more. Assuming decreased emissions from very wet soils and increased emissions from drier soils under scenario (2) can increase the total flux even without changing the emission rate from water bodies, which, however, will also increase due to the mechanism discussed above. This thought experiment demonstrates that on a landscape scale, the effects of weather-induced changes in methane emission can easily be the opposite of what is observed on a small scale or expected based on previous (mostly closed chamber) studies.

These discrepancies in the results on the different scales highlight the need for integrated investigations of methane dynamics on multiple nested scales, and in particular the need for more non-intrusive and spatially integrating measurements such as by eddy covariance or airborne instruments, allowing to develop up-scaling procedures in small verifiable steps without skipping scales.

However, despite the different controls and methane dynamics on the two scales, closed-chamber measurements from within the eddy covariance footprint can be scaled by an area-weighting approach of landcover classes to match the total ecosystem-scale emission remarkably well. On the other hand, another up-scaling study by Schneider et al. (2009) reports total emissions from the same types and distribution of landcover classes that are about 34% lower than in this study. The closed chamber measurements forming the basis of the Schneider et al. (2009) upscaling were located 700 m south of the eddy covariance tower in a generally drier and more elevated area (Wagner et al., 2003). The classification used in their upscaling, however, was based on two aerial image scenes, both of which cover wetter areas in the center of the island. If

a classification of the actual measurement site results in the same landcover classes, the discrepancy between the two studies implies that either differences in flux calculation from closed chamber data (linear regression in Schneider et al. (2009) vs. nonlinear regression here) or spatial heterogeneities cause the significant difference between these two estimates. If differences in the flux calculation caused the discrepancy, this underlines the importance of accurate flux determination as discussed in Kutzbach et al. (2007). If spatial heterogeneity is the reason, it demonstrates clearly that small-scale measurements of methane can not readily be applied to scales beyond the "next step" in the scaling ladder. And if the classification of the actual measurement site results in different landcover classes, it emphasizes the importance of obtaining data and information intended to be integrated under as similar conditions as possible.

The difficulties in upscaling emissions governed by highly local controls were already identified by Bubier and Moore (1994) and multi-scale studies were recommended. Attempts at up-scaling methane emissions from point measurements or at deriving globally valid statements on methane dynamics based on very small-scale studies are thus not recommended.

In addition, larger-scale methane emission models that have previously been developed exclusively on the basis of closed chamber data or other small-scale investigations should be revised to incorporate new findings from eddy covariance or other non-intrusive techniques operating on larger scales.

3.7   Conclusions

The nested approach applied to measurements in this study allowed us to compare results from two scales and to identify some important discrepancies between these two scales. Closed chamber fluxes were roughly an order of magnitude higher in wet polygon centers than on drier rims or in high-center polygons but are only found on 10% of the total area. Depending on weather conditions, the extremely low fluxes from drier sites can end up determining the overall ecosystem flux, because controls and dynamics vary strongly between these two scales.

This heterogeneity, not just in the source strengths of the polygonal tundra but also in terms of controls and seasonal dynamics poses serious challenges to up-scaling exercises, where aggregated results for larger scales cannot be checked against

measurements on that scale. We therefore strongly recommend restricting extrapolation to the next scale up and refraining from skipping scales, in order to get reliable estimates. In order to identify generally valid scaling procedures, a nested measurement approach is necessary to be able and check results – step by step – against real data.

The uncertainties in matching measurements of extremely heterogeneous measurands on different scales using different techniques, especially in highly complex environments, demonstrate that a new method able to estimate spatial contributions to the net ecosystem flux directly from the larger-scale measurements would be highly desirable.

Acknowledgements

4. ENVIRONMENTAL CONTROLS ON ECOSYSTEM-SCALE CH$_4$ EMISSION FROM POLYGONAL TUNDRA IN THE LENA RIVER DELTA, SIBERIA

Torsten Sachs   Christian Wille   Julia Boike   Lars Kutzbach

Abstract

We present the first ecosystem-scale methane flux data from a northern Siberian tundra ecosystem covering the entire snow-free period from spring thaw until initial freeze-back. Eddy covariance measurements of methane emission were carried out from the beginning of June until the end of September in the southern central part of the Lena River Delta (72°22'N, 126°30'E). The study site is located in the zone of continuous permafrost and is characterized by Arctic continental climate with very low precipitation and a mean annual temperature of −14.7°C. We found relatively low fluxes of on average 18.7 mg m^{-2} d^{-1}, which we consider to be because of (1) extremely cold permafrost, (2) substrate limitation of the methanogenic archaea, and (3) a relatively high surface coverage of noninundated, moderately moist areas. Near-surface turbulence as measured by the eddy covariance system in 4 m above the ground surface was identified as the most important control on ecosystem-scale methane emission and

explained about 60% of the variance in emissions, while soil temperature explained only 8%. In addition, atmospheric pressure was found to significantly improve an exponential model based on turbulence and soil temperature. Ebullition from waterlogged areas triggered by decreasing atmospheric pressure and near-surface turbulence is thought to be an important pathway that warrants more attention in future studies. The close coupling of methane fluxes and atmospheric parameters demonstrated here raises questions regarding the reliability of enclosure-based measurements, which inherently exclude these parameters.

4.1 Introduction

Approximately 24% of the Northern Hemisphere's exposed land area is underlain by permafrost (Zhang et al., 1999). Permafrost-affected Arctic tundra has been a major carbon sink throughout the Holocene and is a globally significant carbon reservoir, although estimates of its size vary. For example, Post et al. (1982) estimate Arctic tundra environments to account for 190 Gt or 13–15% of the global soil organic carbon pool, while more recent studies suggest a carbon content of 500 Gt in frozen yedoma sediments alone. Yedoma is a Pleistocene-age loess permafrost with high volumetric ice content of 50–90% and 2–5% organic carbon (Zimov et al., 2006a). An additional carbon content of 400 Gt is estimated for nonyedoma permafrost excluding peatlands. This would exceed the carbon content of the atmosphere (730 Gt) and that of vegetation (650 Gt) (Zimov et al., 2006a). Because of the high sensitivity of high-latitude ecosystems to climate changes, as well as their large proportion of the terrestrial earth surface, these landscapes are critically important for the Earth System, in particular for the global carbon cycle (Chapin et al., 2000), as recent warming of the Arctic makes an increasing amount of previously frozen organic carbon available for decomposition.

Where permafrost thaws, organic matter is decomposed by microbial activity. Yedoma soils contain very labile organic carbon, a large fraction of which is respired quickly upon thaw (Zimov et al., 2006b). Under aerobic conditions, this process produces carbon dioxide. Under anaerobic conditions, however, microbial decomposition produces methane.

Northern wetlands and tundra are a major source of methane, contributing about 20% of the annual natural emissions (Fung et al., 1991; Cao et al., 1996; Christensen et

al., 1996). With growing concern about climate change and the need to quantify emissions on a large scale, the greenhouse gas (GHG) budgets of arctic wetlands have come into the focus of attention. Because methane has a 23-fold global warming potential compared to carbon dioxide (time horizon of 100 years (Intergovernmental Panel on Climate Change, 2001)), even a modest change in methane sources can change the sign of the GHG budget of these landscapes (Friborg et al., 2003; Corradi et al., 2005) and feed back on the radiative forcing of the climate system. Furthermore, global climate models rely on predictions of future GHG concentrations, which require the ability to accurately model sinks and sources of methane as a powerful greenhouse gas.

However, there is still much uncertainty about the source strength and the driving forces of methane flux of tundra landscapes. Existing studies of high-latitude methane fluxes were mostly based on the closed-chamber technique, which provides measurements representative on the very small scale. Because of the high temporal and spatial variability of methane fluxes (Christensen et al., 1995, 2000; Kutzbach et al., 2004, Whalen and Reeburgh, 1992), this technique alone does not give reliable information on landscape-scale fluxes. In addition, during chamber measurements the soil surface is isolated from the atmosphere so that the coupling of atmosphere and methane emission cannot be studied. The eddy covariance technique provides nonintrusive spatially integrated flux data at the landscape scale. However, to our knowledge only five studies reported eddy covariance methane flux data from Arctic tundra ecosystems, namely Fan et al. (1992) from western Alaska, Harazono et al. (2006) from northern Alaska, Friborg et al. (2000) from Greenland, and Hargreaves et al. (2001) from a semiarctic Finnish site. Wille et al. (2008) reported data from the Lena River Delta, Siberia, using measurements from 2 years to construct a "synthetic" growing season.

Here, we present the first eddy covariance methane flux data covering an entire contiguous growing season in a Siberian Arctic tundra landscape. The objective of this study is (1) to quantify the methane emission over the full course of the growing season from snowmelt to freeze-back of the active layer, (2) to identify the biological and physical parameters which control the methane fluxes on the ecosystem scale, and (3) to
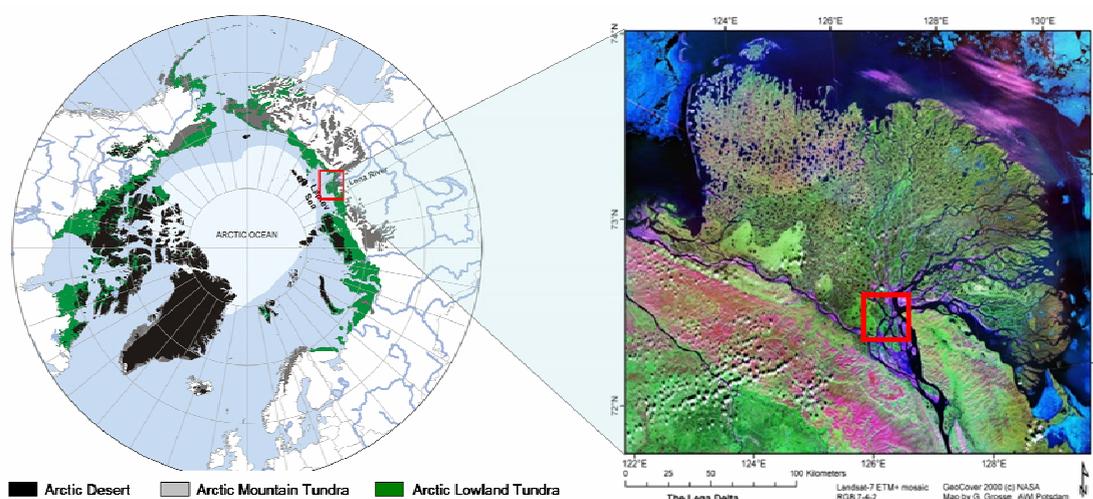
Figure 4.1: (left) Location of the investigation area and vegetation zones in the Arctic (modified after work by UNEP/GRID-Arendal (1996)). **(right)** Location of the study site Samoylov Island in the Lena River Delta (marked by the square (satellite image: Landsat 7 Enhanced Thematic Mapper (on Nimbus 6)+ GeoCover 2000, NASA (Landsat imagery courtesy of NASA Goddard Space Flight Center and U.S. Geological Survey))).

test a model proposed by Wille et al. (2008) for the same investigation site and validate it with a new and continuous data set. We found relatively low methane fluxes, which were predominantly controlled by atmospheric parameters (turbulence and pressure). A model based on turbulence, pressure, and soil temperature performed significantly better than a model without an atmospheric pressure term by Wille et al. (2008).

4.2 Site description

The study site is located on Samoylov Island, 120 km south of the Arctic Ocean in the southern central Lena River Delta (72°22'N, 126°30'E) (Fig. 4.1). With an area of approximately 32,000 km^2 it is the largest delta in the Arctic and one of the largest in the world (Walker, 1998). A maze of river channels and more than 1500 islands make up three main geomorphological terraces, only the youngest of which represents modern delta landscapes (Are and Reimnitz, 2000). Samoylov Island (Fig. 4.2) is considered representative of this Late Holocene terrace, which covers about 65% of the total delta area. Over the past ten years it has been the focus of a wide range of studies on surface-atmosphere gas and energy exchange, soil science, hydrobiology, microbiology, cryogenesis, and geomorphology (Hubberten et al., 2006).
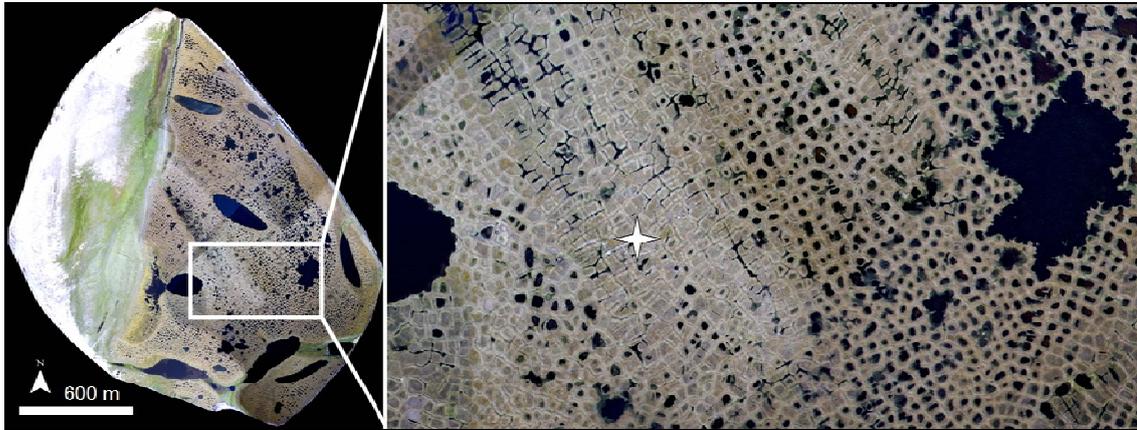
Figure 4.2: Aerial images of the study site. **(left)** Mosaic of aerial images of Samoylov Island taken in August 2007 (mosaic by Boike et al. (2008)). **(right)** The central part of Samoylov Island in August 2007. The asterisk marks the position of the micrometeorological tower.

The region is characterized by true arctic continental climate with very low temperatures and low precipitation. Mean annual air temperature at the meteorological station on Samoylov Island was –14.7°C and mean summer precipitation was 137 mm, ranging from 72 mm to 208 mm in a period from 1999 to 2005 (Boike et al., 2008). Frequent cyclones moving through the area cause rapidly changing weather conditions throughout the growing season by advection of cold and moist air from the Arctic Ocean or warm and dry air from continental Siberia, respectively. Polar day lasts from 7 May to 8 August, and polar night lasts from 15 November to 28 January. Typically, snowmelt and river break up start in the first half of June, and the growing season lasts from mid-June through mid-September. The continuous permafrost in the delta reaches depths of 500 to 600 m (Grigoriev, 1960) and is characterized by very low temperatures between –13°C and –11°C (Kotlyakov and Khromova, 2002).

Samoylov Island covers an area of 7.5 km^2 with two main geomorphological units (Kutzbach, 2006). The western part of the island (3.4 km^2) is a modern floodplain with elevations from 1 to 5 m above sea level (asl). The study site is located in the center of the eastern part (4.1 km^2), a Late Holocene river terrace with elevations from 10 to 16 m asl. The surface of the terrace is characterized by wet polygonal tundra. It has a flat macrorelief with slope gradients less than 0.2% except at the shores of larger lakes, where elevation differences of up to 2.5 m occur. However, because of the

development of low-center ice wedge polygons, the surface is structured by a regular microrelief with typical elevation differences of around 0.5 m between depressed polygon centers and elevated polygon rims. Typical soil types in the poorly drained and hence mostly inundated centers are *Typic Historthels*, while *Glacic* or *Typic Aquiturbels* dominate at the dryer but still moist polygon rims (Soil Survey Staff, 1998; Kutzbach et al., 2004). In the course of the summer, these soils thaw to a depth of 30 cm to 50 cm.

Hydrophytic sedges such as *Carex aquatilis*, *Carex chordorrhiza*, and *Carex rariflora* as well as mosses (e.g., *Drepanocladus revolvens*, *Meesia triquetra*, and *Aulacomnium turgidum*) dominate the vegetation in the wet polygon centers and on their edges (Kutzbach et al., 2004; M. Minke, personal communication, 2006). Mesophytic dwarf shrubs such as *Dryas octopetala* and *Salix glauca*, forbs (*Astragalus frigidus*), and mosses (*Hylocomium splendens*, *Timmia austriaca*) dominate the polygon rims. Surface classification of aerial photographs taken in 2003 shows, that elevated and dryer polygon rims cover approximately 60% of the area surrounding the study site, while depressed and wet polygon centers and troughs cover 40% of the area (G. Grosse, personal communication, 2005).

4.3   Methods

4.3.1 Eddy covariance setup

The eddy covariance system was set up in the center of the eastern part of Samoylov Island and was surrounded by a relatively homogenous fetch of wet polygonal tundra. Larger lakes were located at the periphery of a 600 m radius around the tower. Successful measurements (i.e., measurements that did not have to be discarded because of technical problems) were conducted on 103 days from 9 June to 19 September 2006, covering an entire growing season from the middle of snowmelt until initial freeze-back.

Wind velocity components and sonic temperature were measured using a three-dimensional sonic anemometer (Solent R3, Gill Instruments Ltd., UK) installed 4 m above ground level. A vacuum pump (RB0021, Busch Inc., Germany) drew sample air at 20 L min^{-1} from a sample intake 15 cm below the anemometer measurement point through a CO_2/H_2O infrared gas analyzer (LI-7000, LI-COR Inc., USA) and a tunable

diode laser spectrometer (TGA 100, Campbell Scientific Ltd., USA) for CH$_4$ analysis. Before entering the tunable diode laser spectrometer (TDL), sample air was dried in a reversed flow membrane gas dryer (PD-200T-48 SS, Perma Pure Inc., USA). The analyzers and the gas dryer were arranged in series and housed in a temperature-regulated case at the base of the tower. All analog signals were synchronously digitized at 20 Hz and logged on a laptop PC running EdiSol software (J. Massheder, University of Edinburgh, UK). The system was powered by a diesel generator located 100 m southwest from the tower in the least frequent wind direction. An uninterruptible power supply ensured continuous operation.

Additional instruments installed on or near the tower include sensors for air temperature and relative humidity (MP103A, ROTRONIC AG, Switzerland), incoming and outgoing solar and infrared radiation (CNR1, Kipp and Zonen B.V., The Netherlands), photosynthetically active radiation (QS2, Delta-T Devices Ltd., UK), and barometric pressure (RPT410, Druck Messtechnik GmbH, Germany). Precipitation and soil temperature data were recorded at a long-term monitoring station 700 m south of the eddy covariance tower (Boike et al., 2008). Additional daily manual measurements at five sites in the footprint of the tower included thaw depth using a steel probe, soil temperatures in 5 cm depth intervals, water level, and soil moisture where no standing water was present. These sites differed with regard to inundation, vegetation, and polygon degradation.

4.3.2 Data processing

Raw data processing and flux calculation was done using the software EdiRe (R. Clement, University of Edinburgh, UK). Because of relatively low methane fluxes we used an averaging interval of 60 min in order to increase the signal-to-noise ratio of the correlation calculation. Two coordinate rotations were applied to the wind components so that the mean transverse and the mean vertical wind components were reduced to zero. We then removed the time lag between wind measurements at the sonic anemometer and methane concentration measurements in the TDL. The effects of instrument drift and instationary conditions were removed using a recursive high pass filter with a 30 s time constant that was applied to the methane concentration time series. After the initial methane flux calculation, fluxes were corrected for the

differences between the flux frequency spectrum and the spectral response of the eddy covariance system, tube attenuation effects, the separation of anemometer and methane analyzer, as well as for the effects of the recursive high pass filter following Moore (1986) and Moncrieff et al. (1996). On average, 35.4% were added to the calculated flux. The correction of the analyzer response accounted for 27.9%, while the high pass filtering of the methane signal accounted for 5.4% of that correction.

The corrected methane flux data were screened thoroughly. Excessively noisy measurements with peaks in the cross-correlation function greater than the flux peak were rejected. We found this procedure to reliably reject measurements which were disturbed for example by instationary conditions, instrument drift, or high wind speeds. Additionally, an integral turbulence characteristics test (Foken and Wichura, 1996) was used for the final screening. The integral turbulence characteristics (ITC) are similarity characteristics of the atmospheric turbulence with a close connection to the correlation coefficient. They characterize whether turbulence is well developed or not, and it is possible to discover some typical effects of nonhomogeneous terrain, such as obstacles or inhomogeneities in surface temperature or moisture conditions (Foken and Wichura, 1996). Where the ITC parameter deviated more than 30% from the model, the turbulence was assumed to have been disturbed and data were rejected. In total, the screening removed 34.6% of the hourly flux data. However, as we only considered average daily fluxes for all subsequent analyses and there were hourly flux data available for all days (minimum four, average 15), no gap-filling procedures were applied. Measurement errors were estimated using the standard deviation of the cross correlation function and the average random error was 1.7 mg CH_4 m^{-2} d^{-1}. Systematic errors for any individual flux measurement have been estimated by Wesely and Hart (1985) to be in the range of 10–20%. The system performance agrees well with the performance other investigators using the TGA 100 have reported and is described in more detail by Wille et al. (2008).

The area from which 80% of the cumulative methane flux originated was calculated using a footprint analysis according to Schuepp et al. (1990). The upwind distance of this flux contribution was on average 518 m. The maximum contribution originated from an average distance of 116 m.

4.3.3 Ecosystem-scale flux modeling

We used two approaches to determine flux controlling parameters and set up a small-scale model for the growing period, all of which were based on daily averages of the measured fluxes.

The first approach was purely data based. We used classification and regression tree analysis (CART) as a flexible and robust tool, which can deal with nonlinear relationships, complex interactions, and missing data (Breiman et al., 1984). Regression trees aim to explain variation in a dependent variable by recursive splitting of the data set into more homogenous subgroups, each of which is characterized by typical values of the dependent variable, the number of data points in the group, and the specific values of the independent variables that define the group. Splitting is continued until an overlarge tree is grown, which is then pruned by cross-validation. We used tenfold cross validation, were the data is divided into ten subsets of approximately equal size, each of which is dropped once in turn while growing a series of trees from the remaining subsets to predict the response of the omitted subset. The estimated error for each subset is summed over all subsets, and after repeating the procedure for each tree size, the tree with the smallest estimated error rate is selected. A more detailed description of this method and its advantages for the exploration, description, and prediction of patterns and processes in ecological data is given by De'ath and Fabricius (2000). We required a minimum of ten data points in order to allow further splitting and ran a series of 100 tenfold cross validations to select the most frequently occurring tree with the minimum mean squared error.

After identifying the main controls of methane emission, the objective of the second approach was to propose a multiplicative and semideterministic model following the work by Friborg et al. (2000), where the flux is a product of an ecosystem reference flux and a set of environmental parameters, each with its specific regulation factor. This approach was also applied by Wille et al. (2008), who initially chose parameters for the model on the basis of previously well established relationships, such as the temperature dependence of soil microbial methane production (e.g., Arrhenius, 1909; Conrad, 1989), and on direct correlation between methane flux and the respective parameter. The general form of this model can be written as:

$$FCH_4 = a \cdot b^{((T-\bar{T})/10)} \cdot \prod_{i=1}^{n} f_i(X_i) \qquad (1)$$

where FCH_4 is the methane flux time series, a is the reference flux determined through the fit process, b is a fit parameter, T and $\bar{T}$ are a temperature and reference temperature, respectively, and $f_i(X_i)$ describe the flux regulation by environmental parameters, where f_i can be linear or exponential. A weighting factor of σ_{FCH4}^{-2} was applied to each square of residuals before summing the squares of residuals during the fitting process, with σ_{FCH4} being the daily mean of the errors of the hourly flux data points.

Models were compared by variance reduction RV, where positive values indicate improvement in model performance. For RV to be significantly different from zero ($\alpha = 5\%$), a required minimum value RV_{min} is computed following Balzer (1997):

$$RV_{min} \approx \frac{186}{(N-2)^{0.415}} \qquad (2)$$

4.4   Results

4.4.1 Meteorology

During setup of the instruments at the end of May/ beginning of June, the ground around the eddy covariance tower was still mostly snow covered. Only a few snow-free patches occurred on elevated polygon rims. However, mean daily air temperatures were already approaching 0°C and reached 1.5°C on 2 June (Fig. 4.3). Light rainfall starting on 7 June and air temperatures of up to 8.8°C on 6 June and the following days further accelerated snowmelt and by the time continuous measurements started on 9 June, the tundra was almost completely snow free. Thawing of the ice cover on polygonal ponds and thermokarst lakes continued until the end of June, when remaining ice from ponds and smaller lakes that was frozen to the bottom surfaced. After snowmelt, water levels in the polygon centers were more than 11 cm above soil level and slowly decreased throughout June and July to about 2 cm. A storm with precipitation of up to 23 mm per

day in the first week of August caused the water levels to rise up to 10 cm above soil level again and they never fell below soil level in the subsequent drying throughout August. Another storm system in the first week of September yielded 34 mm of precipitation within three days causing water levels to rise once more to about 10 cm, where they remained until the end of the measurement period. At a total of 158 mm, liquid precipitation during the study period was above average. Snow started to accumulate on 12 September and reached depths of 8–10 cm in polygon centers and 2–6 cm on elevated areas, but advection of warmer air from the south caused the mean daily air temperature to increase from its minimum at −5.3°C on 12 September to +4.2°C on 19 September and all snow had disappeared on 18 September. While mean daily air temperature was 4.5°C during the first half of June and reached a monthly maximum of 13.0°C on 15 June, soil temperature in a polygon center at 10 cm depth remained slightly below freezing until 14 June. It reached its first of two distinct maxima at 8.1°C on 11 July, after air temperature had reached daytime maxima of up to 28.9°C and a mean daily temperature of 18.9°C. Soil temperature subsequently declined to about 5°C until the second peak was reached at 8.4°C on 2 August, following a second peak in mean daily air temperature of 18.5°C. From there, soil temperature steadily declined, and refreezing of the soil in 10 cm depth began on 14 September, and on 10 September in the top soil layers, respectively. By mid-September, all water bodies except for the large thermokarst lakes were covered with ice up to 8 cm thick and soils were frozen up to approximately 10 cm depth. The maximum thaw depth of the soil was reached in the beginning of September at 46 cm. The minimum air temperature during the study period was reached at −7.2°C on 9 September and the minimum mean daily temperature was −3.9°C on 10 September. Despite the high temperatures in July and August, the mean monthly air temperature never exceeded 10°C. Long-term temperature data are available from Tiksi, which is located 110 km southeast of Samoylov Island but characterized by very similar temperatures. Temperature conditions in 2006 were almost 5°C warmer than the long-term average in June (2°C) but within ±1°C of the long-term average in July (7°C), August (7°C), and September (1°C). The average daily wind speed was 5.1 m s⁻¹ during the study period, which is 0.4 m s⁻¹ higher than in 2003 and 2004 (Kutzbach, 2006). Winds from east-southeast were clearly predominant, but west-northwesterly and southern winds also
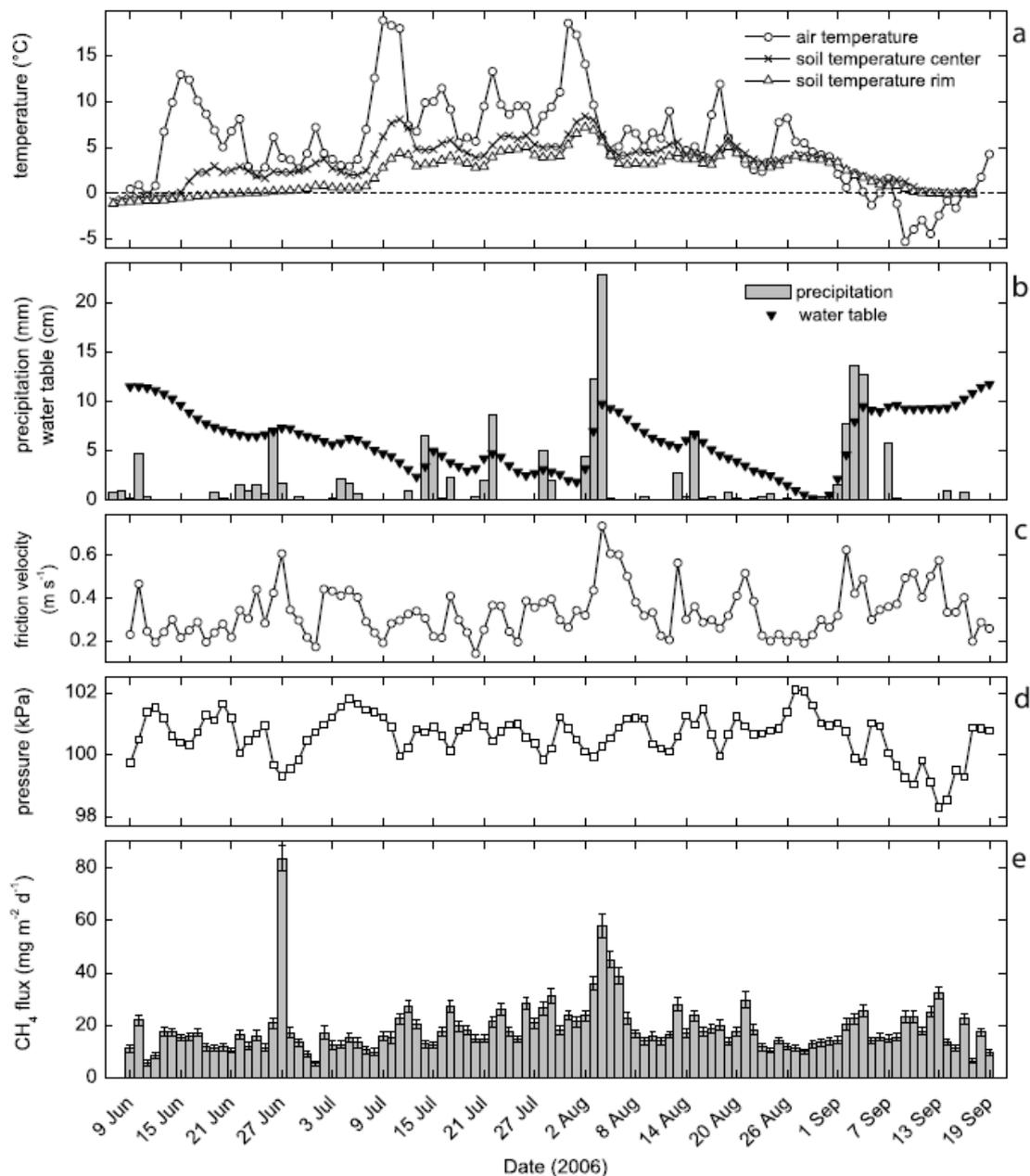
Figure 4.3: Data of the 2006 growing season. **(a)** Air temperature at 2 m above surface, soil temperature at a polygon center in 0.10 m depth, and soil temperature at a polygon rim in 0.20 m depth; **(b)** liquid precipitation and water table relative to the soil surface in a polygon center; **(c)** friction velocity u_*; **(d)** atmospheric pressure; and **(e)** methane flux as measured by eddy covariance (Error bars denote the average random error.). All data are shown as daily means.

occurred frequently (data not shown).

4.4.2 Ecosystem-scale methane flux

Mean daily methane flux was 18.7 mg m^{-2} d^{-1} during the study period and showed relatively small seasonal variation (Fig. 4.3). However, strong variations could be observed, which coincided with pronounced decreases in air pressure, higher wind speed after calm periods, and precipitation events.

In the first two weeks of measurements, average daily methane fluxes were already 13.8 mg m^{-2} d^{-1}, with high variability from 5.7 mg m^{-2} d^{-1} to 22.0 mg m^{-2} d^{-1}. Soil temperature was still below 0°C when measurements started and showed very little variation in the early part of the thawing period. The lowest methane flux was observed during days with relatively high air pressure and low wind speed. Methane fluxes increased to an average of 25.0 mg m^{-2} d^{-1} in the third week; however, this increase was mainly due to an extreme peak on 27 June, which coincided with the lowest observed air pressure during the summer and high wind speeds. The last ice from the bottom of ponds and smaller lakes surfaced and melted around this time.

Methane fluxes dropped to an average of 12.3 mg m^{-2} d^{-1} during the calm period at the end of June, and then steadily increased to the highest measured fluxes of on average 35.1 mg m^{-2} d^{-1} in the first week of August, roughly following variations in soil temperature and closely following variations in wind speed. Throughout July, above-average methane fluxes frequently correlated with sudden decreases in air pressure. Until the third week of August, fluxes remained between 17.0 and 20.0 mg m^{-2} d^{-1} and then decreased to less than 13.0 mg m^{-2} d^{-1} during a longer calm high-pressure period at the end of August.

During the first and second week of September, which were characterized by rapidly decreasing air pres-sure, partly strong winds, and rain or snow events, methane fluxes increased to an average of 18.2 mg m^{-2} d^{-1} and 21.6 mg m^{-2} d^{-1}, respectively, despite a decrease in soil temperature and refreezing of the top soil layers and water bodies. By mid-September, all water bodies except for the large thermokarst lakes where covered with ice up to 8 cm thick. During the calm high-pressure period after 13 September, methane fluxes decreased markedly to below 10.0 mg m^{-2} d^{-1} at the end of the measurement period.

Classification and regression tree analysis (CART) of the measured methane flux data and environmental variables showed that variation in methane fluxes could
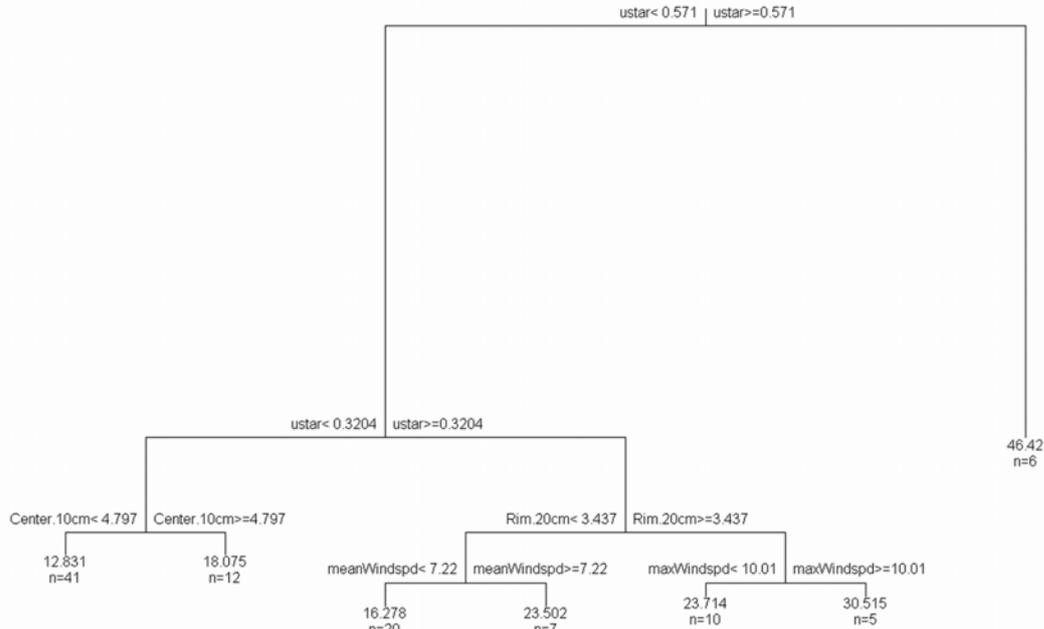
Figure 4.4: Regression tree determined by 100 tenfold cross validations and pruning to the level of the smallest mean square error. The most frequently occurring tree was selected. The label at each split denotes the splitting criterion (the first split here is at $u* = 0.571$ m s^{-1}), and the labels at the "leaves" of the tree indicate the number of data points n in the respective "leaf" as well as the mean of the respective data points. Near-surface turbulence (friction velocity $u*$) explains most of the variability in methane emissions through the first two splits. In the next two splits, a considerably smaller amount of variability is explained by soil temperatures in a polygon center at 10 cm depth and in a polygon rim at 20 cm depth. In the final splits, more variability is explained by atmospheric parameters, i.e., by mean horizontal wind speed u, which directly correlates with $u*$, and by maximum horizontal wind speed. Terminal nodes are labeled with means of the respective variable and the number of observations in the subgroup.

best be explained by friction velocity $u*$ and soil temperatures at 10 cm depth in a polygon center and 20 cm depth in a polygon rim, respectively. Friction velocity alone accounted for 57% of the variance in methane emissions and another 3% could be explained by wind speed, which is closely correlated with friction velocity and its main surrogate variable in the CART analysis. Soil temperatures on the other hand only explained about 8% of the variance (Fig. 4.4).

This combination of $u*$ and T conformed to the model proposed by Wille et al. (2008) using the following equation:

$$FCH_4 = a \cdot b^{((T-\bar{T})/10)} \cdot c^{(u*-\overline{u*})} \tag{3}$$

Table 4.1: Input and fit parameters for the model proposed here (equation (4)), and the model proposed by Wille et al. (2008) (equation (3))[a]

Model	$\overline{T}$ (°C)	$\overline{u_*}$ (m s^{-1})	$\overline{p}$ (kPa)	a (mg m^{-2} d^{-1})	b	c	d	R^2	R^2_{adj}	RV (%)
This paper	3.44	0.34	100.617	16.68 ± 0.16	2.28 ± 0.10	11.16 ± 0.94	0.86 ± 0.01	0.69	0.68	33.07
This paper (excl. pressure)	3.44	0.34	_	16.79 ± 0.16	2.07 ± 0.09	14.41 ± 1.12	_	0.63	0.62	18.07
Wille et al. (2008)	1.94	0.28	_	15.67 ± 0.46	3.93 ± 0.50	25.26 ± 7.23	_	0.40	0.39	_

[a]R^2_{adj} is the adjusted R^2 taking into consideration the number of explanatory variables. Models were compared to the model proposed by Wille et al. (2008) using variance reduction RV, where positive values indicate improvement in model performance. For RV to be significantly different from zero (α = 5%), a minimum value of RV_{min} = 27.40% was calculated using equation (2). The extended model proposed here is significantly better than the model proposed by Wille et al. (2008).

where T is the soil temperature at a depressed polygon center in 20 cm depth, u_* is the friction velocity, and $\overline{T}$ and $\overline{u_*}$ are the mean values of the respective variables. Applying this model with the fit parameters determined by Wille et al. (2008) (Table 4.1) to the data of the 2006 measurement period explained only about 40% of the variance seen in the flux data and tended to overestimate fluxes larger than 25 mg m^{-2} d^{-1} while underestimating some of the lower fluxes (Fig. 4.5). It also did not adequately capture variation in methane fluxes associated with decreases in air pressure that could be seen throughout July. Model performance was improved by using a soil temperature at 10 cm depth in a polygon center, where methane production takes place, as identified by CART and renewed fitting; however, the best agreement (R^2_{adj} = 0.68; Table 4.1) of modeled and measured data was obtained by expanding the model proposed by Wille et al. (2008) with an exponential term that accounts for the observed influence of air pressure:

$$FCH_4 = a \cdot b^{((T-\overline{T})/10)} \cdot c^{(u*-\overline{u*})} \cdot d^{(p-\overline{p})} \tag{4}$$

where T is the soil temperature at 10 cm depth in a polygon center, u_* is the friction velocity, p is the air pressure, and $\overline{T}$, $\overline{u_*}$, and $\overline{p}$ are the mean values of the respective variables.

Thaw depth, which increased gradually and without variation throughout the season, did not improve the model, and neither did water level, which remained above the soil surface at all times in the polygon centers.
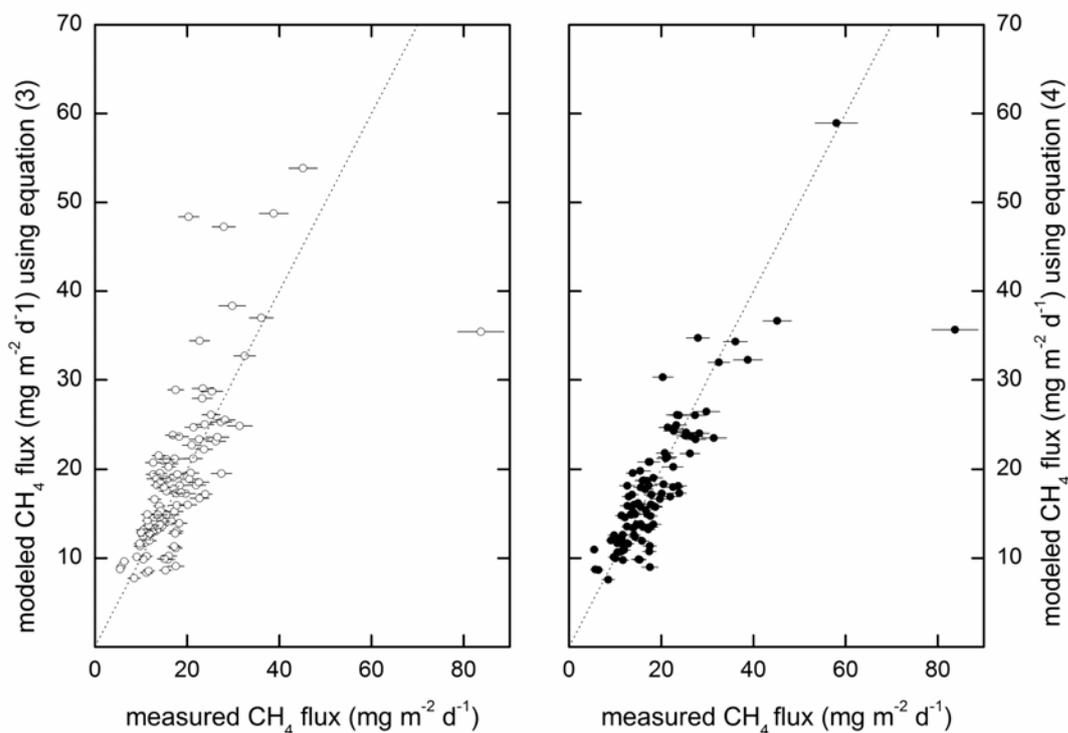
Figure 4.5: Modeled flux versus mean daily flux. **(left)** Using the model as proposed by Wille et al. (2008) (equation (3)), larger fluxes are overestimated. **(right)** Using the extended model proposed here (equation (4)), fluxes agree well over the entire range of fluxes.

While fluxes modeled using equation (4) agreed well with measured fluxes, Figure 4.6 shows that measured fluxes during the thaw period, when soil temperature variation was low, were underestimated. Also, less than 50% of the actual methane emission on 27 June could be modeled using either of the approaches described above. Substituting air temperature for soil temperature in equation (4) does not significantly improve the model as a whole, but underestimation of fluxes during the thaw period was reduced substantially (Fig. 4.6).

The cumulative methane emission during the 2006 growing season was 1.93 g m^{-2}, which agrees well with the cumulative flux during the same period of a combined 2003 and 2004 data set, which amounted to 1.87 g m^{-2} (Wille et al., 2008). The extended model (equation (4)) underestimated the cumulative measured flux by less than 5%.
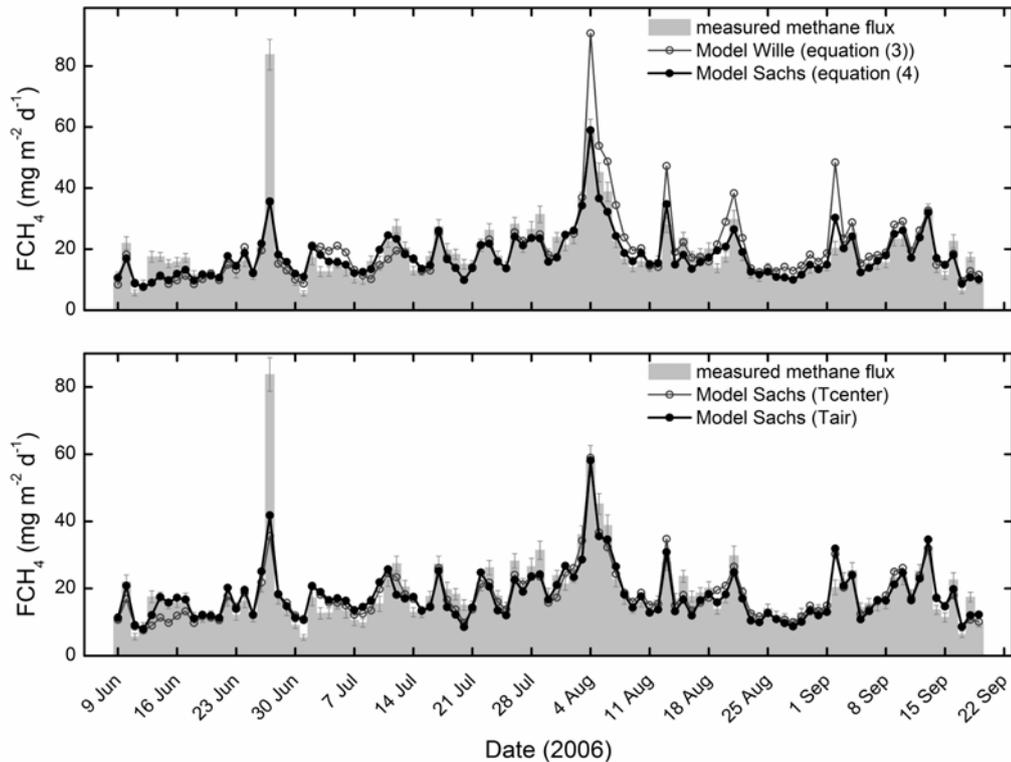
Figure 4.6: Time series of measured and modeled daily mean CH$_4$ fluxes. **(top)** Fluxes modeled using equations (3) and (4). The model by Wille et al. (2008) tends to overestimate larger methane fluxes. **(bottom)** Fluxes modeled using equation (4) and a modified version of equation (4), where soil temperature in 10 cm depth was replaced by 2 m air temperature. The underestimation of methane fluxes during the early thaw period is reduced substantially.

4.5 Discussion

4.5.1 Environmental controls on methane emission

To our best knowledge, we here present the first ecosystem-scale methane exchange data from the Siberian Arctic covering an entire contiguous growing season from spring thaw to initial freeze-back by the eddy covariance method. The measurement period included a wide range of meteorological and soil conditions, allowing for a comprehensive analysis of the environmental controls of methane fluxes. The most important parameter controlling methane emissions from our site was near-surface turbulence, which closely correlates with horizontal wind speed. Though few other studies have reported this effect, our results confirm the conclusions by Wille et al. (2008), who observed the same relationship during a "synthetic" growing season of

2003/2004 eddy covariance data from the same site (Table 4.1). Fan et al. (1992) found emissions from lakes in Alaskan Arctic tundra to be dependent on wind speed and Hargreaves et al. (2001) described a close relationship between momentum flux and methane emissions for short periods of up to one day at a tundra site in Finnish Lapland. The concurrent observation of ebullition in the latter study indicates a water table above the soil surface. Our site features a large fraction of polygon centers with water tables above the surface, deep thermokarst cracks, and small polygonal ponds of various depths. Thus the methane flux dependence on near-surface turbulence could at least partly be explained by diffusive and turbulent gas transfer between water surface and atmosphere, which several lake studies have shown to be proportional to $u^{1.6}$, with u being the horizontal wind speed (MacIntyre et al., 1995).

Increased turbulence and wind speed on noninundated surfaces such as polygon rims and, probably more so, high-center polygons, which are dominated by thick moss layers, could lead to a thinning of the laminar boundary layer in the moss canopy, resulting in a higher concentration gradient from the methane-enriched soil to the turbulent boundary layer and hence to an increased diffusive flux of methane. In addition, increased turbulence could lead to increased aeration and a transient flushing of methane stored in these layers during calm periods. Increased methane emissions during high wind speeds after calm periods were also reported by Hargreaves et al. (2001). However, this storage flushing is of highly transient nature and thus might only play a role on shorter timescales.

Another important mechanism for methane emissions from lakes and water inundated areas is bubble ebullition, which is often ignored because of its patchiness and resulting difficulties in quantifying it. Hargreaves et al. (2001) have observed ebullition during spring thaw and periods of high wind speed. Walter et al. (2006) reported methane release by ebullition from eastern Siberian thermokarst lakes, which was continuous and large enough to prevent some emission hot spots in the investigated lakes from freezing. During closed chamber flux measurements in close proximity to the eddy covariance tower, we captured ebullition events using floating chambers on thermokarst cracks (data not shown) and repeatedly observed ebullition from polygonal ponds during the thawing period. We suggest two main triggers for methane ebullition: (1) increased atmospheric turbulence and (2) decreased atmospheric pressure. Increased

turbulence could lead to the release of gas bubbles that adhere to surfaces below the water table, such as plants, roots, or shallow sediments through wind induced turbulence in the water, agitation of plants, or wave action. Decreasing atmospheric pressure, which frequently correlated with increased methane emission from our study site, can release free-phase gas and resulting ebullition was shown to contribute 50–64% to total emissions reported from a Japanese peatland by Tokida et al. (2007). Laboratory experiments by Tokida et al. (2005) also demonstrated the importance of atmospheric pressure on methane ebullition, and including the pressure term in our model (equation (4)) improved model performance significantly (Table 4.1).

Soil temperature in a polygon center at 10 cm depth was identified as the third parameter controlling methane fluxes from our site. The dependence of soil microbial activity on temperature was already described almost a century ago by Arrhenius (1909) and has been confirmed by several studies since (e.g., Conrad, 1989; Hargreaves et al., 2001; Christensen et al., 2001). However, while Hargreaves et al. (2001) found a very strong relationship between methane emission and peat temperature, Rinne et al. (2007) for example, found a good exponential relationship only for temperatures <12°C. Other studies, such as Wickland et al.'s (2006), did not find a relationship between methane emission and soil temperature. At our study site, we found soil temperature to play a minor role, explaining 8% of the observed methane fluxes. However, during spring thaw, substituting air temperature for soil temperature resulted in a better model fit and reduced the underestimation of early season methane fluxes. This is considered to be due to the fact, that deeper soil layers were still frozen and most of the methane emitted during that early phase originated from methanogenesis in the uppermost soil layers and from release of trapped methane from lake ice and ponds. Temperatures in these sources are likely to be directly influenced by air temperature rather than soil temperature in several centimeters depth. Increased temperature would increase melt/thaw rates, resulting in higher emissions of stored methane.

Some studies do not separate methane production or even potential microbial activity from actual methane release (e.g., Wagner et al., 2003). However, the clear dominance of atmospheric parameters over soil temperature found here has two main implications:

1. It suggests that methane production and methane emission are not necessarily closely linked, particularly on shorter timescales. Instead, storage of methane in soils and sediments leads to a certain degree of decoupling between temperature-dependent methane production and meteorology-dependent methane release. Light disturbance of sediments underneath a floating chamber using a steel probe resulted in rapid fivefold increase of the methane concentration inside the chamber, suggesting that large amounts of free-phase methane are stored in sediments of polygon ponds and lakes as well as thermokarst cracks.

2. When measuring gas exchange by the closed chamber method, near-surface turbulence and, depending on chamber design, also air pressure are inherently eliminated, while many other parameters including air and soil temperature are altered inside the chamber (Kutzbach et al., 2007). As most studies on the quantification and source strengths of methane emissions (including those that upscale emission estimates to the landscape or regional scale) are currently based on closed chamber methods, this finding raises questions about the reliability of reported field data based on chamber measurements and highlights the need for studies based on nonintrusive measurement techniques such as the eddy covariance approach.

While other studies found thaw depth to be correlated with methane emission (Friborg et al., 2000; van Huissteden et al., 2005), we did not find a significant influence of thaw depth on methane emission at our site, confirming the findings discussed by Wille et al. (2008).

As methane is produced under anaerobic conditions in the soil column and oxidized under aerobic conditions, water table depth is another variable, which has often been identified as predictor for methane emissions (e.g., Friborg et al., 2000; Suyker et al., 1996). However, Rinne et al. (2007) found only a weak anticorrelation between methane emission and water table position, and Hargreaves et al. (2001) did not find any relationship between these parameters. At our site, we did not find any relationship between ecosystem-scale methane emission and water table position. However, simultaneous closed chamber measurements on fifteen plots at five different microsites in close proximity to the eddy covariance tower showed a high small-scale variability of methane fluxes between sites with low water tables (i.e., polygon rims and high-center polygons) and sites with water tables near the surface (i.e., polygon

centers). While emissions from rim and high-center polygon plots frequently did not reach/exceed the detection limit of the analyzer, large fluxes of up to 400 mg m^{-2} d^{-1} were measured in inundated polygon centers (data not shown). Since the water table in these polygon centers never dropped below the soil surface and precipitation quickly drained from elevated polygon rims into polygon centers, there were no significant temporal changes in the ratio of aerobic and anaerobic areas in the soil column and thus no temporal changes in methane emission related to water table position.

4.5.2 Seasonal dynamics

Although soils were still frozen at the beginning of the 2006 measurement period, substantial methane emission could already be observed, confirming the observations from the same site in 2004 (Willie et al., 2008). These early emissions were highly variable and dependent on atmospheric conditions. The highest emission peak of the entire season was observed on 27 June, toward the end of the thawing period. Rinne et al. (2007) also reported an emission pulse during snowmelt, which was independent of soil temperature. Hargreaves et al. (2001) found methane fluxes in the range of summer emissions during the thaw period, which were attributed to the release of methane trapped in and below the ice cover. Harazono et al. (2006) on the other hand, did not observe an increase in methane emission during spring thaw at a wet tundra site in Barrow, Alaska.

Visual observation of ebullition from thawing lake shores and lake ice suggests that this pathway played a major role in early methane emission on Samoylov Island. The large emission peak on 27 June coincided with the end of the thawing period, when remaining ice from ponds and lakes, which were frozen solid, broke loose from the lake bottoms and surfaced, presumably disturbing bottom sediments and thus causing free-phase methane to be released. In addition, through the processes described above, strong winds and a pronounced drop in air pressure might have caused unusual high emission of methane produced and stored during the winter.

Monthly average methane fluxes of 17.1 mg m^{-2} d^{-1} in June, 18.3 mg m^{-2} d^{-1} in July, 20.6 mg m^{-2} d^{-1} in August, and 18.2 mg m^{-2} d^{-1} in September agree well with fluxes from the same site reported by Wille et al. (2008). Emissions are similar to the average methane flux reported by Fan et al. (1992) from an Alaskan subarctic tundra

site, which was characterized by a mix of dry and wet microsites as well as lakes with a ratio of wet/dry sites comparable to Samoylov Island. The other eddy covariance flux studies from Arctic sites reported higher fluxes. Friborg et al. (2000) reported August methane fluxes of 50 mg m^{-2} d^{-1} from a rich fen near Zackenberg (Greenland), Hargreaves et al. (2001) measured emissions of typically 38 mg m^{-2} d^{-1} from a wetland in Finnish Lapland, and Harazono et al. (2006) reported methane fluxes from a coastal wet sedge tundra in Barrow, Alaska, of 50 mg m^{-2} d^{-1} until the end of August. However, all these sites have a considerably larger fraction of wet or inundated surfaces than our site on Samoylov Island, where relatively dry polygon rims make up about 60% of the surface area. Thus, less than half the area covered by the eddy covariance footprint actually contributes significant methane emissions. In addition, extremely cold permafrost in northern Siberia might inhibit microbial activity. Methanogenesis is also impeded by unfavorable conditions, such as sandy soils and substrate limitation because of only weakly decomposed organic matter (Ganzert et al., 2006).

Relatively high fluxes could also be observed in September. However, with the top soil layer frozen and water bodies covered by up to 8 cm of ice, these high fluxes are harder to explain by turbulence or atmospheric pressure influence, especially in the last two weeks of measurements. The remaining pathway for methane emission while soil and water bodies freeze from the top, is via plant mediated transport through the aerenchyma of wet-adapted aerenchymatous sedges and grasses such as *Carex aquatilis*, which was shown to account for 27% to 66% of overall methane fluxes on Samoylov Island (Kutzbach et al., 2004). However, this study also suggested that plant-mediated transport was only driven by diffusion and presumably limited by the diffusion resistance of dense root exodermes, leading Wille et al. (2008) to hypothesize that near-surface turbulence is not likely to increase methane emission via this pathway. However, in light of the 2006 data this should be qualified as the diffusion resistance of the root exodermes has not been quantified and the correlations between increased turbulence and methane emission, and decreasing atmospheric pressure and methane emission were still apparent during refreezing of soil and water bodies. Similar to the effect of increased aeration in moss canopies, higher wind speed and lower atmospheric pressure would decrease the aerodynamic resistance in the turbulent boundary layer and

the thickness of the laminar boundary layer at the leaf surfaces, thus allowing the diffusion from aerenchyma to the atmosphere to increase.

In addition, incidental observations in the field indicate that refreezing of the top soil pressurizes the unfrozen layer underneath, possibly forcing increased emission from unfrozen patches or through cracks. These increased emissions could result from the added effect the freezing has on two usually opposing processes: (1) it limits the transportation of oxygen from the atmosphere to the soil, thus promoting the net formation of methane in the unfrozen layers (Yu et al., 2007), and (2) it early on reduces methane consumption in the freezing upper layers, as methane oxidizing bacteria in these layers were found to have a higher temperature optimum (Liebner and Wagner, 2007) and thus reduce their activity earlier than the psychrotolerant methanogens in the still unfrozen lower horizons (Ganzert et al., 2006). Hence, an increased net amount of methane is available for emission.

However, the poorly understood effects of freezing induced structural properties of cold soils on methane transport processes and pathways, and the lack of ecosystem-scale data on cold season methane fluxes highlight the need for long-term nonintrusive studies, which extend well beyond the growing season.

4.6   Conclusions

In comparison to three other Arctic eddy covariance studies from Alaska, Greenland, and Finland, methane emission was low at our site, probably because of (1) extremely cold permafrost, (2) substrate limitation of the methanogens, and (3) a relatively high surface coverage of noninundated, moderately moist areas.

Near-surface turbulence was identified as the most important control on ecosystem-scale methane emission, while soil temperature explained only 8% of the seasonal emission. In addition, atmospheric pressure was found to significantly improve a model based on turbulence and soil temperature.

Ebullition from waterlogged areas triggered by falling atmospheric pressure and near-surface turbulence is thought to be an important pathway that warrants more attention in future studies. In this context, available free-phase gas in lake and thermokarst crack sediments should be quantified in order to estimate potential emissions by ebullition.

The close coupling of methane fluxes and atmospheric parameters demonstrated here raises questions regarding the reliability of enclosure-based measurements, which inherently exclude these parameters. Long-term, nonintrusive measurements on the ecosystem scale are needed to adequately quantify high-latitude methane emissions and correct potentially biased estimates based on chamber measurements, to identify processes governing the emission of methane on various scales, and to address interannual and long-term variations of methane emission from a range of Artic ecosystems.

Acknowledgements

5. DETECTING SPATIAL HETEROGENEITY OF POLYGONAL TUNDRA IN EDDY COVARIANCE COSPECTRA

Torsten Sachs   Werner Eugster

Abstract

The eddy covariance (EC) method has become the preferred method to measure turbulent fluxes of climate relevant gases such as carbon dioxide and methane between terrestrial ecosystems and the atmosphere. One important assumption in the eddy covariance theory is homogeneity of the surface over which measurements are conducted. However, in reality the method is often applied in very heterogeneous areas and the effect of that heterogeneity on the measurement time series is discussed controversially in the scientific community. We hypothesize that heterogeneity of the flux strength within the EC fetch leads to deviations of the shape of the cospectra from the idealized curves. Using Taylor's frozen turbulence field assumption, we further hypothesize that the cospectral frequencies can be translated into distances which allows an association of the observed deviations in the cospectrum with landscape features in the EC fetch. Assuming that this should be easiest to detect where the

observed heterogeneity is characterized by a strong small-scale spatial contrast of fluxes while also exhibiting certain regularity, we used EC data from a polygonal tundra site as a test data set. The site was characterized by a regular micro-relief of very wet polygon depressions with high rates of photosynthesis and methane emission on the one hand and relatively "dry" elevated polygon rims with lower rates of photosynthesis, higher rates of respiration, and extremely low methane emissions on the other hand. In this case study, we demonstrate that eddy covariance cospectra of water vapor, carbon dioxide and methane from the Lena River Delta, Siberia, can be correlated with surface features in high-resolution aerial photographs. If successful beyond this first case study, our method could be of wide interest wherever fluxes are measured over spatially heterogeneous surfaces. It would be especially helpful to move towards more accurate upscaling in areas where emission rates and processes vary greatly across scales, such as the vast and hard to access high latitude tundra ecosystems.

5.1   Introduction

The eddy covariance (EC) method is a non-intrusive, spatially integrating method for *in-situ* measurements of gas fluxes between ecosystems and the atmosphere and has become the preferred method for studies of land-atmosphere interactions. Initially, the method was mostly used on flat and uniformly vegetated surfaces, for example on agricultural land or over forests (Baldocchi et al., 2001). In recent years, however, more and more non-traditional sites were investigated using EC, including complex terrain (mountains, urban settings) and strongly heterogeneous ecosystems, such as Arctic tundra (Sachs et al., 2008; Wille et al., 2008). One important assumption in the conventional eddy covariance method, however, is horizontal homogeneity of the surface over which measurements are conducted (Lee et al., 2004; Foken, 2006). It is not entirely clear yet, how eddy covariance data are affected by different degrees of violation of the homogeneity assumption.

In addition, eddy covariance provides high temporal resolution of net fluxes over a larger area but no high spatial resolution, which is of interest in complex landscapes. Multi-scale studies and attempts at upscaling flux data from heterogeneous or patchy surfaces have shown disagreements between eddy covariance and other methods (Fox et al., 2008; Sachs et al., submitted). Fox et al. (2008) measured net

ecosystem exchange (NEE) in heterogeneous tundra near Abisko and found a 60% bias in the magnitude of cumulative NEE over a 40 day period between EC observations and closed chamber based calculations. Sachs et al. (submitted) found differing controls on methane emissions and contradicting seasonal dynamics measured by EC vs. closed chambers.

The unclear effects of spatial heterogeneity on the quality of EC flux data and the difficulties and uncertainties arising from attempts to reconcile and upscale measurements from different scales and methods suggest it would be highly desirable to develop a method to identify spatial disturbance and estimate its effect on ecosystem-scale flux data directly from eddy covariance time series.

Taylor (1938) suggested that turbulence can be considered "frozen" ("Taylor's frozen turbulence hypothesis"), i.e. turbulence elements move horizontally with a mean wind speed u without changing their characteristics while moving from one point to the next (Foken, 2006). Wind speed can be used to translate turbulence measurements to corresponding measurements in space (Stull, 1988; von Randow et al., 2002). Because of this time-for-space substitution concept of the EC method, in a very broad sense, temporal autocorrelation translates to spatial autocorrelation which might be of interest for flux studies carried out over heterogeneous terrain.

In this paper, we present a proof of concept and preliminary work on such a method allowing the detection of spatial heterogeneities and their contributions to the net flux directly from eddy covariance raw data. The method was developed and tested using EC data of water vapor, carbon dioxide, and methane from polygonal tundra in the Lena River Delta, Siberia. The tundra surface is characterized by a pronounced but regular microrelief due to low-center polygons, as well as strongly contrasting methane fluxes and photosynthesis rates between wet polygon centers and relatively drier polygon rims (Kutzbach et al., 2004; Sachs et al., 2008; Wille et al., 2008) and was therefore assumed to provide clear and readily detectable disturbances. Using high-resolution aerial images we were able to show that spatial heterogeneity correlates significantly with eddy covariance cospectra of water vapor, carbon dioxide, and methane after translation into a spatial wavelength scale.

5.2   Theoretical background and methods

The turbulent flux measured by the eddy covariance method is the covariance between the vertical (or streamline-normal) wind speed w and the concentration of interest c:

$$F = \overline{w'c'} \tag{1}$$

where primes indicate the instantaneous deviation from the mean and the overbar denotes the mean. Turbulence data are usually described and interpreted by frequency analysis where the data series is converted from the time domain into the frequency domain by Fast Fourier Transformation (FFT). The cospectrum of two times series describes how eddies of different frequencies contribute to the covariance and the integral of the spectral density of a cospectrum equals the covariance of the time series. Kaimal et al. (1972) empirically determined idealized cospectra which are an important statistical reference for calculating frequency response corrections for eddy covariance data. When using cospectra to correct for frequency response of sensors, cospectral densities below the ideal cospectral curve indicate flux losses, for example due to deficiencies in the frequency response of the instrument set-up. Here, we do not aim at such an application, but will use the same technique to quantify in a relative measure which areas within the footprint area of our flux measurements contribute below average to the overall eddy covariance flux measured during a given time period, and which other areas contribute more strongly to the flux.

We believe that strong departures in the cospectra from the ideal cospectra can provide information on heterogeneity-induced disturbance of the time series data. To translate cospectra from the frequency scale to a spatial wavelength scale that allows an analysis of such disturbances in relation to surface features in the upwind direction of the measurement tower, we use Taylor's frozen turbulence hypothesis. The general form of Taylor's hypothesis is (Stull, 1988):

$$\frac{\partial \xi}{\partial t} = -U \frac{\partial \xi}{\partial x} - V \frac{\partial \xi}{\partial y} - W \frac{\partial \xi}{\partial z} \tag{2}$$

where ζ is any variable. The turbulence is frozen, when $\delta\zeta/\delta t = 0$. x, y, and z are the three directions of the wind vector and U, V, and W are is the wind speed of the respective direction. The hypothesis is only valid if the horizontal movement is much faster than the vertical evolution of the eddy. Taylor's hypothesis can also be stated in terms of a wavenumber κ and the frequency f (Stull, 1988):

$$\kappa = 2 \cdot \pi \cdot \frac{f}{\bar{u}} \qquad (3)$$

where $\kappa = 2\pi/\lambda$ for wavelength λ (Wyngaard and Clifford, 1977). Using $\lambda = 2\pi/\kappa$ and equation (3) yields:

$$\lambda = \frac{\bar{u}}{f} \qquad (4)$$

Equation (4) can be used to translate a frequency into a distance. We hypothesize that when the frequency axis of the co-spectrum is translated using eq. (4), the resulting distance at a given frequency indicates the distance from the eddy tower of the point of origin of the flux contribution at that frequency.

Data were collected from a wet polygonal tundra site during June 9–September 19, 2006 at the Russian-German Research Station Samoylov Island in the southern central Lena River Delta, Siberia. The measurements and the instrument set-up are described in detail in Sachs et al. (2008). Hence we limit our description here to a brief summary. The deployed eddy covariance system was set up as a closed-path system with a Solent R3 three-dimensional sonic anemometer-thermometer (Gill Instruments Ltd., UK) installed at 4 m above the surface, a LI-7000 CO_2/H_2O infrared gas analyzer (LI-COR Inc., USA) and a TGA100 tunable diode laser absorption spectrometer (Campbell Scientific Ltd., USA) for CH_4 analysis. We used 60 min composites of eddy covariance rawdata and R (version 2.7.0 2008-04-22) to perform Fast Fourier Transformations (FFT) and calculate cospectra of the vertical wind w and concentrations c of H_2O, CO_2, and CH_4. Since measurements were made using a closed path system, lag times were determined and the lag was removed for each constituent
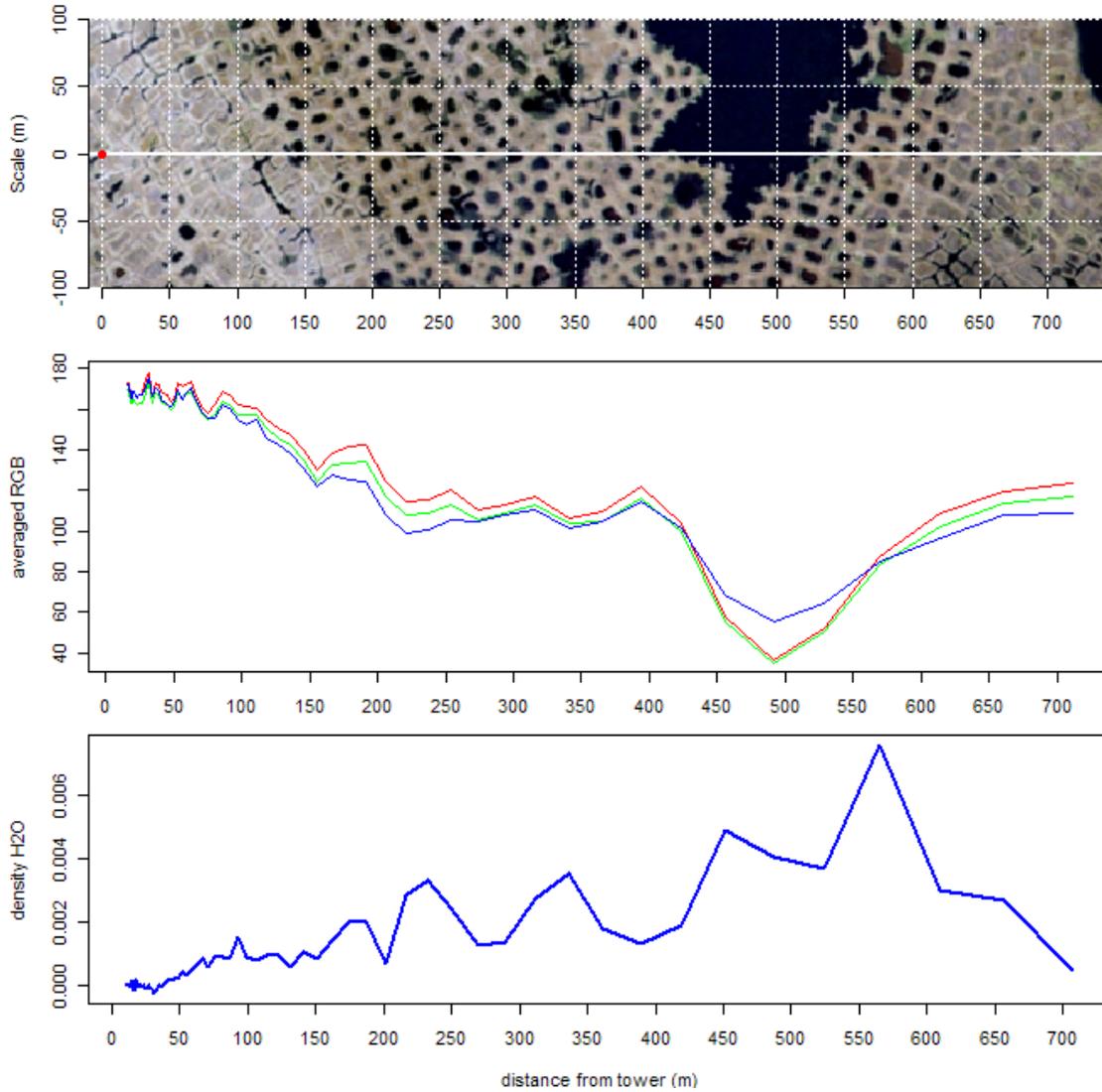
Figure 5.1: Relation between surface conditions and relative spatial-explicit contributions to ecosystem-scale water vapor flux. **(top)** Rotated and cropped aerial image (750 x 200 m). The eddy covariance tower is marked by the red dot. **(middle)** Extracted RGB channels from image above. **(bottom)** $\overline{w'H_2O'}$ cospectrum after translation into the spatial scale. The general trend of increasing wetness from the tower towards the larger lake is visible both in the RGB channels and in the increase in evaporation as shown by the H_2O flux.

before calculating the cospectra. The cospectra were then translated into the spatial scale using equation (4). An orthorectified aerial image mosaic of the investigation area (S. Muster, unpublished data) was rotated so that the mean wind direction during each 60 min data composite was aligned with the x-axis. Translated cospectra were bandwidth-averaged (150 bands) and the red, green, and blue channel of a 200 m wide
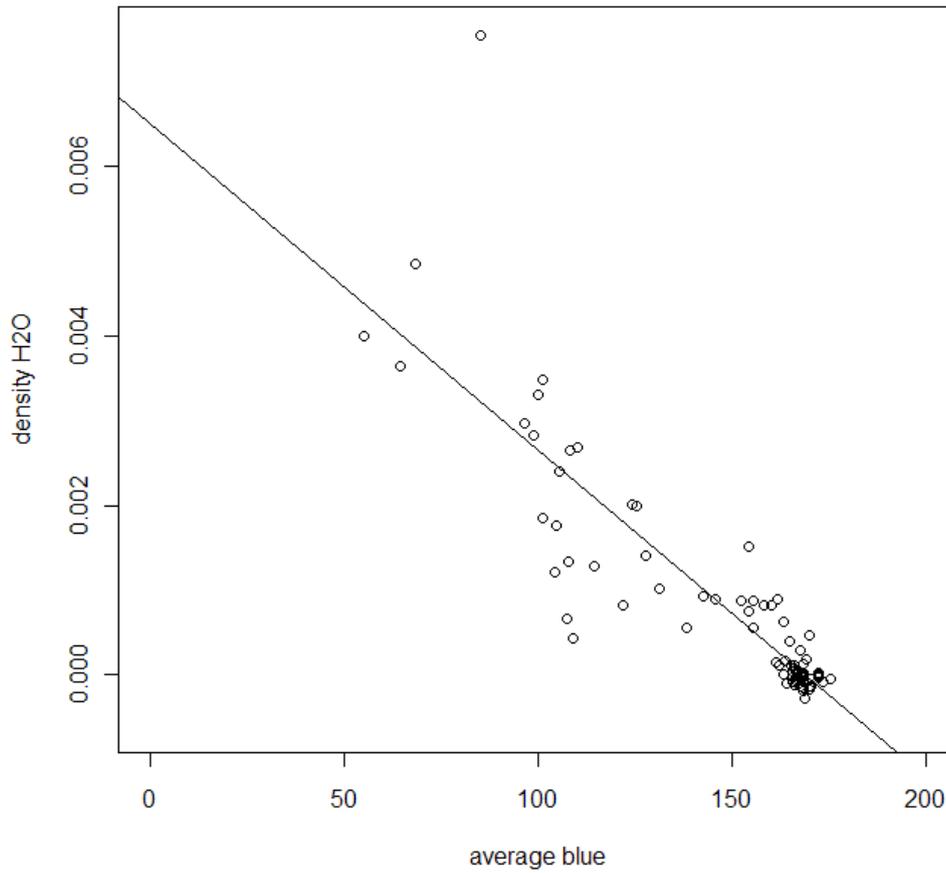
Figure 5.2: Regression of the bandwidth-averaged blue channel and the translated H_2O cospectrum.

Table 5.1: Fraction of significant correlations between cospectra and blue channel and associated ranges of R^2_{adj} at different p.

	Percent significant correlations between image and cospectra					
	$p < 0.1$	R^2_{adj}	$p < 0.05$	R^2_{adj}	$p < 0.01$	R^2_{adj}
H_2O	64%	0.02…0.75	57%	0.03…0.75	45%	0.05…0.75
CO_2	47%	0.02…0.59	39%	0.03…0.59	26%	0.05…0.59
CH_4	38%	0.02…0.56	30%	0.03…0.56	18%	0.05…0.56

and up to 800 m long section of the aerial image were extracted and averaged accordingly (Fig. 5.1). We then correlated the 2426 translated cospectra with the red, green, and blue channels of the corresponding image sections.

5.3   Results

We found significant correlations between the translated cospectra and different channels of an RGB aerial image of the study site in many cases (Table 5.1). Although we had access to true-color images, our results would not differ had we used grayscale images for our analysis. This is due to the fact that we did not find any significant differences in the correlations of the three different color channels of the image (RGB) with the cospectra of H_2O, CO_2 and CH_4. This suggests that all spatial correlations are simply based on the brightness of the image. Wet areas such as inundated polygon centers or ponds and lakes appear darker on the aerial image and emit at least an order of magnitude more methane than drier areas (Sachs et al., submitted). If emergent vegetation is present, then evapotranspiration and photosynthesis are high. Relatively drier areas such as polygon rims (the areas on top of the ice wedges forming the outlines of each polygon) or high-centered polygons, drained areas and sandy river banks appear brighter and are characterized by minimal methane emission, lower evapotranspiration and less intensive photosynthesis.

An example is given in Figure 5.1: The general trend from a relatively "drier" area around the eddy covariance tower (at left) towards more open water surfaces (at right) and an overall wetter area around the larger lake in the right part of the aerial image correlates very well with the cospectral density representing the respective distance from the tower (Fig. 5.2). Since the integral of the cospectral curve equals the ecosystem-scale flux, the interpretation of this example is that the highest water vapor flux can be found between 450 and 600 m upwind from the tower.

In general, results of the correlations between H_2O cospectra and the image brightness values are clearest and easy to interpret. With a random uncertainty of $p < 0.05$, about 57% of all correlations between H_2O cospectra and the image were significant (R^2_{adj} up to 0.75; n=2426), while ~40% of the CO_2 cospectra (R^2_{adj} up to 0.59) and ~30% of the CH_4 cospectra (R^2_{adj} up to 0.56) were significant (Table 5.1).

5.4   Discussion

Since no significant differences were found between the three channels of the RGB image (i.e., the correlations H_2O/CO_2/CH_4–red channel, H_2O/CO_2/CH_4–green channel, H_2O/CO_2/CH_4–blue channel were extremely similar) the correlations were essentially

determined by the brightness of the image. The tundra surface at the investigation site is characterized by polygonal tundra with very wet or inundated low-center polygons, thermokarst cracks, ponds, and lakes on one hand and relatively dry polygon rims or high-center polygons, drained areas and sandy river banks on the other hand. These spatially distributed surface features are associated with distinctly differing vertical exchange fluxes of H_2O, CO_2, and CH_4. Very wet areas emit large amounts of methane, while drier areas emit almost no methane. Similarly, evaporation from very wet areas is higher than that from drier areas, whereas photosynthesis is much higher than respiration in vegetated wet areas, resulting in a negative net ecosystem exchange and thus large negative fluxes of CO_2.

Contrary to our expectation, the method worked best with H_2O cospectra. This may be because of the relatively large coverage of open water surfaces. However, we expected to find the best correlations with methane flux cospectra, as methane fluxes exhibit the steepest gradient between extremely high fluxes from wet low-center polygons and very low fluxes from the surrounding polygon rims, all of which is repeated with a fairly regular pattern at a small scale of typically 10–20 m. Depending on atmospheric stability, the flux footprint area with our measurement height of 4 m, was rather large and thus the statistical information that could be retrieved from narrow frequency bands of flux cospectra were too large to resolve the small-scale pattern of polygonal tundra. In fact, a lower measurement height would most likely have been a benefit for this kind of analysis.

Additionally, our methane flux cospectra did not follow the expected power law in the inertial subrange, a limitation of the TDL system which has also been found by Wille et al. (2008) and Billesbach et al. (1998). This attenuation of the highest frequencies beyond the effect that is expected from a closed-path system (Eugster and Senn 1995), which translates to reduced statistical information from the shorter distances, in combination with the generally very low methane emissions at our investigation site (less than 20 mg m^{-2} d^{-1} on average, see Sachs et al. 2008) appear to be the reason for the smaller number of significant correlations for methane flux cospectra.

However, our results clearly show that translated flux cospectra can be correlated with surface characteristics and thus, strong departures of the flux cospectra

from the idealized cospectra can correspond to surface heterogeneities and could therefore be used to identify flux hotspots within a footprint directly from eddy covariance data as opposed to labor-intensive small-scale measurements. Thus, if proven beyond this first case study, the method could be of interest to the wider FLUXNET community for use at increasingly heterogeneous sites.

5.4.1 Future research

Further research is needed to make this method more generally applicable under different conditions. With the concept shown here we made the important simplification that we only relate one distance with one frequency, thereby assuming that there is not too much complexity in the spatial distribution of different flux densities. We expected our polygonal tundra site to be a simplified case of the more general case of heterogeneous surface where many different small-scale land surface units contribute to ecosystem-scale fluxes. For polygonal tundra, we expected two classes, one related to moist or wet surface conditions, the other for dry conditions of the polygon rims. In reality, each frequency band in the cospectrum (and spectrum) relates to all the distances within the flux footprint area, and thus the more complex the heterogeneity of the surface, the more difficult it might be to relate time-domain or frequency-domain statistical flux information to spatial distributions of fluxes. To advance our method for applicability at such general cases, the theoretical background of Taylor's (1938) frozen turbulence field concept needs to be further developed.

The key issues to be addressed in detail include the assessment of:

(1) The role of mean horizontal wind speed $\bar{u}$ which is dependent on the measurement height z, as wind profiles tend to be logarithmic. Thus, when translating from the frequency domain to spatial wavelength scales, the measurement height should be included in the calculations.

(2) The relationship $\lambda = \bar{u} / f$ which is only correct for the center of a eddy passing the sensor. This, however, is mostly not the case and a relationship that is valid for any part of the eddy passing the sensor needs to be found.

(3) The shape of the eddies, which are usually not exactly circular but anisotropic. In the present form of our equation set, any differences between horizontal and vertical dimensions of the eddies do not have any effect on the results.

Once these aspects of our new method are fully understood, the next step would be the coupling of the spatial-explicit cospectral density information with a detailed footprint model. Since diffusive footprint models require homogenous surfaces (Foken, 2006) a combination of the method with a Lagrangian model (Kljun et al., 2002) would help to gain a comprehensive picture of the composition of flux footprints in inhomogeneous terrain.

5.5 Conclusions

In this first case study, we demonstrated that significant correlations exist between eddy covariance flux cospectra of H_2O, CO_2, and CH_4 and surface features in the footprint, which were identified by their brightness on high-resolution aerial images. Once the theoretical background of the method is further refined, tests and validations under different conditions could make this method a beneficial tool for the wider FLUXNET community to estimate the effect of non-ideal terrain or patchy source distributions on eddy covariance flux data. It could be especially helpful to move towards more accurate upscaling in areas where emission rates and processes vary greatly on small spatial scales, such as the vast and hard to access high latitude tundra ecosystems.

Acknowledgements

6.   DISCUSSION AND SYNTHESIS

The aim of this study was to improve our mechanistic understanding of processes and controls involved in the Arctic methane cycle, to investigate differences between spatial scales, and to evaluate the implications these differences may have on upscaling. Methane fluxes between wet polygonal tundra in Northern Siberia and the atmosphere were investigated at two different scales, the micro-site scale and the ecosystem scale. The results differed in terms of the identified driving factors, as well as the overall magnitude and seasonal balance of the fluxes. Upscaling fluxes from micro-sites to the ecosystem was possible but may have led to a serious bias had the nested measurement approach not allowed to check the upscaled fluxes against measured data.

On the micro-site scale, fluxes were measured using the closed chamber technique. The commonly used method of linear regression for the calculation of fluxes from concentration change over time was assessed in detail with regard to CO_2 fluxes from vegetated wetland soils. It was proven to be often not the adequate approach to derive accurate flux estimates and the application of linear regression was shown to lead to a systematic underestimation of CO_2 fluxes at four different investigation sites. This underestimation was unevenly distributed between CO_2 uptake and emission situations which can cause serious biases in carbon balances. For example, Oechel et al. (1993, 2000) found Alaskan tundra ecosystems to have switched from being a carbon sink to a source in the 1980s and back to a sink in the 1990s. The switching appears to coincide with changes in measurement methods. In particular, measurements in the 1980s predominantly utilized the closed chamber method. If fluxes were calculated by

the traditional linear regression, which is not clearly stated in these publications, results from Chapter 2 imply the possibility for erroneously identifying a carbon source simply because the sink strength was underestimated. Thus, re-analyzing these data with the developed nonlinear flux calculation approach could be a worthwhile and interesting future project.

For the assessment of the linear regression flux calculation, the first theory-based model of CO_2 concentration change in closed chambers over vegetated surfaces was developed. Such biophysical models are helpful in identifying deficiencies of the chamber set-up and measurement design such as leaks or altered environmental conditions, which would cause curvatures not explainable by the model if all model assumptions are met. One such altered environmental parameter that is likely to cause errors in chamber-based flux estimates is near-surface turbulence which was found to be a dominant driver of methane emissions on a larger scale, measured by the non-intrusive eddy covariance method (Chapter 4).

A non-linear regression method was implemented and applied to the analysis of CO_2 and also CH_4 chamber flux measurements. The latter is especially important, as most of the work on methane emissions from high latitudes so far was based on closed chamber flux measurements, some of which were subsequently used for upscaling methane emissions from small measurement plots to regional or global scales (Whalen and Reeburgh, 1988, 1990, 1992; Christensen et al., 1995, Reeburgh et al., 1998; Schneider et al., 2009). The errors associated with the use of linear regression in CO_2 or CH_4 flux calculation, even if they are small compared to natural variability, lead to biases in the summary statistics and propagate during upscaling (e.g. Hutchinson et al., 2000). Thus, the use of linear regression may introduce strong additional biases in large-scale estimates, which are already affected by the extreme spatial heterogeneity of methane emissions.

In Chapter 3, the proposed exponential model for closed chamber flux calculation was applied to determine chamber-based methane fluxes from different micro-sites on Samoylov Island. These fluxes exhibit a strong heterogeneity even within micro-sites assumed to be relatively homogeneous in their characteristics and differ both in their seasonal dynamics and the dominant environmental controls from the simultaneous eddy covariance measurements discussed in Chapter 4. Specifically,

surface temperature had the most explanatory power for chamber-based methane fluxes while near-surface turbulence explained most of the variability on the ecosystem scale. In addition, seasonal variation was much stronger in chamber-based fluxes than on the ecosystem scale. Both of these findings imply that vegetation type and productivity have a major influence on both methane production and methane transport, as has been documented by a number of earlier studies (Morrissey et al., 1993; Whiting and Chanton, 1993; Bubier, 1995; Schimel, 1995; Bellisario et al., 1999; King et al., 1998, 2002; Joabsson and Christensen, 2001). As both vegetation characteristics and surface temperature can be remotely sensed, this relationship would allow upscaling of micro-site fluxes by area-weighted approaches as shown in Chapter 3. However, once a scale is reached where other parameters and processes dominate the emissions, the scaling should not go beyond that respective scale without adjusting the scaling method.

The closed-chamber measurements were nested in the footprint of an eddy covariance tower which provided flux data on the ecosystem scale. The publications by Sachs et al. (2008) in Chapter 4 and Wille et al. (2008) in the appendix constitute the first reports of eddy covariance methane flux measurements from the Russian Arctic and expanded the total number of published eddy covariance methane flux data sets from Arctic tundra by 100% (50% if subarctic sites investigated by Fan et al. (1992) and Hargreaves et al. (2001) are included). The dominant control on methane flux identified for the ecosystem scale was near-surface turbulence. Fan et al. (1992) found methane emissions measured by eddy covariance that originated from a sector characterized by lakes to be dependent on wind speed, but otherwise wind speed or turbulence have not been described as a driver of emissions before and are currently not included in process-based models for methane emissions (e.g. Walter et al., 1996). The same is true for atmospheric pressure which improved the model developed in Chapter 4 significantly and was found to trigger methane ebullition (Tokida et al., 2005, 2006), which may contribute significantly to overall methane emissions (Walter et al., 2006).

The surprisingly low methane emissions on the ecosystem scale indicate that the traditional closed chamber approach may be associated with strong investigator biases and thus heavily skewed to the selection of high-emission micro-sites, which do not adequately reflect the spatial distribution of stronger and weaker methane sources. Fan

et al. (1992) found similarly low emissions from a subarctic Alaskan tundra as measured by eddy covariance, but most other estimates are based on closed chambers.

Community feedback on the publication in Chapter 4 indicated that the proposed model has some general validity and is not restricted to the study site on Samoylov Island. For example, the model, which was based on daily averages, was successfully applied to 30-minute averages of methane flux data at a Canadian site operated by the University of Lethbridge, Alberta (K. Long, personal communication). Interestingly, the site does not have open water surfaces but the model still appears to work very well and even produces improved fits when the atmospheric pressure term is included vs. when it is not included. This indicates that near-surface turbulence and varying atmospheric pressure influence methane emission not only from water bodies through the processes described in Chapter 3 and 4 but through additional mechanisms. One such additional mechanism could be convective flux through plants induced by the Venturi-effect under higher wind speeds (Armstrong et al., 1996).

This study newly identified or "re-identified" processes involved in methane dynamics that demonstrate clearly the interconnections between atmosphere and biosphere on a daily timescale. While methane production takes place in anaerobic soils (and possibly in plants under aerobic conditions (Keppler et al., 2006)), the eventual methane emission to the atmosphere is by no means controlled predominantly by microbial processes. Microbial methane production and oxidation obviously determine the net amount of methane available for eventual release to the atmosphere, thus constraining the potential amount of methane released. However, the energy and matter fluxes coupling different compartments of the biosphere (i.e. soils, vegetation) with each other and with the atmosphere are driven by physical and biological factors and processes within and between these compartments that all affect each other. For example, as shown in this dissertation, atmospheric conditions and processes, primarily pressure fluctuations and turbulent motion, clearly exert a direct influence on transport processes at the soil/vegetation/water-atmosphere interface. While the importance of vegetation has been recognized previously, the atmosphere's role thus far was limited to providing precipitation and solar radiation and receiving the methane emitted from the surface. Other non-biological processes influencing methane emission continue to be identified, such as soil freezing which forces methane produced in unfrozen soil layers

out of the soil at the onset of winter, as outlined in Chapter 4 and recently reported by Mastepanov et al. (2008).

The differences between the dominant controls on methane flux on the two scales as well as the different seasonal dynamics have implications for upscaling those measurements to larger areas. In particular, crossing several scales, i.e. extrapolating from micro-site measurements to regional or global scales should be avoided. Kulmala et al. (2007) found upscaled gross photosynthesis even between neighbored scales at a relatively homogeneous site to differ and identified dense vegetation in chambers as a potential source of overestimation. Fan et al. (1992) found errors of a factor of two when upscaling closed chamber measurements to tower measurements. Thus, even for scaling from micro-sites to the ecosystem scale, it is essential that all micro-sites occurring within the targeted scale are adequately identified and sampled at sufficient spatial resolution, which is often difficult and in any case either labor- or cost-intensive. The closed-chamber measurements from Samoylov Island presented in this dissertation, for example, did not cover all relevant micro-sites, notably lakes and other open water surfaces. Water bodies potentially contribute significantly to the overall ecosystem flux, for example by bubble ebullition (Walter et al., 2006). While the massive amount of emitted methane reported by Walter et al. (2006) is not likely at our site, McEnroe et al. (2009) found methane emissions from open water pools in a northern peatland to depend on pool size, with higher emissions found from smaller, shallower pools. Small and shallow ponds occur frequently on Samoylov Island but their importance to the net ecosystem flux and in particular the process understanding on larger scales was in part only identified by the comparison of results from closed-chambers and eddy covariance and the dominant controls identified for the latter. Thus, without the ability to check chamber-based results against results from the next larger scale and fill identified gaps with results from earlier studies, an upscaling of chamber-based methane fluxes may have resulted in a seriously biased flux estimate because the sampled micro-sites were not representative of the footprint they were nested in.

As a result of the demonstrated strong small-scale heterogeneity, the discrepancies it causes when comparing different methods and scales, and the potential problem in upscaling such measurements, a proof of concept is presented to derive estimates of spatial heterogeneity and contributions from different source areas directly

from eddy covariance data. For methane, this was complicated by the analyzer's attenuation of the high frequencies, but for water fluxes and under simplifying assumptions, a correlation between surface features and spatially translated co-spectra could be shown. This chapter constitutes work in progress and needs to be presented to the larger eddy covariance community for thorough testing, evaluation, and further development, which initial feedback indicates strong interest in.

This dissertation argues strictly scale-dependent and the results from different scales suggest that a certain degree of restraint is advisable when measurements are upscaled. The development of reliable upscaling procedures relies on detailed multi-scale studies at representative key sites where scaling results can be checked against real data. On a much larger scale than possible in this study in terms of human and financial resources, several multi-scale studies are currently in progress in different parts of the Arctic. Under U.S. National Science Foundation Office of Polar Programs grant 0421588, a large-scale water table manipulation experiment is conducted at the Barrow Environmental Observatory, including closed chamber measurements, automated tramlines for spectral measurements, multiple eddy covariance towers, and airplanes for gas flux measurements. All investigations are conducted in a nested approach as advocated in Chapter 3. Previously in the US, NASA's Atmospheric Boundary Layer Expedition (ABLE 3A) in 1988 already applied a multi-scale and nested approach at a subarctic tundra site in Alaska and produced results very much in agreement with the results presented here (e.g. Fan et al., 1992).

In Europe, the ABACUS (Arctic Biosphere Atmosphere Coupling at mUltiple Scales) consortium of UK scientists currently conducts multi-scale investigations of carbon fluxes using chambers, towers, and aircraft near Abisko, Sweden, and near Kevo, Finland (Fox et al., 2008). To really understand the Arctic system with its tightly coupled and interconnected processes, more multi-scale and longterm observations are necessary.

One ideal candidate site for this kind of integrated ecosystem-atmosphere research would be the study site introduced in this dissertation. It has a long history of intensive research into various aspects of the environment to draw from and the groundwork for truly scale-conscious investigations has been laid by this study. As methane flux measurements resume in 2009 with more resources and eddy covariance

towers available and small-scale investigations of the microbiology involved in methane production and oxidation supplemented by subsurface methane gradient and transport studies, intensified multi-scale studies become more feasible. With closed chamber measurements nested in the footprints of eddy covariance towers on two distinctly different terraces in the southern Lena River Delta, the logical next step would be aircraft measurements of methane fluxes and mixing ratios and supporting concentration gradient measurements in the lower atmosphere using balloons or blimps for ground-truthing the aircraft measurements. The GFZ and University of Bremen operated Methane Airborne Mapper (MAMap) would be the ideal tool to complement the resuming flux studies and to enable verifiable upscaling of ecosystem-scale flux measurements to the regional scale or even global scale by closing the gap between satellite data provided by SCIAMACHY and ground-based measurements. With all tools at hand, every effort should be made to implement the first and only known site in the vast Russian Arctic, where methane fluxes can be investigated intensively on all relevant scales from microbial and physical subsurface processes to the interface between soil/vegetation and atmosphere to transport and distribution within the atmosphere.

7. BIBLIOGRAPHY

ACIA (2005), *Arctic Climate Impact Assessment*, Cambridge Univ. Press, 1042 pp.

Abramova, E., I. Vishnyakova, and T. Sachs (2007), Hydrobiological investigations in the Lena Delta, In *Russian-German Cooperation SYSTEM LAPTEV SEA: The Expedition Lena 2006*, Alfred-Wegener-Institut für Polar- und Meeresforschung, Bremerhaven.

Akaike, H. (1974), A new look at the statistical model identification, *IEEE T. Automat. Contr.*, *19*, 6, 716–723.

Alm, J., A. Talanov, S. Saarnio, J. Silvola, E. Ikkonen, H. Aaltonen, H. Nykanen, and P. Martikainen (1997), Reconstruction of the carbon balance for microsites in a boreal oligotrophic pine fen, Finland, *Oecologia*, *110*(3), 423-431.

Alm, J., S. Saarnio, H. Nykänen, J. Silvola, and P. J. Martikainen (1999) Winter CO_2, CH_4 and N_2O fluxes on some natural and drained boreal peatlands. *Biogeochemistry*, *44*, 163–186.

Alm, J., Shurpali, N. J.., Tuittila, E.-S., Laurila, T., Maljanen, M., Saarnio, S., and K. Minkkinen (2007), Methods for determining emission factors for the use of peat and peatlands – flux measurements and modelling, *Boreal Environ. Res.*, *12*, 85-100.

Amthor, J. S. (2000) Direct effect of elevated CO2 on nocturnal in situ leaf respiration in nine temperate deciduous tree species is small, *Tree Physiol.*, *20*, 139-144.

Are FE, Reimnitz E (2000) An overview of the Lena River Delta setting, geology, tectonics, geomorphology, and hydrology. *Journal of Coastal Research*, *16*(4), 1083-1093.

Arrhenius, S. (1909), Theorien der Chemie, Nach Vorlesungen gehalten an der Universität von Kalifornien zu Berkeley, 2nd ed., Akademische Verlagsgesellschaft m.b.H., Leipzig, Germany.

Are, F. E., and E. Reimnitz (2000), An overview of the Lena River Delta setting, geology, tectonics, geomorphology, and hydrology, *Journal of Coastal Research*, *16*(4), 1083-1093.

Baldocchi, D. D., B. B. Hincks, and T. P. Meyers (1988), Measuring Biosphere-Atmosphere Exchanges of Biologically Related Gases with Micrometeorological Methods, *Ecology*, 1331-1340.

Baldocchi, D. D., E. Falge,L. Gu, R. Olson, D. Hollinger, S. Running, P. Anthoni, C. Bernhofer, K. Davis, R. Evans, J. Fuentes, A. Goldstein, G. Katul, B. Law, X. Lee, Y. Malhi, T. Meyers,W. Munger, W. Oechel, K. T. Paw U, K. Pilegaard, H. P. Schmid, R. Valentini, S. Verma, T. Vesala, K. Wilson, and S. Wofsy (2001), FLUXNET: A New Tool to Study the Temporal and Spatial Variability of Ecosystem-Scale Carbon Dioxide, Water Vapor, and Energy Flux Densities, *Bulletin of the American Meteorological Society*, *82*, 11, 2415-2434.

Balzer, K. (1997), Mindest RV, Beitrag zum Langfristprognoseseminar beim gemeinsamen Seminar am Institut für Meteorologie der FU, Berlin, Germany.

Bellisario, L. M., J. L. Bubier, T. R. Moore, and J. P. Chanton (1999), Controls on CH4 Emissions From a Northern Peatland, *Global Biogeochemical Cycles*, *13*(1), 81–91.

Billesbach DP, Kim J, Clement RJ, Verma SB, Ullman FG (1998) An Intercomparison of Two Tunable Diode Laser Spectrometers Used for Eddy Correlation Measurements of Methane Flux in a Prairie Wetland. *Journal of Atmospheric and Oceanic Technology*, *15*, 197–206.

Boike J, Hinzman L, Overduin P, Romanovsky V, Ippisch O, Roth K (2003) A comparison of snow melt at three circumpolar sites: Spitsbergen, Siberia, Alaska. In: *Permafrost: Proceedings of the 8th International Conference on Permafrost 2003* (eds Arenson LU, Phillips M, Springman SM), pp. 79–84. Balkema Publishers, Lisse.

Boike, J., D. Y. Bolshiyano, and M. Grigoriev (Eds.) (2007), *Russian-German Cooperation SYSTEM LAPTEV SEA: The Expedition Lena 2006*, Alfred-Wegener-Institut für Polar- und Meeresforschung, Bremerhaven.

Boike, J., C. Wille, and A. Abnizova (2008), The climatology, and summer energy and water balance of polygonal tundra in the Lena River Delta, Siberia, *J. Geophys. Res.*, doi:10.1029/2007JG000540,

Boike, J., D. Y. Bolshiyano, L. Schirrmeister and S. Wetterich (Eds.) (2009), *Russian-German Cooperation SYSTEM LAPTEV SEA: The Expedition Lena – New Siberian Islands 2007 during the International Polar Year 2007/2008*, Alfred-Wegener-Institut für Polar- und Meeresforschung, Bremerhaven.

Breiman, L., J. H. Friedman, R. A. Olshen, and C. J. Stone (1984), *Classification and Regression Trees*, The Wadsworth Statistics/Probability Series, Chapman & Hall/CRC, Boca Raton, Florida, USA.

Bubier, J. L. (1995), The relationship of vegetation to methane emission and hydrochemical gradients in northern peatlands, *Journal of Ecology*, *83*(3), 403-420.

Bubier, J. L., and T. R. Moore (1994), An ecological perspective on methane emissions from northern wetlands, *Trends in Ecology & Evolution*, *9*(12), 460-464.

Bubier, J., P. Crill, and A. Mosedale (2002), Net ecosystem CO_2 exchange measured by autochambers during the snow-covered season at a temperate peatland, *Hydrological Processes*, *16*(18), 3667-3682.

Bunce, J. A (2005), Response of respiration of soybean leaves grown at ambient and elevated carbon dioxide concentrations to day-to-day variation in light and temperature under field conditions, *Ann. Bot.-London*, *95*, 1059-1066.

Burnham, K. P., and D. R. Anderson (2004), Multimodel inference: understanding AIC and BIC in model selection, *Sociol. Method. Res.*, *33*, 2, 261-304.

Burrows, E. H., Bubier, J. L., Mosedale, A., Cobb, G. W., and P. M. Crill (2004), Net Ecosystem exchange of carbon dioxide in a temperate poor fen: a comparison of automated and manual chamber techniques, *Biogeochemistry*, *76*, 21-45.

Cao, M., S. Marshall, and K. Gregson (1996), Global carbon exchange and methane emissions from natural wetlands: Application of a process-based model, *J. Geophys. Res.*, *101*(D9), 14,399–14,414.

Chapin III, F. S., A. D. McGuire, J. Randerson, R. Pielke Sr., D. Baldocchi, S. E. Hobbie, N. Roulet, W. Eugster, S. Kasischke, E. B. Rastetter, S. A. Zimov, and S. W. Running (2000), Arctic and boreal ecosystems of western North America as

components of the climate system, *Global Change Biology*, *6*(s1), 211-223, doi:10.1046/j.1365-2486.2000.06022.x.

Christensen, T. R., S. Jonasson, T. V. Callaghan, and M. Havström (1995), Spatial variation in high-latitude methane flux along a transect across Siberian and European tundra environments, *J. Geophys. Res.*, *100*(D10), 21,035–21,046.

Christensen, T. R., I. C. Prentice, J. Kaplan, A. Haxeltine, and S. Sitch (1996), Methane flux from northern wetlands and tundra: An ecosystem source modelling approach, *Tellus Chemical and Physical Meteorology*, *48B*(5), 652-661.

Christensen, T. R., Jonasson, S., Michelsen, A., Callaghan, T. V., and M. Havström (1998), Environmental controls on soil respiration in the Eurasian and Greenlandic Arctic. *J. Geophys. Res.*, *103*, D22, 29,015-29,021.

Christensen, T. R., T. Friborg, M. Sommerkorn, J. Kaplan, L. Illeris, H. Soegaard, C. Nordstroem, and S. Jonasson (2000), Trace gas exchange in a high-arctic valley 1. Variations in CO_2 and CH_4 flux between tundra vegetation types, *Global Biogeochem. Cycles*, *14*(3), 701–714.

Christensen, T., D. Lloyd, B. Svensson, P. Martikainen, R. Harding, H. Oskarsson, H. Soegaard, T. Friborg, and N. Panikov (2002), Biogenic controls on trace gas fluxes in northern wetlands, *Global Change Newsletter*, *51*, 9-15.

Conen, F. and K. A. Smith (1998), A re-examination of closed flux chamber methods for the measurement of trace gas emissions from soils to the atmosphere, *Eur. J. Soil Sci.*, *49*, 701-707.

Conrad, R. (1989) Control of methane production in terrestrial ecosystems, in: *Exchange of Trace Gases between Terrestrial Ecosystems and the Atmosphere,* edited by M. O. Andreae and D. S. Schimel, pp. 39-58, John Wiley and Sons, Chichester, UK.

Corradi, C., O. Kolle, K. Walter, S. A. Zimov, and E.-D. Schulze (2005), Carbon dioxide and methane exchange of a north-east Siberian tussock tundra, *Global Change Biology*, 11, 1–16, doi: 10.1111/j.1365-2486.2005.01023.x

D'Agostino, R. B. (1971), An omnibus test of normality for moderate and large size samples, *Biometrika*, *58*, 2, 341-348.

D'Agostino, R. B. (1986), Tests for normal distribution, in Goodness-Of-Fit Techniques edited by D'Agostino R. B. et al., Marcel Dekker Ltd., New York.

Davidson, E. A., Savage, K., Verchot, L. V., and R. Navarro (2002), Minimising artefacts and biases in chamber-based measurements of soil respiration, *Agric. Forest Meteorol.*, *113*, 21-37.

De'ath, G., and K. E. Fabricius (2000), Classification and Regression Trees: A Powerful Yet Simple Technique for Ecological Data Analysis, *Ecology*, *81*, 11, 3178-3192.

Denmead, O. T. and D. C. Reicosky (2003), Tillage-induced gas fluxes: Comparison of meteorological and large chamber techniques, *Proceedings of the 16th Triennial Conference of International Soil Tillage Research Organizations*, 13-18 July 2003, Brisbane, Australia.

Dise, N.B. (1992), Winter fluxes of methane from Minnesota peatlands, *Biogeochemistry*, *17*(2), 71-83.

Drake, B. G., Azcon-Bieto, J., Berry, J., Bunce, J., Dijkstra, P., Farrar, J., Gifford, R. M., Gonzalez-Meler, M. A., Koch, G., Lambers, H., Siedow, J., and S. Wullschleger (1999), Does elevated atmospheric CO2 inhibit mitochondrial respiration in green plants?, *Plant, Cell Environ.*, *22*, 649-657.

Drösler, M. (2005), Trace gas exchange of bog ecosystems, Southern Germany, PhD thesis, Technische Universität München, Munich, 179 pp..

Dugas, W. A., Reicosky, D. C., and J. R. Kiniry (1997), Chamber and micrometeorological measurements of CO2 and H2O fluxes for three C4 grasses, *Agric. Forest Meteorol.*, *83*, 1, 113-133.

Durbin, J. and G. S. Watson (1950), Testing for serial correlation in least squares regression I, *Biometrika*, *37*, 409-428.

Eugster, W., and W. Senn (1995), A cospectral correction model for measurement of turbulent NO2 flux, *Boundary Layer Meteorol.*, *74*, 321– 340.

Fan, S. M., S. C. Wofsy, P. S. Bakwin, D. J. Jacob, S. M. Anderson, P. L. Kebabian, J. B. McManus, C. E. Kolb, and D. R. Fitzjarrald (1992), Micrometeorological measurements of CH4 and CO2 exchange between the atmosphere and subarctic tundra, *J. Geophys. Res.*, *97*(D15), 16,627–16,643.

Farquhar, G. D., von Caemmerer, S., and J. A. Berry (1980), A biochemical model of photosynthetic CO2 assimilation in leaves of C3 species, *Planta*, *149*, 78-90.

Fisher, R. A. (1924), On a distribution yielding the error functions of several well known statistics, *Proceedings of the International. Congress of Mathematicians*, Toronto, 2, 805-813.

Foken, T., and B. Wichura (1996), Tools for quality assessment of surface-based flux measurements, *Agricultural and Forest Meteorology*, *78*(1-2), 83-105.

Foken, T. (2006), *Angewandte Meteorologie*, Springer-Verlag, Berlin.

Fox, A. M., B. Huntley, C. R. Lloyd, M. Williams, and R. Baxter (2008), Net ecosystem exchange over heterogeneous Arctic tundra: Scaling between chamber and eddy covariance measurements, *Global Biogeochem. Cycles*, *22*. [online] Available from: http://dx.doi.org/10.1029/2007GB003027

Friborg, T., T. R. Christensen, B. U. Hansen, C. Nordstroem, and H. Soegaard (2000), Trace gas exchange in a high-arctic valley 2. Landscape CH_4 fluxes measured and modeled using eddy correlation data, *Global Biogeochem. Cycles*, *14*(3), 715–724.

Friborg, T., H. Soegaard, T. R. Christensen, C. R. Lloyd, and N. S. Panikov (2003), Siberian wetlands: Where a sink is a source, *Geophys. Res. Lett.*, *30*(21), 2129, doi:10.1029/2003GL017797.

Frolking S., and P.Crill (1994), Climate controls on temporal variability of methane flux from a poor fen in southeastern New Hampshire: Measurement and modeling, *Global Biogeochemical Cycles*, *8*(4), 385-397.

Fung, I., J. John, J. Lerner, E. Matthews, M. Prather, L. P. Steele, and P. J. Fraser (1991), Three-dimensional model synthesis of the global methane cycle, *J. Geophys. Res.*, *96*(D7), 13,033–13,065.

Ganzert, L., G. Jurgens, U. Münster, and D. Wagner (2006), Methanogenic communities in permafrost-affected soils of the Laptev Sea coast, Siberian Arctic, characterized by 16S rRNA gene fingerprints, *FEMS Microbiology Ecology, 59*(2), 476–488. doi:10.1111/j.1574-6941.2006.00205.x

Gorham, E. (1991), Northern Peatlands: Role in the Carbon Cycle and Probable Responses to Climatic Warming, *Ecological Applications*, *1*(2), 182-195.

Granberg, G., Sundh, I., Svensson, B. H., and M. Nilsson (2001), Effects of temperature, and nitrogen and sulphur deposition, on methane emission from a boreal mire, *Ecology*, *82*, 7, 1982-1998.

Griffin K. L. and Y. Luo (1999), Sensitivity and acclimation of Glycine max (L.) Merr. leaf gas exchange to CO2 partial pressure, *Environ. Exp. Bot.*, *42*, 141-153.

Grigoriev, N. F. (1960), The temperature of permafrost in the Lena delta basin – deposit conditions and properties of the permafrost in Yakutia, *Yakutsk*, *2*, 97-101 (in Russian).

Grulke, N. E., Riechers, G. H., Oechel, W. C., Hjelm, U., and C. Jaeger (1990), Carbon balance in tussock tundra under ambient and elevated atmospheric CO2, *Oecologia*, *83*, 485-494.

Goulden, M. L. and P. M. Crill (1997), Automated measurements of CO2 exchange at the moss surface of a black spruce forest, *Tree Physiol.*, *17*, 537–542.

Hanson, P. J., Wullschleger, S. D., Bohlman, S. A., and D. E. Todd (1993), Seasonal and topographic patterns of forest floor CO2 efflux from upland oak forest, *Tree Physiol.*, *13*, 1–15.

Harazono, Y., M. Mano, A. Myiata, M. Yoshimoto, R. C. Zulueta, G. L. Vourlitis, H. Kwon, and W. C. Oechel (2006), Temporal and spatial differences of methane flux at arctic tundra in Alaska, *Mem. Natl. Inst. Polar Res.*, *Spec. Issue 59*, 79-95.

Hargreaves, K. J., D. Fowler, C. E. R. Pitcairn, and M. Aurela (2001), Annual methane emission from Finnish mires estimated from eddy covariance campaign measurements, *Theor. Appl. Climatol.*, *70*, 203-213.

Healy, R. W., Striegl, R. G., Ressel, T. F., Hutchinson, G. L., and G. P. Livingston (1986), Numerical evaluation of static-chamber measurements of soil-atmosphere gas exchange identification of physical processes, *Soil Sci. Soc. Am. J.*, *60*, 740-747.

Heijmans, M. M. P. D., Arp, W. J., and F. S. Chapin III (2004), Carbon dioxide and water vapour exchange from understorey species in boreal forest, *Agric. Forest Meteorol.*, *123*, 135-147.

Hibbert, D. B. (2005), Further comments on the (miss-)use of r for testing the linearity of calibration functions, *Accredit. Qual. Assur.*, *10*, 300-301.

Houghton, J. T., Y. Ding, D. J. Griggs, M. Noguer, P. J. van der Linden, and D. Xiaosu (Eds.) (2001), Climate Change 2001: The Scientific Basis. Contribution of Working Group I to the Third Assessment Report of the Intergovernmental Panel on Climate Change, 944 pp., Cambridge University Press, UK.

Hubberten H.-W., D. Wagner D, E.-M. Pfeiffer, J. Boike, A. Y. Gukov (2006), The Russian-German research station Samoylov, Lena Delta – a key site for polar research in the Siberian Arctic, *Polarforschung*, *73*(2/3), 111-116.

Huber, W. (2004), On the use of the correlation coefficient r for testing the linearity of calibration functions, *Accredit. Qual. Assur.*, *9*, 726.

Hutchinson, G. L. and G. P. Livingston (2001), Vents and seals in non-steady state chambers used for measuring gas exchange between soil and the atmosphere, *Eur. J. Soil Sci.*, *52*, 675-682.

Hutchinson G. L. and A. R. Mosier (1981), Improved soil cover method for field measurement of nitrous oxide fluxes, *Soil Sci. Soc. Am. J.*, *45*, 311-316.

Hutchinson, G. L., Livingston, G. P., Healy, R. W., and R. G. Striegl (2000), Chamber measurement of surface-atmosphere trace gas exchange: numerical evaluation of dependence on soil, interfacial layer, and source/sink properties, *J. Geophys. Res.*, *105*, D7, 8865-8875.

IPCC (2007), *Climate Change 2007: The Physical Science Basis: Contribution of Working Group I to the Fourth Assessment Report of the Intergovernmental Panel on Climate Change*, edited by S. Solomon, D. Qin, M. Manning, Z. Chen, M. Marquis, K. B. Averyt, M. Tignor, and H. L. Miller, Cambridge University Press, Cambridge, UK and New York, NY, USA.

Joabsson, A., and T. Christensen (2001), Methane emissions from wetlands and their relationship with vascular plants: an Arctic example, *Global Change Biology*, *7*(8), 919-932.

Jensen, L. S., Mueller, T., Tate, K. R., Ross, D. J., Magid, J., and N. E. Nielsen (1996), Soil surface CO2 flux as an index of soil respiration in situ: a comparison of two chamber methods, *Soil Biol. Biochem.*, 28, 1297-1306.

Kaimal, J. C., J. C. Wyngaard, Y. Izumi, O. R. Coté (1972), Spectral characteristics of surface layer turbulence, *Quarterly Journal of the Royal Meteorological Society*, 98, 563–589.

Keppler, F., J. T. G. Hamilton, M. Braß, and T. Rockmann (2006), Methane emissions from terrestrial plants under aerobic conditions, *Nature*, *439*(7073), 187-191, doi:10.1038/nature04420.

King, J., W. Reeburgh, and S. Regli (1998), Methane emission and transport by arctic sedges in Alaska: Results of a vegetation removal experiment, *J. Geophys. Res.-Atmos.*, *103*(D22), 29083-29092.

King, J., W. Reeburgh, K. Thieler, G. Kling, W. Loya, L. Johnson, and K. Nadelhoffer (2002), Pulse-labeling studies of carbon cycling in Arctic tundra ecosystems: The contribution of photosynthates to methane emission, *Global Biogeochemical Cycles*, *16*(4).

Kljun, N., M. W. Rotach, and H. P. Schmid (2002), A three-dimensional backward lagrangian footprint model for a wide range of boundary-layer stratifications, *Boundary Layer Meteorology*, 103, 205-226.

Kormann, R., H. Mueller, and P. Werle (2001), Eddy flux measurements of methane over the fen "Murnauer Moos", 11°11'E, 47°39'N, using a fast tunable diode laser spectrometer, *Atmospheric Environment*, *35*(14), 2533-2544.

Kotlyakov, V., and T. Khromova (2002), Permafrost, Snow and Ice, in: *Land Recources of Russia* [CD-ROM, Eds. Stolbovoi, V and I. McCallum], International Institute of Applied Systems Analysis and the Russian Academy of Science, Laxenburg, Austria.

Kulmala, L., S. Launiainen, J. Pumpanen, H. Lankreijer, A. Lindroth, P. Hari, and T. Vesala (2008), H2O and CO2 fluxes at the floor of a boreal pine forest, *Tellus B*, *60*(2), 167-178, doi:10.1111/j.1600-0889.2007.00327.x.

Kutzbach, L. (2006), The exchange of energy, water and carbon dioxide between wet arctic tundra and the atmosphere at the Lena River Delta, Northern Siberia, *Reports on Polar and Marine Research*, *541*, 157 pp., Alfred Wegener Institute, Bremerhaven, Germany.

Kutzbach, L., Wagner, D., and E.-M. Pfeiffer (2004), Effect of microrelief and vegetation on methane emission from wet polygonal tundra, Lena Delta, Northern Siberia, *Biogeochemistry*, *69*, 341-362.

Kutzbach, L., J. Schneider, T. Sachs, M. Giebels, H. Nykänen, N. J. Shurpali, P. J. Martikainen, J. Alm, and M. Wilmking (2007), CO_2 flux determination by closed-chamber methods can be seriously biased by inappropriate application of linear regression, *Biogeosciences*, *4*, 1005-1025.

Kutzbach, L., C. Wille, and E.-M. Pfeiffer (2007),The exchange of carbon dioxide between wet arctic tundra and the atmosphere at the Lena River Delta, Northern Siberia, *Biogeosciences*, *4*, 869-890.

Laurila,T., J. P. Tuovinen, and A. Lohila (2005), Measuring methane emissions from a landfill using a cost-effective micrometeorological method, *Geophysical Research Letters*, *32*, 1-5.

Laine, A., Sottocornola, M., Kiely, G., Byrne, K. A., Wilson, D., and E.-S. Tuittila (2006), Estimating net ecosystem exchange in a patterned ecosystem: Example from blanket bog, *Agric.Forest Meteorol.*, *18*, 231-243.

Law, B. E., Ryan, M. G., and P. M. Anthoni (1999), Seasonal and annual respiration of a ponderosa pine ecosystem, *Glob. Change Biol.*, *5*, 169-182.

Le Dantec, V., Epron, D., and E. Dufrene (1999), Soil CO2 efflux in a beech forest: comparison of two closed dynamic systems, *Plant Soil*, *214*, 125-132.

Lee, X, W. Massman, and B. E. Law (2004), Handbook of micrometeorology. A guide for surface flux measurement and analysis, Kluwer Academic Press, Dordrecht, 250 pp.

Liebner, S., and D. Wagner (2007), Abundance, distribution and potential activity of methane oxidizing bacteria in permafrost soils from the Lena Delta, Siberia, *Environmental Microbiology*, *9*(1), 107–117. doi:10.1111/j.1462-2920.2006.01120.x

Livingston G. P. and G. L. Hutchinson (1995), Enclosure-based measurement of trace gas exchange: applications and sources of error, in: Biogenic Trace Gases: Measuring Emissions from Soil and Water, edited by Matson, P. A. and Harriss, R. C., Blackwell Science Ltd, Oxford, UK, pp. 15-51.

Livingston, G. P., Hutchinson, G. L., and K. Spartalian (2005), Diffusion theory improves chamber-based measurements of trace gas emissions, *Geophys. Res. Lett.*, *32*, L24817, doi:10.1029/2005GL024744.

Livingston, G. P., Hutchinson, G. L., and K. Spartalian (2006), Trace Gas Emission in Chambers A Non-Steady-State Diffusion Model, *Soil Sci. Soc. Am. J.*, *70*, 1459-1469.

Luo, Y. and H. A. Mooney (1996), Stimulation of global photosynthetic carbon influx by an increase in atmospheric carbon dioxide concentration, in: Carbon Dioxide and

Terrestrial Ecosystems, edited by G. W .Koch and H. A. Mooney, pp. 381-397, Academic, San Diego.

Luo, Y., Sims, D. A., Thomas, R. B., Tissue, D. T., and J. T. Ball (1996), Sensitivity of leaf photosynthesis to CO2 concentration is an invariant function for C3 plants: A test with experimental data and global applications, *Global Biogeochem. Cycles*, *10*, 2, 209-222.

MacIntyre, S., R. Wanninkhof, and J. P. Chanton (1995), Trace gas exchange across the air-water interface in freshwater and coastal marine environments, in: *Biogenic Trace Gases: Measuring Emissions from Soil and Water,* edited by P. Matson and R. Harriss, pp. 52-97, Blackwell.

Maljanen M., Martikainen P. J., Walden J., and J. Silvola (2001), CO2 exchange in an organic field growing barley or grass in eastern Finland, *Glob.Change Biol.*, *7*, 679-692.

Mastepanov, M., C. Sigsgaard, E. J. Dlugokencky, S. Houweling, L. Strom, M. P. Tamstorf, and T. R. Christensen (2008), Large tundra methane burst during onset of freezing, *Nature*, *456*(7222), 628-630, doi:10.1038/nature07464.

Matson, P. A. and R. C. Harriss (editors) (1995), Measuring Emissions from Soil and Water, Blackwell Science Ltd, Oxford, UK, 383 pp..

Matthias, A. D., Yarger, D. N., and R. S. Weinback (1978), A numerical evaluation of chamber methods for determining gas fluxes, *Geophys. Res. Lett.*, *5,* 765-768.

McGuire, A. D., J. M. Melillo, D. W. Kicklighter, Y. Pan, X. Xiao, J. Helfrich, B. M. III, C. J. Vorosmarty, and A. L. Schloss (1997), Equilibrium Responses of Global Net Primary Production and Carbon Storage to Doubled Atmospheric Carbon Dioxide: Sensitivity to Changes in Vegetation Nitrogen Concentration, *Global Biogeochemical Cycles*, *11*(2), 173–189.

McMillen, R. (1988), An eddy correlation technique with extended applicability to non-simple terrain, *Boundary-Layer Meteorology*, *43*, 231-245.

Meyer, H. (2003), Studies on recent cryogenesis. In: *Russian-German Cooperation SYSTEM LAPTEV SEA, The Expedition LENA 2002, Reports on Polar and Marine Research 466* (eds Grigoriev MN *et al.*) pp. 8-16, Alfred-Wegener-Institute, Bremerhaven, Germany.

Moncrieff, J. B., Y. Mahli, and R. Leuning (1996), The propagation of errors in long-term measurements of land-atmosphere fluxes of carbon and water, *Global Change Biology*, *2*, 231-240.

Moore, C. J. (1986), Frequency response corrections for eddy correlation systems, *Boundary-Layer Meteorology*, *37*, 17-35.

Morrissey, L. A., D. B. Zobel, and G. P. Livingston (1993), Significance of stomatal control on methane release from -dominated wetlands, *Chemosphere*, *26*(1-4), 339-355.

Nakano, T., S. Kuniyoshi, and M. Fukuda (2000), Temporal variation in methane emission from tundra wetlands in a permafrost area, northeastern Siberia, *Atmospheric Environment*, *34*(8), 1205-1213, doi:doi: DOI: 10.1016/S1352-2310(99)00373-8.

Nakano, T., Sawamoto, T., Morishita, T., Inoue, G., and R. Hatano (2004), A comparison of regression methods for estimating soil-atmosphere diffusion gas fluxes by a closed-chamber technique, *Soil Biol. Biochem.*, *36*, 107-113.

Norman, J. M., Kucharik, C. J., Gower, S. T., Baldocchi, D. D., Crill, P. M., Rayment, M., Savage, K., and R. G. Striegl (1997), A comparison of six methods for measuring soil-surface carbon dioxide fluxes, *J. Geophys. Res.*, *102D*, 28771-28777.

Nykänen H, Heikkinen JEP, Pirinen L, Tiilikainen K, and P. J. Martikainen (2003), Annual CO2 exchange and CH4 fluxes on a subarctic palsa mire during climatically different years, *Global Biogeochem. Cycles*, *17*, 1, 1-18.

Oechel, W. C., Hastings, S. J., Vourlitis, G. L., Jenkins, M., Riechers, G., and N. Grulke (1993), Recent Change of Arctic ecosystems from a net carbon dioxide sink to a source, *Nature*, *361*, 520-523.

Oechel, W. C., Vourlitis, G. L., Brooks, S., Crawford, T. L., and E. Dumas (1998), Intercomparison among chamber, tower, and aircraft net CO2 and energy fluxes measured during the Arctic System Science Land-Atmosphere-Ice Interactions (ARCSS-LAII) Flux Study, *J. Geophys. Res.*, *103*, D22, 28993-29003.

Oechel, W. C., Vourlitis, G. L., Hastings, S. J., Zulueta, R. C., Hinzman, L., and D. Kane (2000), Acclimation of ecosystem CO2 exchange in the Alaskan Arctic in response to decadal climate warming, *Nature, 406*, 978-981.

Panikov, N.S., and S. N. Dedysh (2000), Cold season CH_4 and CO_2 emission from boreal peat bogs (West Siberia): Winter fluxes and thaw activation dynamics, *Global Biogeochemical Cycles*, *14*(4), 1071-1080.

Panikov, N.S., S. N. Dedysh, O. M. Kolesnikov, A. I. Mardini, and M. V. Sizova (2001), Metabolic and environmental control on methane emission from soils: mechanistic studies of mesotrophic fen in West Siberia, *Water, Air, & Soil Pollution: Focus*, *1*(5-6), 415-428.

Pedersen, A. R. (2000), Estimating the nitrous oxide emission rate from the soil surface by means of a diffusion model, *Scand. J. Stat.*, *27*, 385-403.

Pedersen, A. R., Petersen, S. O., and F. P. Vinther (2001), Stochastic diffusion model fro estimating trace gas emissions with static chambers. *Soil Sci. Soc. Am. J.*, *65*, 49-58.

Pfeiffer, E.-M., Akhmadeeva, I., Becker, H., Wagner, D., Quass, W., Zhurbenko, M., and E. Zöllner (1999), Modern processes in permafrost affected soils, in: Expeditions in Siberia in 1998, edited by Rachold, V., *Reports on Polar Research*, *315*, Alfred Wegener Institute, Bremerhaven, Germany, pp. 19-79.

Post, W. M., W. R. Emanuel, P. J. Zinke, and A. G. Stangenberger (1982), Soil carbon pools and world life zones, *Nature*, *298*(5870), 156-159, doi:10.1038/298156a0.

Potthoff, R. F. (1965), Some Scheffé-type tests for some Behrens-Fisher type regression problems, *J. Am. Stat. Assoc.*, *60*, 1163-1190.

Pumpanen, J., Ilvesniemi, H., Perämäki, M., and P. Hari (2003), Seasonal patterns of soil CO2 efflux and soil air CO2 concentration in a Scots pine forest: comparison of two chamber techniques, *Glob. Change Biol.*, *7*, 371-382.

Pumpanen, J., Kolari, P., Ilvesniemi, H., Minkkinen, K., Vesala, T., Niinisto, S., Lohila, A., Larmola, T., Morero, M., Pihlatie, M., Janssens, I. A., Yuste, J. C., Grunzweig, J. M., Reth, S., Subke, J. A., Savage, K., Kutsch, W., Ostreng, G., Ziegler, W., Anthoni, P. M., Lindroth, A., and P. Hari (2004), Comparison of different chamber techniques for measuring soil CO2 efflux, *Agric. Forest Meteorol.*, *123*, 159-176.

Rawlings, J. O., Pantula, S. G., and D. A. Dickey (1998), Applied regression analysis: a research tool, 2nd edition, Springer, New York.

Reeburgh, W., J. King, S. Regli, G. Kling, N. Auerbach, and D. Walker (1998), A CH4 emission estimate for the Kuparuk River basin, Alaska, *J. Geophys. Res.-Atmos.*, *103*(D22), 29005-29013.

Reicosky, D. C. (2003), Tillage-induced soil properties and chamber mixing effects on gas exchange, *Proceedings of the 16th Triennial Conference of International Soil Tillage Research Organizations*, 13-18 July 2003, Brisbane, Australia.

Reth, S., Gödecke, M., and E. Falge (2005), CO2 efflux from agricultural soils in eastern Germany − comparison of a closed chamber system with eddy covariance measurements, *Theor. Appl. Climatol.*, *80*, 105-120.

Rinne, J., T. Riutta, M. Pihlatie, M. Aurela, S. Haapanala, J.-P. Tuovinen, E.-S. Tuittila, and T. Vesala (2007), Annual cycle of methane emission from a boreal fen measured by the eddy covariance technique, *Tellus B*, doi:10.1111/j.1600-0889.2007.00261.x

Rivkina, E, K. Laurinavichius, J. McGrath, J. Tiedje, V. Shcherbakova, and D. Gilichinsky (2004), Microbial life in permafrost, *Advances in Space Research*, *33*(8), 1215-1221.

Riutta, T., J. Laine, M. Aurela, J. Rinne, T. Vesala, T. Laurila, S. Haapanala, M. Pihlatie, and E. Tuitulla (2007), Spatial variation in plant community functions regulates carbon gas dynamics in a boreal fen ecosystem, *Tellus B*, *59*(5), 838-852, doi:10.1111/j.1600-0889.2007.00302.x.

ROSHYDROMET, Russian Federal Service for Hydrometeorology and Environmental Monitoring (2004), http://www.worldweather.org/107/c01040.htm.

Saarnio, S., Alm, J., Silvola, J., Lohila, A., Nykänen, H., and P. J. Martikainen (1997), Seasonal variation in CH4 emissions and production and oxidation potentials at microsites on an oligotrophic pine fen, *Oecologia*, *110*, 414-422.

Sachs, L. (1992), Angewandte Statistik, 7th edition, Springer, Berlin, Heidelberg.

Sachs, T., C. Wille, J. Boike, and L. Kutzbach (2008), Environmental controls on ecosystem-scale CH4 emission from polygonal tundra in the Lena River Delta, Siberia, *J. Geophys. Res.*, *113*. http://dx.doi.org/10.1029/2007JG000505

Sage, R. F. (1994), Acclimation of photosynthesis to increasing atmospheric CO2: The gas exchange perspective, *Photosynth. Res.*, *39*, 351-368.

Schimel, J. (1995), Plant transport and methane production as controls on methane flux from arctic wet meadow tundra, *Biogeochemistry*, *28*(3), 183-200, doi:10.1007/BF02186458.

Schneider J, Grosse G, Kutzbach L, Wagner D (2006) Land cover classification of tundra environments in the arctic Lena Delta based on Landsat 7 ETM+ data and its application for upscaling of methane emissions. In: Proceedings of Globwetland Symposium: Looking at Wetlands from Space (ed Lacoste H) ESA SP-634, ESA Publication Division, Noordwijk.

Schneider, J., G. Grosse, and D. Wagner (2009), Land cover classification of tundra environments in the Arctic Lena Delta based on Landsat 7 ETM+ data and its application for upscaling of methane emissions, *Remote Sensing of Environment*, *113*(2), 380-391, doi:doi: DOI: 10.1016/j.rse.2008.10.013.

Schuchard-Ficher, C., K. Backhaus, U. Humme, W. Lohrberg, W. Plinke, and W. Schreiner (1982), Multivariate Analysemethoden. Eine anwendungsorientierte Einführung. Berlin, Heidelberg, New York: Springer-Verlag, 346 pages

Schuepp, P.H., M. Y. Leclerc, J. I. MacPherson, and R. L. Desjardins (1990), Footprint prediction of scalar fluxes from analytical solutions of the diffusion equation, *Boundary-Layer Meteorology*, *50*(1-4), 355-373.

Schütz H, Schröder P, Rennenberg H (1991) Role of plants in regulating the methane flux to the atmosphere. In: *Trace Gas Emissions by Plants* (eds Sharkey TD, Holland EA, Mooney HA) pp. 29-63. Academic Press, San Diego.

Schwamborn, G., V. Rachold, and M. N. Grigoriev (2002), Late Quaternary sedimentation history of the Lena Delta, *Quaternary International*, *89*, 119-134.

Shurpali, N. J., Hyvönen, N. P., Huttunen, J. T., Nykänen, H., Pekkarinen, N., and P. J. Martikainen (2008), Bare soil and reed canary grass ecosystem respiration measurements from a peat extraction site, *Tellus-B*, 2008 (in press).

Smart, D. R. (2004), Exposure to elevated carbon dioxide concentration in the dark lowers the respiration quotient of Vitis cane wood, *Tree Physiol.*, *24*, 115-120.

Soil Survey Staff (1998), *Keys to Soil Taxonomy 8th Edition*, Soil Conservation Service, USDA, Pocahontas, Blacksburg, Virginia, USA.

Spott, O. (2003) Frostmusterbedingte Seen der Polygonalen Tundra und ihre Funktion als Quellen atmospärischen Methans. Unpublished Diploma Thesis, University of Leipzig, Leipzig, Germany, 125 pp.

Steduto, P., Ö. Cetinkökü, R. Albrizio, and R. Kanber (2002), Automated closed-system canopy-chamber for continuous field-crop monitoring of CO2 and H2O fluxes, *Agric. Forest Meteorol.*, *111*, 171-186.

Stitt, M. (1991), Rising CO2 levels and their potential significance for carbon flow in photosynthetic cells, *Plant, Cell Environ.*, *14*, 741-762.

Stull, R. B. (1988), *An Introduction to Boundary Layer Meteorology*, 666 pp., Kluwer Acad., Norwell, Mass.

Suyker, A. E., S. B. Verma, R. J. Clement, and D. P. Billesbach (1996), Methane flux in a boreal fen: Season-long measurement by eddy correlation, *J. Geophys. Res.*, *101*(D22), 28,637–28,648.

Taylor, G. I. (1938), The spectrum of turbulence, *Proceedings of the Royal Society of London Series A*, *164*, 919, pp. 476–490.

Tjoelker, M. G., Oleskyn, J., Lee, T. D., and P. B. Reich (2001), Direct inhibition of leaf dark respiration by elevated CO2 is minor in 12 grassland species, *New Phytol.*, *150*, 419-424.

Tokida, T., T. Miyazaki, and M. Mizoguchi (2005), Ebullition of methane from peat with falling atmospheric pressure, *Geophys. Res. Lett.*, *32*, L13823, doi:10.1029/2005GL022949

Tokida, T., T. Miyazaki, M. Mizoguchi, O. Nagata, F. Takakai, A. Kagemoto, and R. Hatano (2007), Falling atmospheric pressure as a trigger for methane ebullition from peatland, *Global Biogeochem. Cycles*, *21*, GB2003, doi:10.1029/2006GB002790.

Tuittila, E.-S., Komulainen, V. M., Vasander, H., and J. Laine (1999), Restored cutaway peatland as a sink for atmospheric CO2, *Oecologia*, 120, 563-574.

Tsuyuzaki, S., T. Nakano, S-i. Kuniyoshi, M. Fukuda (2001), Methane flux in grassy marshlands near Kolyma River, north-eastern Siberia, *Soil Biology and Biochemistry*, *33*, 1419-1423.

van Gorsel, E., Leuning, R., Cleugh, H. A., Keith, H., and T. Suni (2007), Nocturnal carbon efflux: reconciliation of eddy covariance and chamber measurements using

an alternative to the u*-threshold filtering technique, *Tellus*, DOI: 10.1111/j.1600-0889.2007.00252.x (early online).

van Huissteden, J., T. Maximov, and A. Dolman (2005), High methane flux from an arctic floodplain (Indigirka lowlands, eastern Siberia), *J. Geophys. Res.-Atmos.*, *110*, G02002, doi:10.1029/2005JG000010.

von Randow, C., L. D. A. Sa´, P. S. S. D. Gannabathula, A. O. Manzi, P. R. A. Arlino, and B. Kruijt, Scale variability of atmospheric surface layer fluxes of energy and carbon over a tropical rain forest in southwest Amazonia. 1. Diurnal conditions, *J. Geophys. Res.*, *107*(0), 8062, doi:10.1029/2001JD000379, 2002.

von Storch, J. (2004), On statistical dissipation in GCM-climate, *Climate Dynamics*, *23*(1), 1-15, doi:10.1007/s00382-004-0404-2.

Vourlites, G. L., Oechel, W. C., Hastings, S. J., and M. A. Jenkins (1993), A system for measuring in situ CO2 and CH4 flux in unmanaged ecosystems: an arctic example, *Funct. Ecol.*, 7, 369-379.

Wagner, D., E-.M. Pfeiffer, and E. Bock (1999), Methane production in aerated marshland and model soils: effects of microflora and soil texture, *Soil Biology and Biochemistry*, *31*(7), 999-1006.

Wagner, D., S. Kobabe, E. Pfeiffer, and H. Hubberten (2003), Microbial controls on methane fluxes from a polygonal tundra of the Lena Delta, Siberia, *Permafrost Periglacial Process.*, *14*(2), 173-185.

Wagner, D., A. Lipski, A. Embacher, and A. Gattinger (2005), Methane fluxes in permafrost habitats of the Lena Delta: effects of microbial community structure and organic matter quality, *Environmental Microbiology*, *7*(10), 1582-1592.

Wagner, D., A. Gattinger, A. Embacher, E.-M. Pfeiffer, M. Schloter, and A. Lipski (2007), Methanogenic activity and biomass in Holocene permafrost deposits of the Lena Delta, Siberian Arctic and its implication for the global methane budget, *Global Change Biology*, *13*, 1089-1099.

Wagner, S.W. and D. C. Reicosky (1992), Closed-chamber effects on leaf temperature, canopy photosynthesis, and evapotranspiration, *Agron. J.*, *84*, 4, 731-738.

Wagner, S. W., Reicosky, D. C., and R. S. Alessi (1997), Regression models for calculating gas fluxes measured with a closed chamber, *Agron. J.*, *84*, 731-738, 1997.

Walker, H. J. (1998), Arctic deltas, *Journal of Coastal Research, 14*(3), 718-738.

Walter, B., and M. Heimann (2000), A process-based, climate-sensitive model to derive methane emissions from natural wetlands: Application to five wetland sites, sensitivity to model parameters, and climate, *Glob. Biogeochem. Cycle*, *14*(3), 745-765.

Walter, K. M., S. A. Zimov, J. P. Chanton, D. Verbyla, and F. S. Chapin (2006), Methane bubbling from Siberian thaw lakes as a positive feedback to climate warming, *Nature*, *443*(7107), 71-75, doi:10.1038/nature05040.

Wang, C., Yang, J., and Q. Zhang (2006), Soil respiration in six temperate forests in China, *Glob. Change Biol.*, *12*, 11, 2103-2114.

Wanninkhof R, and W. R. McGillis (1999), A cubic relationship between air-sea CO2 exchange and wind speed, *Geophysical Research Letters*, *26*(13), 1889–1892.

Welles, J. M., Demetriades-Shah, T. H., and D. K. McDermitt (2001), Considerations for measuring ground CO2 effluxes with chambers, *Chem. Geol.*, *177*, 3-13Webb, E., G. Pearman, and R. Leuning (1980), Correction of Flux Measurements for Density Effects Due to Heat and Water-Vapor Transfer, *Quarterly Journal of the Royal Meteorological Society, 106*(447), 85-100.

Wesely, M. L. and R. L. Hart (1985), Variability of short term eddy-correlation estimates of mass exchange, in: *The Forest-Atmosphere Interaction*, edited by B. A. Hutchison and B. B. Hicks, pp. 591-612.

Whalen, S., and W. Reeburgh (1988), Methane Flux Time Series for Tundra Environments , *Global Biogeochemical Cycles GBCYEP*, *2*(4), 399-409.

Whalen, S., and W. Reeburgh (1990), A methane flux transect along the trans-Alaska pipeline haul road, *Tellus Series B-Chemical and Physical Meteorology*, *42*(3), 237.

Whalen, S. C., and W. S. Reeburgh (1992), Interannual Variations in Tundra Methane Emission: A 4-year Time Series at Fixed Sites, *Global Biogeochemical Cycles*, *6*(2), 139–159.

Whalen, S. C., and W. S. Reeburgh (1996), Moisture and temperature sensitivity of CH4 oxidation in boreal soils, *Soil Biology and Biochemistry*, *28*(10-11), 1271-1281.

Whiting, G., and J. Chanton (1993), Primary Production Control of Methane Emission from Wetlands, *Nature*, *364*(6440), 794-795.

Wickland, K. P., R. G. Striegl, J. C. Neff, and T. Sachs (2006), Effects of permafrost melting on CO2 and CH4 exchange of a poorly drained black spruce lowland, *J. Geophys. Res.*, *111*. http://dx.doi.org/10.1029/2005JG000099

Wille, C., L. Kutzbach, T. Sachs, D. Wagner, and E.-M. Pfeiffer (2008), Methane emission from Siberian arctic polygonal tundra: Eddy covariance measurements and modeling, *Global Change Biol.*, *14*, 1 – 14, doi:10.1111/j.1365-2486.2008.01586.x.

Williams T. G. and L. B. Flanagan (1998), Measuring and modelling environmental influences on photosynthetic gas exchange in Sphagnum and Pleurozium, *Plant, Cell Environ.*, *21*, 555-564.

Wyngaard, LC., and S.F. Clifford (1977), Taylor's hypothesis and high-frequency turbulence spectra, *J. Atmos. Sci.*, *34*, 922-929.

Xu, M., and Y. Qi (2001), Soil-surface CO2 efflux and its spatial and temporal variations in a young ponderosa pine plantation in northern California, *Glob. Change Biol.*, *7*, 667-677.

Yu, J., W. Sun, J. Liu, J. Wang, J. Yang, and F. X. Meixner (2007), Enhanced net formations of nitrous oxide and methane underneath the frozen soil in Sanjiang wetland, northeastern China, *J. Geophys. Res.*, *112*, D07111, doi:10.1029/2006JD008025.

Zamolodchikov, D. G., and D. V. Karelin (2001), An empirical model of carbon fluxes in Russian tundra, *Glob. Change Biol.*, *7*, 147-161.

Zhang T., R. G. Barry, K. Knowles, J. A. Heginbottom, and J. Brown (1999), Statistics and characteristics of permafrost and ground-ice distribution in the Northern hemisphere, *Polar Geography*, *23*(2), 132-154.

Zhuang, Q., J. M. Melillo, D. W. Kicklighter, R. G. Prinn, A. D. McGuire, P. A. Steudler, B. S. Felzer, and S. Hu (2004), Methane fluxes between terrestrial ecosystems and the atmosphere at northern high latitudes during the past century: A retrospective analysis with a process-based biogeochemistry model, *Global Biogeochemical Cycles*, *18*, GB3010, doi:10.1029/2004GB002239.

Zimov, S. A., E. A. G. Schuur, and F. S. Chapin III (2006) Permafrost and the Global Carbon Budget, *Science*, *312*(5780), 1612-1613, doi:10.1126/science.1128908

Zimov, S. A., S. P. Davydov, G. M. Zimova, A. I. Davydova, E. A. G. Schuur, K. Dutta, and F. S. Chapin III (2006), Permafrost carbon: Stock and decomposability of

a globally significant carbon pool, *Geophys. Res. Lett.*, *33*, L20502, doi:10.1029/2006GL027484.

Zona, D., and W. C. Oechel (2008), Continuous measurements of methane fluxes by eddy covariance in the Arctic: Results of a large-scale manipulation of water status at Barrow, Alaska., in *Geophysical Research Abstracts*, vol. 10.

APPENDIX

–

Methane emission from Siberian arctic polygonal tundra: Eddy covariance measurements and modeling

Christian Wille   Lars Kutzbach   Torsten Sachs   Dirk Wagner   Eva-Maria Pfeiffer

Abstract

Eddy covariance measurements of methane flux were carried out in an arctic tundra landscape in the central Lena River Delta at 72°N. The measurements covered the seasonal course of mid-summer to early winter in 2003 and early spring to mid-summer in 2004, including the periods of spring thaw and autumnal freeze back. The study site is characterized by very cold and deep permafrost and a continental climate with a mean annual air temperature of −14.7°C. The surface is characterized by wet polygonal tundra, with a micro-relief consisting of raised moderately dry sites, depressed wet sites, polygonal ponds, and lakes. We found relatively low fluxes of typically 30 mg CH_4 m^{-2} d^{-1} during mid-summer and identified soil temperature and near-surface atmospheric turbulence as the factors controlling methane emission. The influence of atmospheric turbulence was attributed to the high coverage of open water surfaces in the tundra. The soil thaw depth and water table position were found to have no clear

effect on methane fluxes. The excess emission during spring thaw was estimated to be about 3% of the total flux measured during June–October. Winter emissions were modeled based on the functional relationships found in the measured data. The annual methane emission was estimated to be 3.15 g m^{-2}. This is low compared to values reported for similar ecosystems. Reason for this were thought to be the very low permafrost temperature in the study region, the sandy soil texture and low bio-availability of nutrients in the soils, and the high surface coverage of moist to dry micro-sites. The methane emission accounted for about 14% of the annual ecosystem carbon balance. Considering the global warming potential of methane, the methane emission turned the tundra into an effective greenhouse gas source.

1   Introduction

Approximately 24% of the Northern Hemisphere's exposed land area is underlain by permafrost (Zhang et al., 1999). Permafrost is a globally significant carbon reservoir, although estimates of its size vary. Post et al. (1982) estimates Arctic tundra environments to account for 190 Gt or 13–15% of the global soil organic carbon pool. More recent studies suggest a carbon content of 500 Gt in frozen yedoma sediments alone and an additional 400 Gt in nonyedoma permafrost excluding peatlands, which exceeds the carbon content of the atmosphere (730 Gt) and that of vegetation (650 Gt) (Zimov et al., 2006). Because of the high sensitivity of high-latitude ecosystems to climate changes, as well as their large proportion of the earth surface, these landscapes are critically important for the Earth System, in particular for the global carbon cycle (Chapin et al., 2000).

Northern wetlands and tundra are a major source of methane, contributing about 20% of the annual natural emissions (Fung et al., 1991; Cao et al., 1996; Christensen et al., 1996). With growing concern about climate change and the need to quantify emissions on a large scale, the greenhouse gas (GHG) budget of arctic wetlands have come into the focus of attention. Because methane has a 25-fold global warming potential compared to carbon dioxide (time horizon of 100 years) (IPCC, 2007), it has a strong influence on the GHG budgets of these landscapes (Friborg et al., 2003; Corradi et al., 2005). Furthermore, global climate models rely on predictions of future GHG

concentrations, which require the ability to accurately model sinks and sources of methane as a powerful greenhouse gas.

However, there is still much uncertainty about the source strength and the driving forces of methane flux of tundra landscapes. Existing studies of high latitude methane fluxes were mostly based on the closed-chamber technique. Due to the high temporal and spatial variability of methane fluxes (Christensen et al., 1995; Christensen et al., 2000; Wagner et al., 2003; Kutzbach et al., 2004), this technique alone does not give reliable information on landscape-scale fluxes. In addition, during chamber measurements the soil surface is isolated from the atmosphere so that the coupling of atmosphere and methane emission cannot be studied. The eddy covariance technique provides nonintrusive spatially integrated flux data at the landscape scale. However, to our knowledge only three studies reported eddy covariance methane flux data from arctic tundra ecosystems, namely Fan et al. (1992) from Alaska, Friborg et al. (2000) from Greenland, and Hargreaves et al. (2001) from Finland.

Here, we present the first eddy covariance methane flux data from a Siberian arctic tundra landscape. The objective of this study was to quantify the methane emission over the full course of the "active" season from early spring to early winter, to analyze the contribution of different parts of the vegetation period, particularly the little studied periods of spring thaw and soil re-freeze, to identify the biological and physical parameters which control the methane fluxes, and to estimate the annual methane emission. Together with the fluxes of carbon dioxide, which were measured concurrently and analyzed elsewhere (Kutzbach et al., 2007), a comprehensive picture of the GHG budget of the tundra was gained.

2 *Materials and methods*

2.1 Study site

The investigation site was located on Samoylov Island in the Lena River Delta at 72°22'N, 126° 30'E (Fig. 1). During the last years, Samoylov Island has been the focus of several studies in the field of microbiology, soil science, and surface-atmosphere fluxes of carbon, energy and water (Hubberten et al., 2006). The Lena River Delta is located in the zone of continuous permafrost with permafrost temperatures between −11
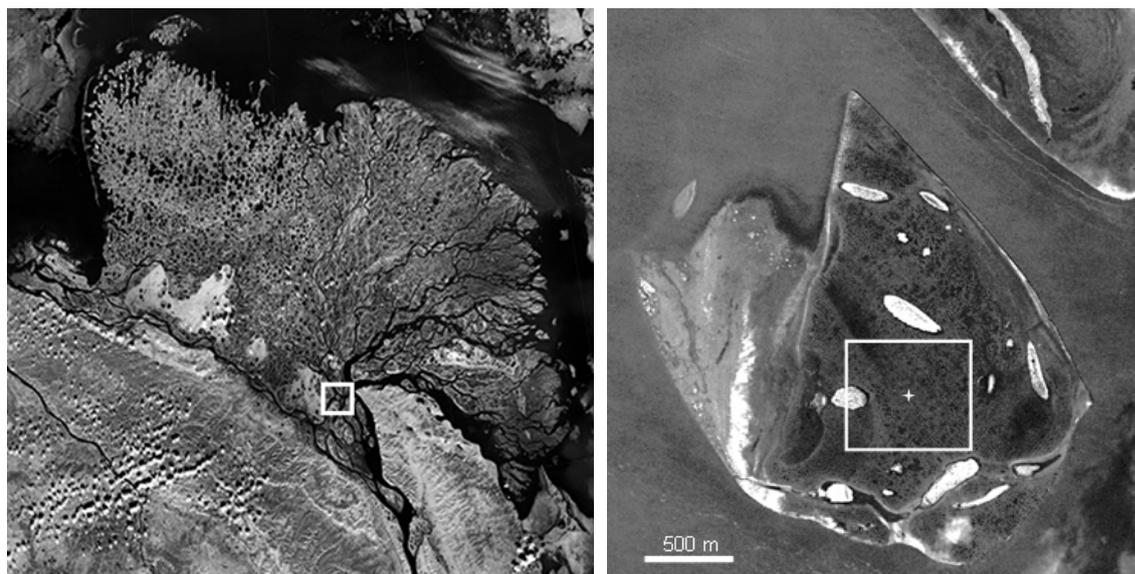
Figure 1: (left) Satellite image of the Lena River Delta (Landsat 7 ETM+ GeoCover 2000, NASA); the location of the investigation area Samoylov Island is marked by a white square.

Figure 2: **(right)** CORONA satellite image of Samoylov Island, taken during the spring flood in June 1964. The white star marks the position of the flux tower; the rectangle indicates the area displayed by the aerial photograph in Fig. 6.

and −13°C (Kotlyakov and Khromova, 2002). Samoylov Island is situated in the southern central part of the river delta, approximately 120 km south of the Arctic Ocean. The central delta region has a dry continental arctic climate, which is characterized by very low temperatures and low precipitation. The 30-year (1961–1999) averages of annual air temperature and precipitation measured at the meteorological station in Tiksi about 110 km east of Samoylov Island are −13.6°C and 319 mm, respectively (ROSHYDROMET, 2004). Data from the meteorological station on Samoylov Island from the period 1999–2005 show a mean annual air temperature of −14.7°C and a highly variable total summer precipitation (rain) between 72 and 208 mm (mean 137 mm). Typically, the ground is snow-covered between the end of September and the beginning of June (Boike et al., 2008), and the growing season lasts from June to August. During spring, summer, and autumn, the weather in the central delta region is characterized by the rapid change between the advection of arctic cold and moist air masses from the north and continental warm and dry air masses from the south.

The flux measurements were carried out on the eastern part of Samoylov Island which is characterized by wet polygonal tundra (Fig. 2). This part of the island

represents the Late-Holocene river terrace which is one of the main geomorphological units in the Lena River Delta, occupying about 65% of the total delta area (Are and Reimnitz, 2000). The eastern part of Samoylov Island has a level surface with slope gradients <0.2%, and an elevation of 10–16 m a.s.l. It is not flooded during the annual spring flood. Larger elevation differences up to 2.5 m occur only along the shorelines of the large lakes. However, the surface of the terrace is structured by a regular micro-relief with elevation differences of up to 0.5 m within a few meters distance, which is caused by the genesis of low-centered ice wedge polygons (Meyer, 2003). In the depressed polygon centers, drainage is impeded by the underlying permafrost, hence the soils are water-saturated and small ponds frequently occur. In contrast, the elevated polygon rims are characterized by a moderately moist water regime. The typical soil types are *Typic Historthels* in the polygon centers and *Glacic* or *Typic Aquiturbels* at the polygon rims. The vegetation in the polygon centers and at the edge of ponds is dominated by hydrophytic sedges (*Carex aquatilis*, *Carex chordorrhiza*, *Carex rariflora*) and mosses (e.g. *Limprichtia revolvens*, *Meesia longiseta*, *Aulacomnium turgidum*). The vegetation on polygon rims is dominated by mesophytic dwarf shrubs (e.g. *Dryas octopetala*, *Salix glauca*), forbs (e.g. *Astragalus frigidus*) and mosses (e.g. *Hylocomium splendens*, *Timmia austriaca*). Aerial photography in July 2003 and subsequent surface classification showed that the surface fraction taken by moderately moist to dry micro-sites, wet micro-sites, and open water bodies in the area surrounding the flux tower was about 60, 10, and 30 %, respectively (Schneider et al., 2006).

2.2   Experimental set-up

Eddy covariance measurements of methane flux were carried out in the periods July 19–October 22, 2003 (96 days), and June 1–July 21, 2004 (51 days). The eddy covariance system was set up at a central position of the eastern part of Samoylov Island (Fig. 2). Wet polygonal tundra of the river terrace extended for 600 m around the tower, with several large lakes protruding into the periphery of the otherwise homogeneous fetch area. The wind vector and sonic temperature were measured with a three-dimensional sonic anemometer (Solent R3, Gill Instruments Ltd, Lymington, UK) at a height of 3.65 m. From a sample intake 15 cm below the anemometer measurement point, the sample air was drawn at a rate of 20 L min^{-1} through a CO_2/H_2O gas analyzer

(LI-7000, LI-COR Inc., Lincoln, NE, USA), a membrane gas dryer (PD-200T-48SS, Perma Pure Inc., Toms River, NJ, USA), and the methane gas analyzer, all of which were housed in a temperature regulated case at the foot of the tower. The methane gas analyzer was a tunable diode laser spectrometer (TGA100, Campbell Scientific Inc., USA). The diode laser was cooled by a closed cycle cryogenic system (Cryo-Tiger, APD Cryogenics, USA). The TGA 100 required a constant flow of a reference gas (0.5% CH_4) which was supplied by calibrated gas bottles. The calibration of the TGA 100 was checked using a zero gas and a span gas (25 ppm CH_4) whenever the reference gas bottles had to be exchanged (about every 5 weeks) or the measurement parameters were adjusted. During the calibration intervals, we observed no appreciable span drift in the methane measurements. The data from the gas analyzers was sampled by the anemometer at a rate of 20 Hz and logged on a laptop PC running the software EDISOL (J. Massheder, University of Edinburgh, UK).

The tower was equipped with additional instruments for the measurement of air temperature and relative humidity (MP103A, ROTRONIC AG, Switzerland), incoming and outgoing solar and infrared radiation (CNR1, Kipp and Zonen B.V., the Netherlands), and barometric pressure (RPT410, Druck Messtechnik GmbH, Germany). Measurements of the water level were carried out at 3 points in the vicinity of the flux tower at intervals of 1–3 days. Precipitation, snow height, and soil temperature data was taken from the long-term monitoring station, which is situated about 700 m south-west of the flux tower (Boike et al., 2008). The thaw depth was measured by probing the soil with a steel rod at 150 regularly spaced grid points near the long-term monitoring station at intervals of 3–7 days.

2.3   Calculation and validation of fluxes

Data analysis was done using the software EDIRE (R. Clement, University of Edinburgh, UK). Two coordinate rotations were performed on the wind components measured by the sonic anemometer, so that the mean transverse and vertical wind components were reduced to zero for each averaging period (McMillen, 1988). The mean absolute value of the angle of the second rotation was $1.0 \pm 0.9°$, hence the error introduced to turbulent fluxes by the rotation should be well below 10% for most measurements (Foken and Wichura, 1996). The time lag between wind and methane concentration
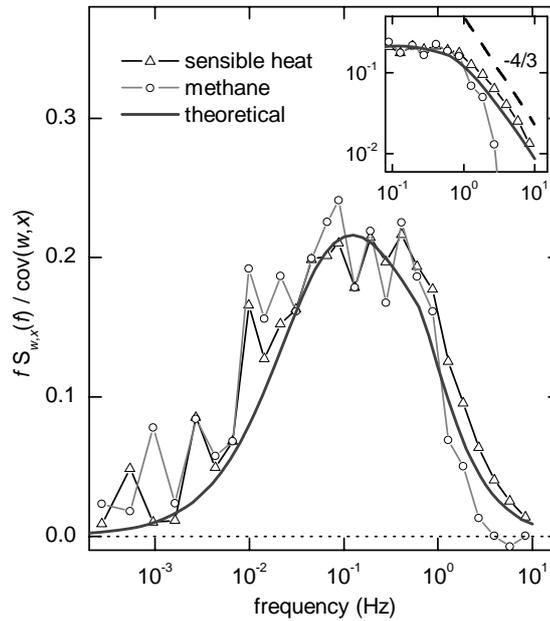
Figure 3: Co-spectra of sensible heat and methane fluxes and theoretical spectrum. The co-spectra are averages of four hourly co-spectra (August 18, 2003, 10:00–14:00 LT) scaled by the corresponding covariance $cov(w,x)$. The theoretical spectrum is the model of the sensible heat flux co-spectrum for the average meteorological conditions of the 4-hour period (wind speed $u = 4.4$ m s^{-1}, stability $z/L = -0.019$). The inset shows the high frequency part of the spectra on a logarithmic scale ordinate.

measurements was determined and removed for each averaging period.

The co-spectra of the fluxes of sensible heat and methane (Fig. 3) show the characteristic features of the surface-layer turbulence spectrum and closely follow the theoretical spectrum for sensible heat flux under unstable atmospheric conditions (Moore, 1986). The co-spectrum of sensible heat follows the expected power law in the inertial sub range, whereas in the methane flux co-spectra the attenuation of high frequencies due to the limited frequency response of the gas analyzer and experimental setup is visible. These observations agree well with reports of the performance of the TGA 100 gas analyzer by other investigators (Billesbach et al., 1998; Laurila et al., 2005).

During the measurement campaigns, a short term drift in the methane concentration measured by the TGA 100 was observed frequently. This drift has been described before as a changing concentration offset caused by optical interference fringes (Billesbach et al., 1998). The analysis of methane power spectra revealed a strong increase in signal intensity at frequencies $<10^{-2}$ Hz. As this feature was not observed in the spectra of the other scalar's time series, it was attributed to the

concentration drift. In order to suppress the drift components in the signal, a recursive high pass filter with a filter constant of 10 s (cut-off wavelength 63 s) was applied to the methane concentration time series before the flux calculation.

A correction was applied to the calculated methane flux to account for the mismatch of the turbulence frequency spectrum and the spectral response of the measurement system. In detail, the correction compensated for the effects of the spectral response of the gas analyzer, the separation of the anemometer and gas analyzer sampling points, the line attenuation in the sample tubing, and the detrending filter (Moore, 1986; Moncrieff et al., 1997). On average, 40% were added to the calculated flux, of which 25% and 13% were related to the effect of the spectral response of the gas analyzer and the high pass filtering of the methane signal, respectively.

As an estimate of the error associated with each individual flux data point, the standard deviation of the cross correlation function of vertical wind speed and methane concentration at time shifts 100–200 s was calculated. This method accounts for the Gaussian error of the individual measurements of wind speed and methane concentration as well as the uncertainty in the stationarity during the averaging period (Kormann et al., 2001). The 30-minute flux time series (screened for instrument malfunctions) showed frequent large outliers and an overall signal-to-noise ratio (SNR) of only 3 (mean flux 12.1 mg m^{-2} d^{-1}, mean flux error 4.0 mg m^{-2} d^{-1}). The reasons for this were thought to be the generally low methane fluxes and high wind speeds at our site, and an insufficient suppression of concentration drift in the methane concentration signal. Stronger high pass filtering of the methane signal did not seem appropriate, because this would also attenuate signal components at the low frequency end of the turbulence spectrum. However, by increasing the averaging time, the statistics of the averaging process for the drift components in the methane signal could be improved (Billesbach et al., 1998). Hence, the averaging interval for the flux calculation was set to 60 minutes. This measure led to an increase of the SNR to 4.5 (mean flux error 2.7 mg m^{-2} d^{-1}). The 60-minute flux time series (Fig. 4) still shows considerable scatter and some negative values. Considering the distribution of wet and dry micro-sites within the eddy covariance fetch and the results of previous static chamber methane flux
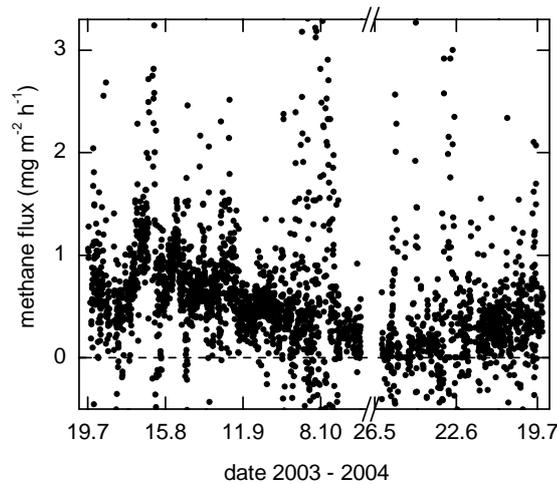
Figure 4: Time series of hourly measured methane fluxes, screened for instrument malfunctions, but not SNR-screened ($N = 2823$).

measurements (Wagner et al., 2003), large negative fluxes of methane are not anticipated in the studied tundra ecosystem. Other investigators have attributed observations of large negative methane fluxes to measurement uncertainties particularly during periods of low flux (Rinne et al., 2007), and have ignored these data points or even included them in further analysis. We think that these negative flux values need to be removed by rigorous data screening based on metrological and micro-meteorological criteria. We used a filter based on the SNR of the flux calculation which rejected all data points showing any signal larger then the flux peak in the cross correlation function of vertical wind and methane concentration. This filter effectively removed all negative fluxes and much of the scatter in the flux time series.

Finally, the data was screened using an integral turbulence characteristics test following Foken and Wichura (1996), which removed data points associated with disturbed and under-developed turbulence. After screening, there remain about 4% of data points with a friction velocity $u_*<0.1$ (Fig. 5a). This data is often rejected in flux studies because under these conditions fluxes are deemed to be disturbed by under-developed turbulence or storage effects. Storage situations were observed a few times in 2003. However, the data associated with these events was rejected by the SNR and turbulence screening procedures. Consequently, in the screened data an increase of methane concentration at low values of u_* which would indicate the influence of storage is not visible (Fig. 5b).
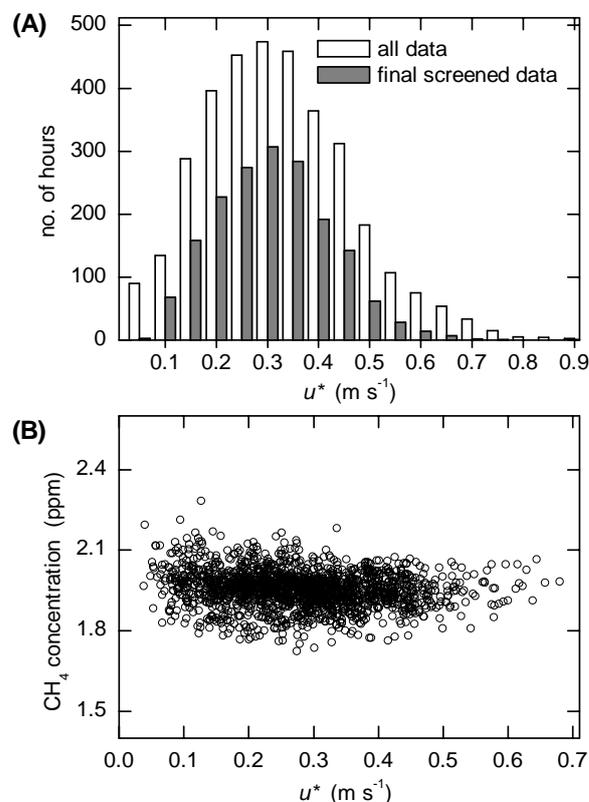
Figure 5: Turbulence characteristics during measurements campaigns 2003 and 2004. **(A)** frequency distribution of hourly friction velocity $u*$ for all data points ($N = 3451$) and final screened data ($N = 1770$); **(B)** mean hourly methane concentration versus friction velocity of final screened data.

A footprint analysis following Schuepp et al. (1990) was carried out for the assessment of the fetch area size of the flux measurements (Fig. 6). During periods of $u* < 0.1$, the 80% cumulative flux distance, (i.e. the upwind distance from which 80% of the observed methane flux originated), occasionally extended beyond 1000 m. Data points associated with these events were removed. Of the screened data, the 80% cumulative flux distance was on average 477 m, and the distance of the point of origin of the maximum contribution to the measured flux was on average 107 m. In 2003, altogether 33% of the data points were rejected by the screening procedures described above. In 2004, due to technical problems during the first half of the measurement campaign the rejection rate was 74%.
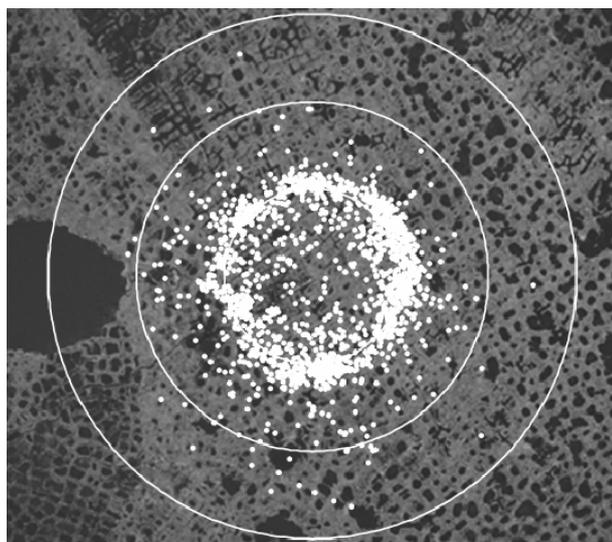
Figure 6: Flux footprint climatology of 2003 and 2004 overlaid on an aerial image of Samoylov Island taken in July 2003. The white dots indicate the position of maximum flux contribution of screened hourly data points ($N = 1770$). The white circles indicate the distance to the flux tower in steps of 100 m.

3   Results

3.1   **Meteorological conditions**

The summer and autumn of 2003 were characterized by above-average temperatures and precipitation (Fig. 7). The advection of warm continental air from the south lead to high air temperatures during the middle of July, at the beginning of August, and during large parts of September. The daily average soil temperature at 20 cm depth in a depressed, wet polygon center reached a maximum of 6.6°C on 9 August. The isothermal state of the thawed layer was reached and re-freeze of the soil began on 30 September. The soil thaw depth was 0.28 m on 15 July and increased to a maximum of 0.48 m at the beginning of September. Measurements of thaw depth stopped on 30 September due to the freezing of the top soil layer. However, the temperature profile measurements showed that the soil was not completely frozen until the middle of November. At 168 mm, the total amount of rainfall during the measurement period was exceptionally large. A great part of the rainfall occurred within one week at the end of July (94 mm), which caused the water table in the investigated polygons close to the eddy tower to rise well above the soil surface. Following a slow decrease, the water level stayed within ±1 cm of the soil surface after the end of August. Snow started to
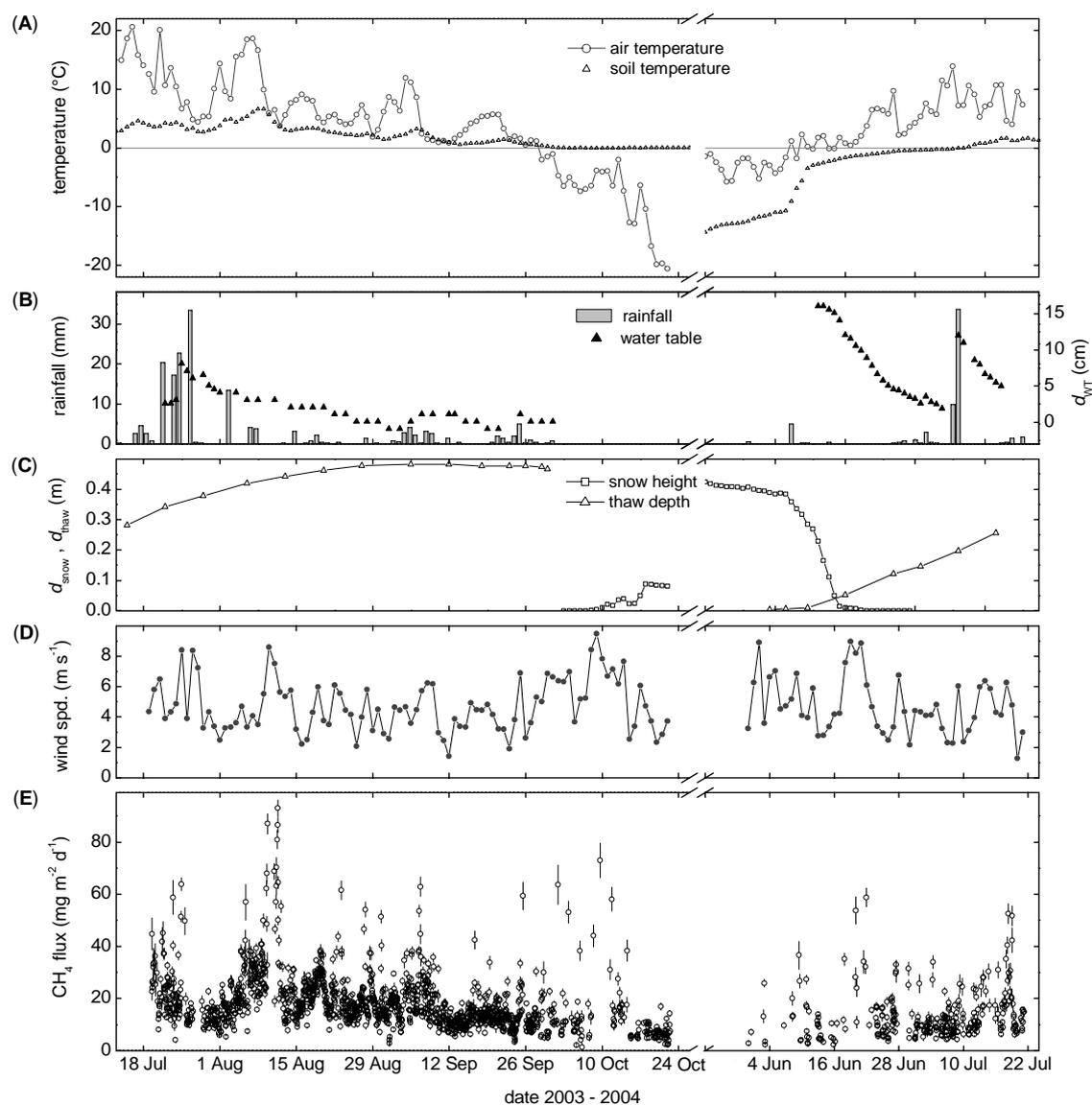
Figure 7: Data of measurement campaigns July 19–October 22, 2003 and June 1–July 21, 2004. **(A)** air temperature, and soil temperature in a wet polygon center at 20 cm depth; **(B)** rainfall, and depth of water table with respect to soil surface in a depressed polygon center; **(C)** snow height in a depressed polygon center, and soil thaw depth; **(D)** wind speed from sonic anemometer measurements at 3.65 m height; **(E)** screened hourly methane flux as measured by eddy covariance ($N = 1770$).

accumulate at the beginning of October. By the end of the measurement campaign, the snow cover had reached a height of 15–25 cm in the polygon centers and just a few centimeters on the polygon rims. The average wind speed during the measurement campaign 2003 was 4.7 m s^{-1}. There was no single predominant wind direction; however, wind directions east-north-east, south, and south-west occurred more frequently than other directions (data not shown).

When methane flux measurements started on June 1, 2004, the ground at the eddy tower site was completely covered with snow. The snow height had already started to decrease but was still 0.4–0.5 m in the polygon centers and about 0.1 m on the polygon rims. The daily average air temperature was in the range –5 to –2°C, and the soil temperature in 20 cm depth was –12°C. The snow thaw period started on 8 June with the occurrence of the first significant rainfall and the air and soil temperatures reaching 0°C. The snow height decreased rapidly, and the polygon rims were largely free of snow after 2 days. Snow thaw in the polygon centers continued until 18 June. The thaw of large ice bodies of polygon ponds and lakes started towards the end of the snow thaw and lasted until about 25 June. At the end of the measurement campaign, daily average air and soil temperatures (20 cm depth) were around 8°C and 1.5°C respectively, and the soil thaw depth had reached about 30 cm (linear extrapolation from measurements). The water table in the polygon centers was generally higher than in 2003 and never fell below the soil surface. The total rainfall up to 21 July was 60 mm. The average wind speed of the measurement period in 2004 was 4.7 m s^{-1}. Unlike 2003, there was a clear dominance of easterly winds, followed by winds from north-westerly directions (data not shown).

3.2   Methane flux

In the first week of measurements in 2003, methane fluxes were on average 23 mg m^{-2} d^{-1} (Fig. 7). During the following cold and rainy period, the fluxes dropped markedly but subsequent warming and further thawing of soils lead to the highest fluxes of on average 30 mg m^{-2} d^{-1} being measured during the second week of August. During periods with high wind speed, the methane flux increased greatly compared to fluxes during calm periods directly before and after, as for instance on August 10, 2003. After the middle of August the measured methane flux showed a general slow decreasing trend until the end of the measurement campaign. No marked influence of the freezing of the top soil layer at the end of September on the methane flux was visible. Average fluxes measured during the first week of October and during the last week of measurements, when snow had accumulated on the ground, were 13 and 7 mg m^{-2} d^{-1}, respectively.
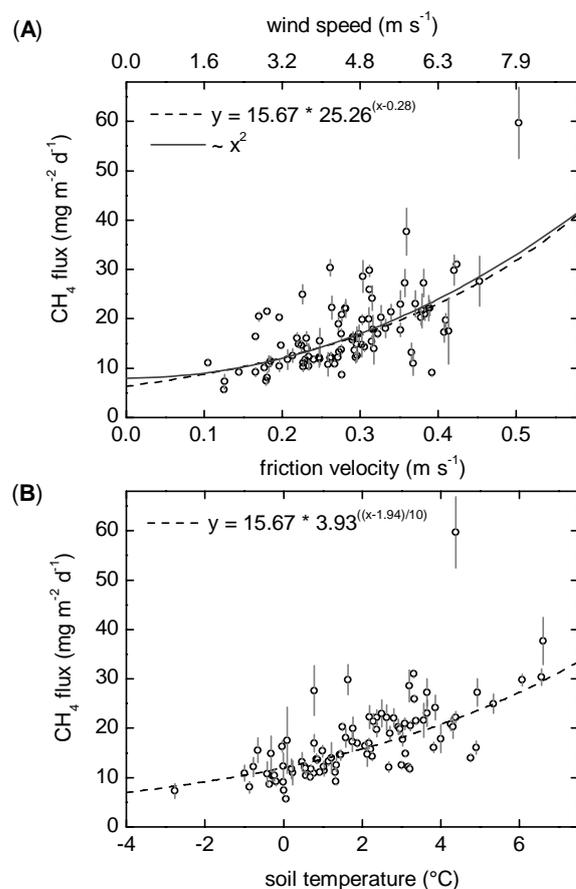
Figure 8: Relationship between average methane flux and environmental parameters of days included in modeling ($N = 91$). **(A)** Methane flux versus friction velocity. The top axis shows the approximate wind speed calculated from the linear regression of friction velocity u_* and wind speed u ($u = 15.84\ u_*$, $R^2 = 0.82$). **(B)** Methane flux versus soil temperature at 20 cm depth in a wet polygon center. The dashed lines in both diagrams are the functional relationships derived by fitting equation (1) to measured fluxes and environmental data.

The average methane flux from the beginning of measurements in 2004 until the end of the snow thaw at 18 June was 11 mg m^{-2} d^{-1}. However, the variation in the flux data during this time was large. Low flux values of about 4 mg m^{-2} d^{-1} occurred frequently throughout this period, but at the beginning of the snow melt methane fluxes of about 30 mg m^{-2} d^{-1} were repeatedly measured. The high variability of the fluxes continued until about 28 June. After this date, the fluxes stabilized at on average 10 mg m^{-2} d^{-1} and increased slowly to on average 17 mg m^{-2} d^{-1} during the last week of measurements. In order to gain a functional relationship between methane flux and environmental drivers which could be used for gap-filling and extrapolation, the correlation between calculated fluxes and environmental variables was studied. For this

Table 1: Input and model parameters for the combined period 2003–2004 using equation (1).

T_{ref} (°C)	1.94
$u*_{ref}$ (m s^{-1})	0.28
a (mg m^{-2} d^{-1})	15.67 ± 0.46
b	3.93 ± 0.50
c	25.26 ± 7.23
R^2	0.74
P	< 0.0001
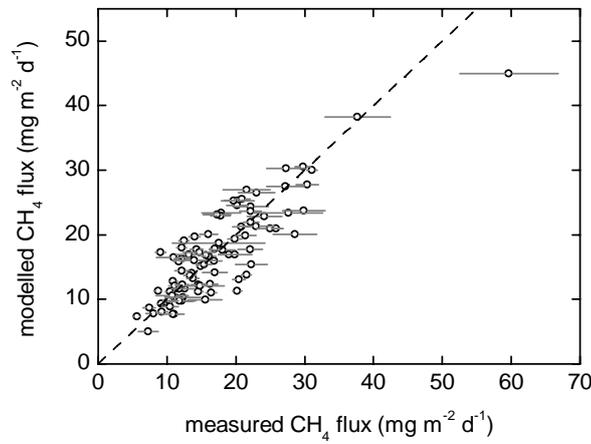
Figure 9: Modeled flux using equation (1) versus daily mean methane flux ($N = 91$).

analysis, only days with a data coverage >33% were used ($N = 91$), and daily averages of methane flux were calculated, so that the variance induced by changes of fetch size and position was reduced. Errors of daily fluxes were calculated as standard errors of the mean. We found a strong correlation between methane flux and friction velocity ($r = 0.62$) and soil temperature in a wet polygon center at 20 cm depth ($r = 0.67$; Fig. 8). These two variables were included in a model following the approach of Friborg et al. (2000). A good agreement ($R^2 = 0.74$) with measured data was found when the methane flux was modeled using the equation

$$FCH_4 = a \times b^{((T-T_{ref})/10)} \times c^{(u*-u*_{ref})} , \qquad (1)$$

where FCH_4 is the measured methane flux, a, b, and c are the parameters determined by the fit process, T is the soil temperature, $u*$ is the friction velocity, and T_{ref} and $u*_{ref}$ are
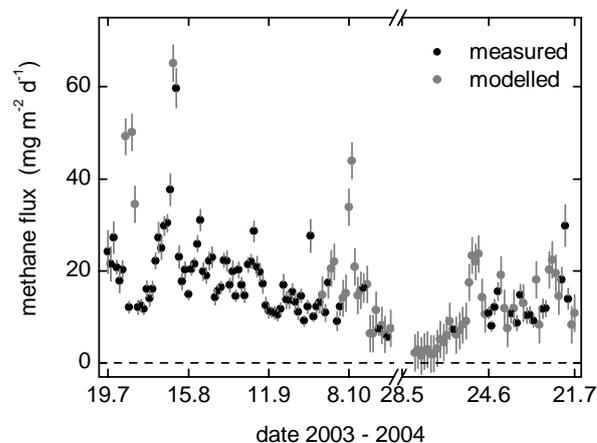
Figure 10: Time series of measured and modeled daily averaged CH_4 fluxes during the periods July 19–October 22, 2003 and June 1–July 21, 2004.

the mean values of the respective variables during the measurement period (Table 1). There was no correlation between methane flux and soil thaw depth or water table position, and expanding the model to include these variables did not improve the fit. Measured fluxes and those modeled by equation (1) agree well over the whole range of measured flux values (Fig. 9), except for the very windy day 11 August (mean wind speed 7.5 m s^{-1}), when the model significantly underestimates the measured flux.

Equation (1) was used for gap-filling of the daily flux time series (Fig. 10). The error of modeled daily fluxes was calculated as the root-mean-square of the fit residuals (3.91 mg m^{-2} d^{-1}). The error of cumulative fluxes was calculated by standard error propagation techniques for a 99% confidence limit. The resulting cumulative methane emission for the combined measurement period June 1–July 19, 2004 and July 20–October 22, 2003 was 2.38 ± 0.09 g m^{-2}.

4   Discussion

4.1   Drivers of methane flux

The combined measurement periods covered a whole vegetation period from spring thaw to refreeze of the soils and thus the most active period of methane emission. The wide range of environmental conditions covered allowed a detailed study of the driving forces of the methane flux. One of the two important parameters controlling methane

emission was the soil temperature. The dependence of methane flux on soil temperature followed an exponential function. This reflects the fundamental dependence of soil microbiological activity on temperature (Conrad, 1989) and was confirmed by numerous studies of methane emission using closed-chamber or eddy covariance techniques (e.g. Nakano et al., 2000; Christensen et al., 2001; Hargreaves et al., 2001).

The turbulence in the near-surface boundary layer, which correlates closely with wind speed, was the second important driving factor of the methane flux in the polygonal tundra. *Fan et al.* (1992) reported a similar effect from a mixed tundra landscape in Alaska, but only when there was a high surface coverage of lakes in the fetch area of the measurement. The exchange of gases between water bodies and the atmosphere proceeds by three primary pathways (MacIntyre et al., 1995): (a) transport through emergent aquatic plants, (b) diffusive and turbulent transfer across the air-water interface, and (c) bubble ebullition. Plant-mediated transport of methane from soil layers or lake sediments to the atmosphere plays an important role in the gas exchange of wet tundra (e.g. Schütz et al., 1991). Using the chamber technique, methane transport via *Carex aquatilis* was shown to account for between 27% and 66% of overall methane emissions from soils on Samoylov Island (Kutzbach et al., 2004). The same study suggested that the transport via this pathway was not limited by the above-soil diffusion resistances (leaf stomata, leaf surface boundary layer) but by the dense root exodermes. Hence, atmospheric turbulence is not likely to have a significant influence on plant mediated transport of methane.

However, the diffusive and turbulent transfer across the water-air interface is well-known to be controlled by wind speed. The results of lake studies suggested a dependence of the gas transfer velocity on wind speed u proportional to $u^{1.6}$ (MacIntyre et al., 1995); studies of air–sea CO_2 exchange suggested a cubic relationship (Wanninkhof and McGillis, 1999). The flux–friction velocity relationship given by equation (1) is very similar to a quadratic function of u_* (Fig. 8). Hence, we hypothesize that the dependence of methane emission on atmospheric turbulence observed at our study site is in a large part due to the high surface coverage of water bodies in the polygonal tundra.

Bubble ebullition, which occurs in lakes and inundated soils, is also likely influenced by atmospheric turbulence. Gas bubbles which tend to adhere to surfaces

under water could be released by wind induced agitation of plants, wave action, and under-water turbulence. However, this process is not well understood. The observation of high methane flux during high wind speeds on August 11, 2003 may be due to turbulence-induced ebullition and indicates a possible threshold of wind speed for the triggering of this process. Ebullition could also be triggered by changes of air pressure. This mechanism has been suggested by other authors (e.g. Frolking and Crill, 1994), and was observed during a study of methane emission from lakes on Samoylov Island in 2002 (Spott, 2003). However, in our data, a relationship between air pressure and methane flux was not found.

Many studies identified the soil thaw depth of soils as an important predictor of methane emission, spatially and temporally (e.g. Friborg et al., 2000; Tsuyuzaki et al., 2001; van Huissteden et al., 2005). In our study, the thaw depth was not correlated with methane flux and, when added as an additional variable, did not improve the performance of flux model [Eqn (1)]. This indicates that during the warm period the majority of the methane emitted originated from the upper soil layers. The small contribution of deep soil layers to methane emissions could be explained by the temperature gradient in the thawed active layer and the temperature dependence of microbial activity. However, since microorganisms in deep soil layers were shown to be cold-adapted (Liebner and Wagner, 2007; Wagner et al., 2006), it is more likely caused by a substrate limitation of microbial activity due to a decreasing bio-availability of soil organic carbon with increasing depth in soils of Samoylov Island (Wagner et al., 2005).

The water table position is another environmental variable which was identified by many studies as a main factor controlling methane emission (e.g. Suyker et al., 1996; Friborg et al., 2000). This was explained with the regulation of the methane production/oxidation balance through the ratio of the aerobic/anaerobic soil column depth. In the spatial domain, this regulation was also observed at our study site. Concurrent measurements of methane emissions by the closed-chamber technique showed that the methane fluxes from water-logged polygon centers were larger by a factor of 8–10 compared with emissions from elevated, moderately moist polygon rims at any time during the measurement campaigns 2003 and 2004 (unpublished data). However, temporally, no significant influence of water table on methane flux was detected. This can be explained with respect to the two micro-sites prevalent in our

study area. Firstly, in the raised polygon rims, the water table was always well below the soil surface, so the ratio of aerobic/anaerobic soil column was always high. Furthermore, process studies have shown that oxidation activity in these soils is greatest near the aerobic-anaerobic interface where the substrate provision is at its optimum (Liebner and Wagner, 2007). Secondly, despite the variations in water table position, in most of the polygon centers the water table was distinctly above the soil surface during both measurement periods. Hence, at both micro-sites the change of water table position did not influence the methane production/oxidation balance significantly. However, extreme draught could lower the water level below the soil surface in many polygon centers and lead to increased oxidation and overall decreased methane flux. This "on-off switch" effect (Christensen et al., 2001) was observed for single polygon center sites on Samoylov Island during the dry summer of 1999 (Wagner et al., 2003; Kutzbach et al., 2004).

4.2 Seasonal dynamics of methane flux

Despite the low data coverage during spring 2004, a description of the processes during the thaw period can be given with reasonable confidence. Large methane fluxes were measured on several occasions during the first days of snowmelt (June 8–13, 2004), which indicate the release of methane from the snow cover during the metamorphosis and settling of snow which is associated with the initial stages of the thaw process (Boike et al., 2003). Furthermore, during a period with strong wind directly after the snow thaw (June 18–21, 2004), fluxes were observed which equaled those measured during the midsummer period of 2003. These large fluxes were very likely caused by the escape of methane trapped in ice covers of ponds and lakes which continued to thaw until at least June 25, 2004. Similar observations were made by Hargreaves et al. (2001) in a Finnish mire. By comparing the measured and modeled methane flux during the period June 8–25, 2004, the contribution of thaw related fluxes to the overall emission during the combined measurement period was estimated to be about 3%. This value is very similar to the spring pulse excess emission of 2.1% of annual emission estimated by Rinne et al. (2007) for a boreal fen.

The average methane emission of the polygonal tundra on Samoylov Island during the "warm" months July, August, and September was 15.7, 22.3 and 15.2 mg m^{-2}

d^{-1}, respectively. These values are at the lower end of summer emissions observed by other flux studies in arctic or sub arctic wetlands. Average methane fluxes observed by eddy covariance were 25 mg m^{-2} d^{-1} during July–August at a tundra site in Alaska (61°N) (Fan et al., 1992), and 38 mg m^{-2} d^{-1} during August at a Finnish mire (69°N) (Hargreaves et al., 2001). The total summer emission (June–August; 1.6 g m^{-2}) was about 60% lower than the value of 3.7 g m^{-2} reported for a tundra site on Greenland (74°N) (Friborg et al., 2000). The geographically closest study based on the closed-chamber method was conducted near Tiksi, about 120 km south-east of Samoylov Island, and reported a mean flux of 23 mg m^{-2} d^{-1} from a tundra site during July and August (Nakano et al., 2000). Generally, closed-chamber flux studies in far north-east Siberia observed significantly higher summer methane emissions: Between 105 and 196 mg m^{-2} d^{-1} at floodplain sites near the Kolyma River (69°N) (Nakano et al., 2000; Tsuyuzaki et al., 2001; Corradi et al., 2005), and 103 mg m^{-2} d^{-1} at a river terrace polygonal tundra of the Indigirka River floodplain (71°N) (van Huissteden et al., 2005).

There are a number of reasons which could explain the differences in methane emission observed. Soil temperature regime, vegetation cover, hydrology and texture of soils, as well as bio-availability of nutrients play an important role in determining microbial activity in the soil and the gas exchange between soils and the atmosphere. The tundra soils at our study site are characterized by a sandy texture. Sand is known to be an unfavorable habitat for microbes (e.g. Wagner et al., 1999). Furthermore, the availability of nutrients is limited because the organic matter in the soils is only weakly decomposed, and there is no input of organic carbon by recent flooding. These conditions appear to impede microbial methane production at our study site compared to other sites in north-east Siberia.

During autumn and early winter, the methane emission of the tundra on Samoylov Island decreased slowly; drastic changes in response to the refreeze of the top soil layer were not observed. The emission of methane through the frozen top soil layer is thought to be facilitated by vascular plants (Hargreaves et al., 2001). It was shown that transport of methane through *Carex aquatilis* is independent of the phenological status of the plant tissues (Kutzbach et al., 2004). Hence, although senescent, the plants keep providing a pathway for diffusion from deeper soil layers to the atmosphere. Moreover, also the accumulation of snow after the middle of October

showed no marked influence on the methane flux. It was shown before that during winter the gas flux into the atmosphere is controlled by production in the soil, and that the snow cover acts as a passive layer only (Panikov and Dedysh, 2000; Corradi et al., 2005). However, we expect the dependence of methane flux on turbulence which was observed during snow-free periods to decrease with increasing snow cover, due to a de-coupling of the turbulence from vegetation, and soil and water surfaces. Though, owing to the lack of data, this hypothesis could not be verified.

Similarly, due to a lack of data, methane emissions during winter, (i.e. during the period of completely frozen soils and low sub-zero soil temperatures) are uncertain. Many studies have stressed the importance of cold season fluxes in boreal wetlands. The contribution of cold season flux to the annual flux was reported to be 4–21% at a Minnesota peatland at 47°N (Dise, 1992), 3.5–11% at a west Siberian peat bog at 57°N (Panikov and Dedysh, 2000), 5–33% at Finnish bogs and fens at 62–65°N (Alm et al. 1999), and 23% at a Finnish mire at 69°N (Hargreaves et al. 2001). However, there exist few studies in permafrost regions which address the question of winter fluxes. Whalen & Reeburgh (1992) observed methane emission during winter which accounted for about 40% of the annual flux, but which they attributed to physical processes during the soil freeze rather than microbial activity. Laboratory experiments have shown only recently that methanogenesis takes places in soils at sub-zero temperatures (Rivkina et al. 2004; Wagner et al. 2007). Based on these findings we assume that the relationship between soil temperature and methane emission derived from measurements in 2003–2004 can be extrapolated for the estimation of winter CH_4 emission. A similar approach was chosen *by Corradi et al. (2*005) for the estimation of winter soil respiration. Using the soil temperature record from 20 cm depth and equation (1), but omitting the u_*-term because of the expected de-coupling of methane flux and turbulence by the snow cover, the cumulative flux of the period October 23, 2003–May 31, 2004 (222 days) was estimated to be 0.77 ± 0.15 g m^{-2} (Fig. 11). Based on this estimate, the integrated emission of the cold season October–May was 1.1 mg m^{-2}, and its contribution to the annual emission was 35%. This estimate is at the upper end of the range of results discussed above which can be explained with the seasonal distribution of fluxes. During summer, methane emission from the tundra of Samoylov Island is generally low compared to other wet tundra sites, while substantial emission continues well into early
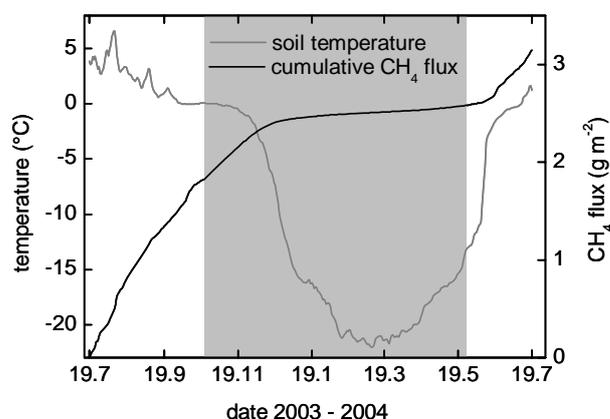
Figure 11: Record of soil temperature at 20 cm depth at a polygon center and cumulative methane flux for the period July 2003–July 2004. The period with modeled data is shaded.

winter. Considering this observation, the method of estimating cold season flux as the product of measured winter flux and number of days with sub-zero air temperature, as used e.g. by Panikov and Dedysh (2000), is likely to systematically underestimate the contribution of the cold season to the annual flux.

4.3   Annual carbon fluxes and GHG budget

Using the estimate of cold season flux, the annual methane flux of the tundra ecosystem during the period July 20, 2003–July 19, 2004 was 3.15 ± 0.17 g m^{-2}. This value is about 40% lower than annual emissions given for wetlands at similar latitudes in Finland (Hargreaves et al., 2001) and Alaska (Reeburgh et al., 1998). As discussed with respect to seasonal fluxes, we hypothesize that the main reasons for the low annual flux observed are the low coverage of wet micro-habitats, the low soil temperature, and the low bio-availability of nutrients in the tundra soils of Samoylov Island.

Measurement and modeling of the fluxes of carbon dioxide showed that the tundra was a CO_2 sink of 72 g m^{-2} during the period July 20, 2003–July 19, 2004 (Kutzbach et al., 2007). Thus, the overall carbon balance of the tundra was -17.3 g C m^{-2}, and the methane emission accounted for about 14% of the carbon balance. A similar value of 19% was given by Friborg et al. (2003) for a west Siberian peat bog, which had a carbon exchange about five times as high as the tundra on Samoylov Island. The high value of 25% reported by Corradi et al. (2005) for a north-east Siberian tussock tundra was due to the high methane emission (10 g C m^{-2} during 60 days in summer) compared

to a moderate annual carbon uptake of -38 mg C m^{-2}. Considering the global warming potential of methane compared to carbon dioxide (factor 25 per unit mass for a time horizon of 100 years) (IPCC, 2007), the GHG balance of the tundra in units of CO_2 equivalents was $+6.8 \pm 4.4$ g m^{-2}. Thus, although the methane emission had only a small influence on the tundra's capacity as a carbon sink, it offset the CO^2 greenhouse gas sink strength of the tundra and even turned it into a small source of greenhouse gases. Other Siberian wetlands were found to be strong GHG sources due to their emission of methane (Friborg et al., 2003; Corradi et al., 2005). Further observation of the tundra ecosystems in the Lena River Delta will be necessary to determine which way their GHG balance will go with the impact of climate change.

5   Conclusions

•   The methane emission at the wet polygonal tundra studied was low regarding daily summer fluxes (typically 30 mg m^{-2} d^{-1}) as well as the annual flux (3.15 g m^{-2}). Reason for this were thought to be the very low permafrost temperature in the study region, the sandy soil texture and low bio-availability of nutrients in the soils, and the high surface coverage (>50%) of moist to dry micro-sites in the polygonal tundra.

•   The soil temperature and near-surface atmospheric turbulence were identified as the main factors controlling methane emission. The dependence of CH_4 fluxes on atmospheric turbulence was attributed to the high coverage of open water bodies in the polygonal tundra and demonstrates the close coupling of the soil and atmosphere systems. The variables soil thaw depth and water table position, which were often identified as (spatial) flux predictors by short term flux studies using the closed-chamber technique were found to have no significant effect in the temporal domain.

•   The relationship between methane flux and soil temperature found during the period spring–early winter was extrapolated to estimate the methane emission during the winter. At 35%, the contribution of the winter period to the annual flux was very large. This was due to the slow freezing of the tundra soils in early winter, the long cold period (October–May), and generally moderate fluxes during summer.

•   During the period July 2003–July 2004, the tundra was a carbon sink of 17.3 g C m^{-2}, and the methane emission accounted for about 14% of the ecosystem carbon balance. Considering the global warming potential of methane compared to carbon

dioxide, the GHG balance of the tundra in units of CO_2 equivalents was $+6.8$ g m^{-2}. Thus, although the methane emission had only a small influence on the tundra's capacity as a carbon sink, it turned the tundra into an effective greenhouse gas source.

Acknowledgements

Methane emission from Siberian wet polygonal tundra on multiple spatial scales: Vertical flux measurements by closed chambers and eddy covariance, Samoylov Island, Lena River Delta

Torsten Sachs   Michael Giebels   Christian Wille   Lars Kutzbach   Julia Boike

Abstract

Ecosystem-scale measurements and investigations of the small-scale variability of methane emission were carried out in northern Siberian wet polygonal tundra using the eddy covariance technique during the entire 2006 growing season. Simultaneous closed chamber flux measurements were conducted daily at 15 plots in four differently developed polygon centers and a polygon rim from July through September 2006. Our study site was located in the southern part of the Lena River Delta, characterized by arctic continental climate and comparatively cold, continuous permafrost. Controls on

methane emission were identified by applying multi-linear and multi-nonlinear regression models. We found a relatively low growing season average methane flux of 18.7 ± 10.2 mg m^{-2} d^{-1} on the ecosystem scale and identified near-surface turbulence, soil temperature, and atmospheric pressure as the main controls on the growing season variation methane emissions. On the micro-site scale, fluxes showed large spatial variability and were best described by soil surface temperature.

1   Introduction

Arctic tundra ecosystems cover an area of about 7.34×10^{12} m^2 (Reeburgh et al., 1998) and are underlain by permafrost. Despite increased research, especially in connection with the much stated concern of potential increased emission of climate-relevant trace gases from warming or thawing tundra areas, these sensitive high-latitude ecosystems with their complex network of interconnected processes and controls are far from being understood. Vegetation, state of the permafrost, soil texture, hydrology, and many other relevant parameters and consequently also processes controlled by these parameters vary greatly on small spatial scales. This is especially valid for methane emission on various scales from arctic wetlands (Christensen et al., 2000; Kutzbach et al., 2004; Whalen and Reeburgh, 1992).

To our knowledge, only four studies reported methane flux data from Arctic tundra on the ecosystem scale using eddy covariance techniques, namely Fan et al. (1992) from western Alaska, Harazono et al. (2006) from northern Alaska, Friborg et al. (2000) from Greenland, and Hargreaves et al. (2001) from Finland. Manuscripts by Wille et al. (2008) and Sachs et al. (2008) reporting data from the Lena River Delta, Siberia, are currently in press.

On the other hand, many studies are available reporting point data using closed chamber methods (e.g. Christensen et al., 2000; Kutzbach et al., 2004; Whalen and Reeburgh, 1992). While closed chamber methods have multiple inherent problems such as the exclusion of atmospheric parameters and induced alteration of concentration gradients underneath the chamber, resulting in disturbed fluxes, they are widely used to investigate the small scale variability of methane fluxes. The eddy covariance method does not allow for a spatial resolution high enough to investigate that kind of variability in heterogeneous areas.

We conducted intensive field studies on the ecosystem (1 ha to 1 km^2) and micro-site scales (0.1-100 m^2) using eddy covariance and closed chamber methods simultaneously in order to investigate the temporal and spatial variability of methane emissions. For the first time, methane flux measurements on the ecosystem scale in Arctic Siberian tundra were carried out during an entire growing season from the beginning of June through September 2006, and measurements on the micro-site scale were conducted within the eddy covariance footprint from July through September 2006.

2　Material and methods

2.1　Study site

The study site was located on Samoylov Island, 120 km south of the Arctic Ocean in the southern central Lena River Delta (72°22'N, 126°30'E) and is considered representative of the active delta landscape. Over the past ten years, Samoylov Island has been the focus of a wide range of studies on surface-atmosphere gas and energy exchange, soil science, hydrobiology, microbiology, cryogenesis, and geomorphology (Boike et al., 2003; Kutzbach et al., 2004, 2007; Liebner and Wagner, 2007; Schwamborn et al., 2002; Sachs et al., 2008; Wille et al. 2008).

Samoylov Island covers an area of about 7.5 km². The western part of the island (3.4 km²) is a modern floodplain with elevations from 1 to 5 meters above sea level (a.s.l.). The study site is located in the center of the Late-Holocene eastern part (4.1 km²) with elevations from 10 to 16 meters a.s.l. The surface of the terrace is characterized by wet polygonal tundra with a flat but regular micro-relief caused by the development of low-center ice wedge polygons. The typical elevation difference between depressed polygon centers and elevated polygon rims is up to 0.5 m (Kutzbach, 2006). The poorly drained and hence mostly inundated centers are characterized by *Typic Historthels*, while *Glacic* or *Typic Aquiturbels* dominate at the dryer but still moist polygon rims (Soil Survey Staff, 1998; Kutzbach et al., 2004). As the summer progresses, these soils typically thaw to a depth of 30 cm to 50 cm.

Hydrophytic sedges as well as mosses dominate the vegetation in the wet polygon centers (Kutzbach et al., 2004). Polygon rims are dominated by mesophytic

dwarf shrubs, forbs, and mosses. Surface classification of aerial photographs taken in 2003 shows that elevated and dryer polygon rims cover approximately 60% of the area surrounding the study site, while depressed and wet polygon centers and troughs cover 40% of the area (G. Grosse, personal communication, 2005).

The climate in the region is arctic continental climate characterized by very low temperatures and precipitation. Mean annual air temperature at the meteorological station on Samoylov Island was −14.7°C and mean precipitation was 137 mm, ranging from 72 mm to 208 mm in a period from 1999 to 2005 (Boike et al., 2008). Snowmelt and river break-up typically start in the first half of June, and the growing season lasts from mid-June through mid-September. The continuous permafrost in the delta reaches depths of 500 to 600 meters (Grigoriev, 1960) and is characterized by very low temperatures between −13°C and −11°C (Kotlyakov & Khromova 2002).

2.2   Ecosystem-scale flux measurements

In-situ ecosystem-scale methane fluxes were measured using the eddy covariance (EC) method with a tunable diode laser spectrometer (TGA 100, Campbell Scientific Ltd., USA) for CH_4 analysis. A more detailed description of the technical set-up can be found in Sachs et al. (2008).

The EC system was set up in the center of the eastern part of Samoylov Island and was surrounded by a relatively homogenous fetch of wet polygonal tundra. Larger lakes were located at the periphery of a 600 m radius around the tower. Successful measurements were conducted on 103 days from 9 June to 19 September 2006, covering an entire growing season (Sachs et al., 2008).

Additional parameters measured at the eddy covariance system and an automated long-term monitoring station 700 m south of the EC tower include air temperature, relative humidity, incoming and outgoing solar and infrared radiation, photosynthetically active radiation (PAR), barometric pressure, precipitation, and soil temperature data at various depths. Additional daily manual measurements at five sites in close proximity to the tower included thaw depth using a steel probe, soil temperatures in 5 cm depth intervals, water level, and soil moisture using a Theta Probe type ML2x (Delta-T Devices Ltd., Cambridge, UK) where no standing water was present.
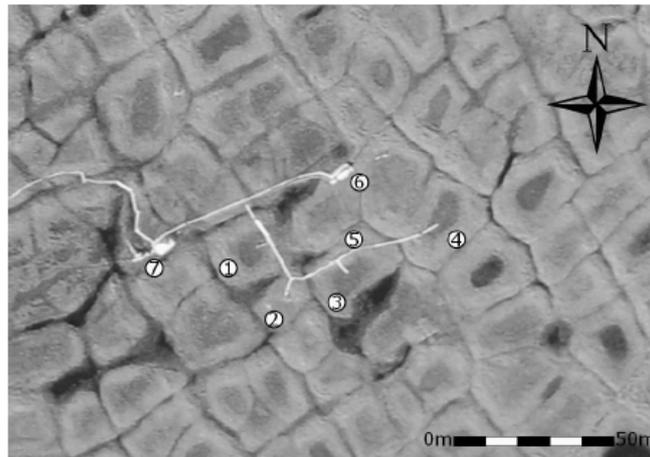
Figure 1: Aerial view of investigation site: 1) low-center polygon, 2) high-center polygon, 3) low-center polygon, 4) low-center polygon, 5) rim, 6) eddy covariance system, 7) tent for equipment (Photo: J. Boike).

The area from which 80% of the cumulative methane flux originated was calculated using a footprint analysis according to Schuepp et al. (1990). The upwind distance of this flux contribution was on average 518 m, the maximum contribution originated from an average distance of 116 m.

2.3   Small-scale flux measurements

For small-scale flux measurements, five different micro-sites characteristic of the prevalent surface and vegetation features within the eddy covariance fetch were established in close proximity to the flux tower (Fig. 1).

Polygon 1 was a low-center polygon with standing water in the center. The northern side of the polygon rim showed signs of beginning degradation, which might serve as a hydraulic connection to surrounding polygon troughs. Vegetation in the center is dominated by *Drepanocladus revolvens* (100% coverage) and *Carex chordorrhiza* (8% coverage).

Polygon 2 was a high-center polygon with no standing water in the center due to drainage into surrounding thermokarst cracks and troughs. The vegetation was dominated by *Hylocomium splendens* (85% coverage) and *Tomentypnum nitens* (10% coverage).

Polygon 3 was a low-center polygon with a massive rim on the western side and a completely degraded rim on the eastern side, where a large thermokarst crack of more than 2 m depth was located. There was standing water in the polygon center and the vegetation was dominated by *Drepanocladus revolvens* (90% coverage), *Carex chordorrhiza* (10% coverage), and *Carex concolor* (10% coverage).

Polygon 4 was a low-center polygon with no apparent rim degradation and no apparent hydraulic connection to surrounding cracks or troughs. It usually maintained the highest water level and was dominated by *Scorpidium scorpidioides* (100% coverage), *Carex chordorrhiza* (8% coverage), and *Carex concolor* (3% coverage).

The polygon rim micro-site was underlain by a massive ice wedge and draining into polygon 3 to the east and the polygon crack to the west. Vegetation was dominated by *Hylocomium splendens* (60% coverage), *Rhytidium rugosum* (30% coverage), and *Carex concolor* (4% coverage).

In each of the four polygon centers and along the rim, three 50 cm x 50 cm PVC chamber collars with a water-filled channel as a seal were inserted 10–15 cm into the active layer. Chambers were made of opaque PVC and clear PVC, respectively, for light and dark measurements. Chamber volume was 12.5 l at the high-center and rim micro-sites and 37.5 l at the other sites, where higher vegetation did not allow for the use of small chambers.

Chamber measurements at all 15 plots were made daily from 12 July through 19 September 2006 with both clear and opaque chambers. Sample air was drawn from a port on top of the chamber every 45 s for 8 to10 minutes for simultaneous analysis of CO_2, CH_4, and water vapor using a photo-acoustic infrared gas spectrometer Innova 1412 with optical filters UA0982 for CO_2, UA0969 for CH_4, and SB0527 for water vapor (INNOVA AirTech Instruments, Denmark). A membrane pump was connected to two other ports and circulated chamber headspace air through perforated dispersive tubes for mixing.

Due to water interference with the CH_4 optical filter sample air was dried prior to entering the analyzer using 0.3 nm molecular sieve (beads, with moisture indicator; Merck KGaA, Darmstadt, Germany). Temperature and pressure inside the chamber were logged continuously by a MinidanTemp 0.1° temperature logger (Esys GmbH, Berlin, Germany) and the Innova 1412, respectively.

2.4   Flux modeling

We used multiple linear regression as well as regression tree analysis to identify the main controls on eddy covariance methane fluxes. All analyses were based on daily averages of measured and quality-controlled fluxes and are reported elsewhere in detail (Sachs et al. 2008). A multiplicative exponential regression model modified and extended after Friborg et al. (2000), was set up and fitted to the in-situ data for small-scale flux modeling. It can be written as

$$FCH_4 = a \cdot b^{((T-\overline{T})/10)} \cdot c^{(u*-\overline{u*})} \cdot d^{(p-\overline{p})} \tag{1}$$

where a, b, c, and d are fitted parameters, T is the soil temperature at 10 cm depth in a polygon center, $u*$ is the friction velocity, p is the air pressure, and horizontal bars denote the mean values of the respective variables. A weighting factor of σ_{FCH4}^{-2} was applied during the fitting process, with σ_{FCH4} being the daily mean of the noise estimates of the hourly flux data points.

For closed chamber measurements, we used multiple linear regression analyses to identify statistically significant controls on methane flux. Data were first tested for multi-collinearity following Schuchard-Ficher (1982) and for parameter significance using a t-test. The regressors were discarded in a stepwise procedure until only independent and significant parameters remained.

3   Results

3.1   Ecosystem-scale methane flux

Mean daily ecosystem methane flux was 18.7 ± 10.17 mg m^{-2} d^{-1} during the study period and showed relatively small seasonal variation (Fig. 2, top panel). However, strong variations could be observed, which coincided with pronounced decreases in air pressure and higher wind speed after calm periods.

In the first two weeks of measurements, average daily methane fluxes were already 13.8 mg m^{-2} d^{-1}, with high variability from 5.7 mg m^{-2} d^{-1} to 22.0 mg m^{-2} d^{-1}. Soil temperature was still below 0°C when measurements started and showed very little variation in the early part of the thawing period. The lowest methane flux was observed
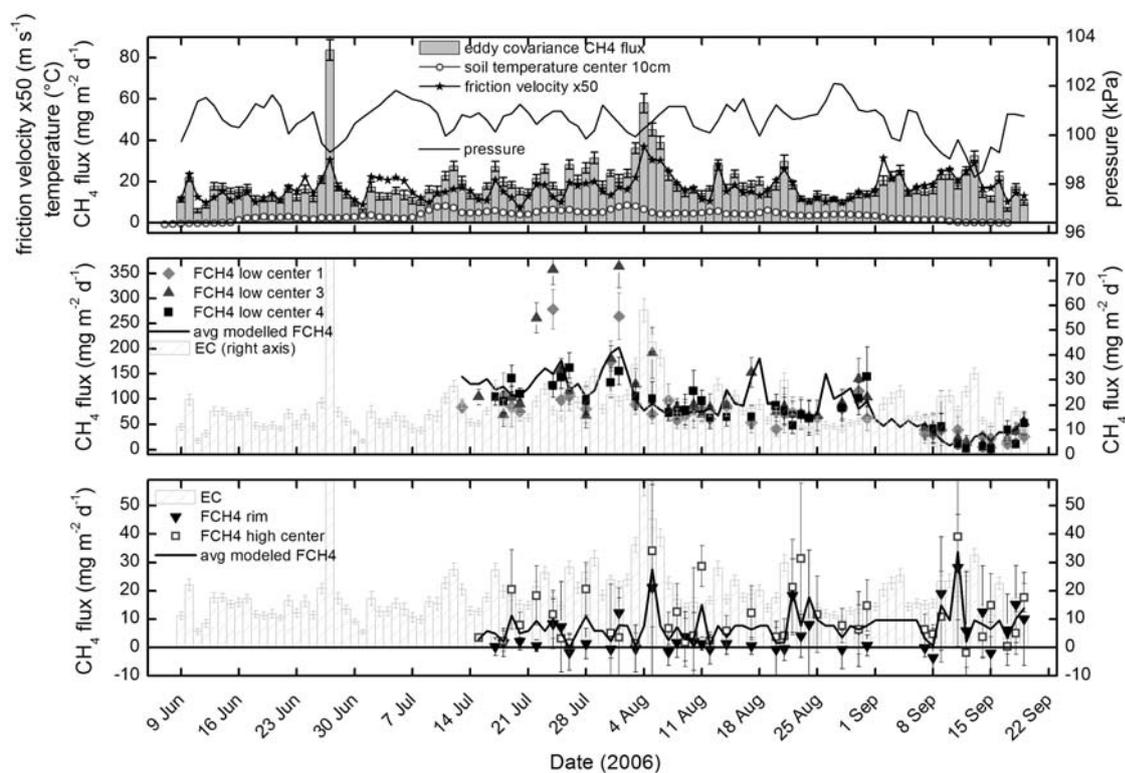
Figure 2: (top) Daily averages of eddy covariance methane fluxes and environmental controls during the 2006 growing season. The error bars of the eddy covariance data indicate the daily average noise level. **(middle)** Closed chamber methane fluxes from low center polygons and average modeled chamber flux. Each point represents the average of six flux measurements in the respective polygon. **(bottom)** Closed chamber methane fluxes from a polygon rim and a high center polygon and average modeled chamber flux. Each point represents the average of six flux measurements at the respective site. The error bars of the chamber data indicate the mean standard errors of the flux estimates. In the middle and bottom panel, the eddy covariance fluxes are given as light-grey columns for comparison. Note the different scale of the two y-axes in the middle panel!

during days with relatively high air pressure and low wind speed. Methane fluxes increased to an average of 25.0 mg m^{-2} d^{-1} in the third week; however, this increase was mainly due to an extreme peak on 27 June, which coincided with the lowest observed air pressure during the summer and high wind speeds. The last ice from the bottom of ponds and smaller lakes surfaced and melted around this time.

Methane fluxes dropped to an average of 12.3 mg m^{-2} d^{-1} during the calm period at the end of June, and then steadily increased to the highest measured fluxes of on average 35.1 mg m^{-2} d^{-1} in the first week of August, roughly following variations in soil temperature and closely following variations in wind speed. Throughout July, above-average methane fluxes frequently correlated with rapid decreases in air pressure. Until the third week of August, fluxes remained between 17.0 and 20.0 mg m^{-2} d^{-1} and then

decreased to less than 13.0 mg m^{-2} d^{-1} during a longer calm high-pressure period at the end of August.

During the first and second week of September, which were characterized by steadily decreasing air pressure, partly strong winds, and rain or snow events, methane fluxes increased to an average of 18.2 mg m^{-2} d^{-1} and 21.6 mg m^{-2} d^{-1}, respectively, despite a decrease in soil temperature and refreezing of the top soil layers and water bodies. By mid-September, all water bodies except for the large thermokarst lakes where covered with ice up to 8 cm thick. During the calm high-pressure period after 13 September, methane fluxes decreased markedly to below 10.0 mg m^{-2} d^{-1} at the end of the measurement period.

All approaches showed that variation in methane fluxes could best be explained by friction velocity u_* and soil temperatures at 10 cm depth in a polygon center and 20 cm depth in a polygon rim, respectively. Friction velocity alone accounted for 57% of the variance in methane emissions and another 3% could be explained by wind speed, which is closely correlated with friction velocity. Soil temperatures on the other hand only explained about 8% of the variance. The best agreement (r^2_{adj} = 0.68) of modeled and measured data was obtained by a model which included an exponential term that accounts for the observed influence of air pressure.

Thaw depth, which increased gradually and without variation throughout the season, did not improve the model, nor did water level, which remained above the soil surface at all times in the polygon centers.

The cumulative methane emission during the 2006 growing season was 1.93 g m^{-2}, which agrees well with the cumulative flux during the same period of a combined 2003 and 2004 dataset that amounted to 1.87 g m^{-2} (Wille et al. 2008). The model underestimated the cumulative measured flux by less than 5%.

3.2   Small-scale methane flux

Small-scale methane emission was similar among low-center polygons (Fig. 2, middle panel) and differed strongly from fluxes at the high-center and rim micro-sites (Fig. 2, bottom panel).

At all three low-center micro-sites, mean daily fluxes in July and August were around 100 mg m^{-2} d^{-1} and decreased at the beginning of September to less than 50 mg

m^{-2} d^{-1}, closely following variations in air temperature. When snow started to accumulate between September 10 and 15 during a period of below-zero temperatures, emissions fluctuated below 20 mg m^{-2} d^{-1}. At polygon 4, the seasonal course was less pronounced and variability was less extreme than at polygon 1 and 3, where peak fluxes exceeded 350 mg m^{-2} d^{-1} and were associated with spatial standard deviations of up to ±300 mg m^{-2} d^{-1}, demonstrating a large spatial variability even within micro-sites. These extreme emissions were generally associated with high temperatures.

It was not possible to construct a multidimensional regression model with independent and significant parameters. The predictor variable with the highest explanatory power within the final one-dimensional model was surface temperature.

At polygon 2 (high center) and at the polygon rim, very low methane concentrations in the closed chamber system frequently caused the analyzer to reach its detection limit, resulting in noisy data and a high exclusion rate during flux calculation. Fluxes that could be calculated were very low throughout the campaign and rarely exceeded 10 mg m^{-2} d^{-1}, which is about 10% of the average fluxes from low-center polygon micro-sites. No seasonal course is evident from the data and no statistically significant correlation with any of the observed environmental parameters was found. Gaps in the time series were filled with monthly average flux values, accounting for the small positive fluxes that were present.

Averaging closed chamber methane fluxes from wet polygon centers and drier sites, respectively, and weighing them according to the distribution of wet (40%) and drier (60%) surfaces classes results in an up-scaled closed chamber flux of 39.11 mg m^{-2} d^{-1}, which is double the eddy covariance flux during the same time period.

4   Discussion

Results from eddy covariance measurements differ from closed chamber data both in terms of the seasonal variation and the identified controls on methane emissions. While ecosystems-scale fluxes do not show much of a seasonal course, results from low-center polygon closed chambers show a pronounced decrease of methane emission towards the end of the season, which is more in agreement with most studies and results from deterministic process-based models used for larger-scale modeling (e.g. Kirschke et al., 2008).

Emission peaks also do not match on the different scales. While ecosystem-scale emission peaks usually coincide with high wind speed, low air pressure, and generally "bad weather" conditions, the largest emission from polygon centers as measured by closed chambers occurred during warm and dry days. However, the very weak peaks visible in closed chamber data from the rim and high-center micro-site tend to be more in agreement with eddy covariance emission peaks.

These differences in the seasonal dynamics may partly be explained by the very different hydrological conditions of the investigated micro-sites in combination with the importance of plant-mediated transport of methane (Kutzbach et al., 2004): in the wet polygon centers, water levels were always at or above the soil surface. Here, higher water levels could lead to decreased methane emission, as more vegetation becomes submerged and plant-mediated transport decreases. In addition, higher temperatures likely increase microbial methane production close to the surface. Hence, warm weather and falling water levels could actually increase emissions as long as the water table remains above the surface. At "drier" micro-sites, on the other hand, storm systems with strong precipitation events lead to a temporary increase in anaerobic soil volume and an increase in methane production, while lower temperatures have a negative effect on the activity of methane oxidizing microbes in the upper horizons of the active layer.

However, a large influence on the ecosystem methane flux can also be ascribed to open-water surfaces such as polygon ponds and thermokarst cracks, which were not covered by the closed chamber measurements but were present in the eddy covariance footprint. Diffusive and turbulent gas transfer between water and atmosphere is known to be proportional to the third power of the wind speed (Wanninkhof and McGillis, 1999) and observation of methane ebullition (Walter et al., 2006) in the field indicates that water bodies are an important contributor to ecosystem methane efflux. These micro-sites must be included in future small-scale measurements within the eddy covariance footprint in order to more accurately scale chamber flux measurements to larger areas. A more detailed analysis of the small-scale variability and the scaling problems is in preparation.

The discrepancies in the results on the different scales also highlight the need for more non-intrusive and spatially integrating measurements from high-latitude ecosystems to verify and understand the results produced by the eddy covariance

method. Larger-scale methane emission models that have previously been developed on the basis of closed chamber data only, should incorporate new findings from eddy covariance or other non-intrusive techniques.

Our findings raise the question to which extent methane fluxes in permafrost ecosystems are controlled by near-surface controls including atmospheric boundary layer conditions and vegetation, or by soil characteristics and processes in the deeper active layer including microbial community structure and activity.

Acknowledgments

Now this is not the end. It is not even the beginning of the end.

But it is, perhaps, the end of the beginning.

(Sir Winston Churchill)